

Turkey-Leg-Tendon: A Model System for Collagen Mineralisation



Paul Adesoji

**This dissertation is submitted for the degree of Master of Medical
Sciences (By Research)**

November 2018

Medical School

Declaration

I declare that this thesis is my own original work and has not been submitted for a higher degree course at any other institution.

Acknowledgements

I would like to give a special thanks to my supervisor Dr Jemma G. Kerns. Her guidance and influence throughout this project has been vital in supporting my research.

I would also like to thank my secondary supervisor Dr David Cheneler for providing the training in mechanical tensile tests and analysis of tensile data using purpose-built codes. I would like to thank Dr Lorna Ashton for the training of the specialist knowledge in Raman spectroscopy.

I am very grateful for the ongoing support in laboratory and throughout the course of master's research provided by Dr Nur Adeelah Binti Che Ahmad Tantowi and Pedro Elston. I would also like to show my appreciation to Dr Chris Jewell for his teaching methods in sample preparation techniques and Mohamed Milad for the training in aspects of mechanical test data analysis.

Finally, I would like to thank my family for the all the support they have given me throughout the year mentally and physically. I have gained an invaluable experience and completion of my master's research would be unobtainable without these people.

Abstract

Turkey leg tendon (TLT) is used as a model system to explore the process of collagen mineralisation. Mineralisation takes place in distinct regions across the length of the tendon and is accompanied by a change in biomechanical properties of collagen. The collagen becomes more aligned and adapted to the mechanical demand of the tendon. This study aimed to: 1) Identify the stages of mineralisation process & associated Raman spectral signatures using the TLT as a model. 2) Determine changes in collagen chemically and mechanically that lead to mineralisation in the maturing TLT. 3) Identify the links between mineralisation in young and old tendons with potential problems which can arise leading to unhealthy ageing of collagenous tissue. These were explored using Raman spectroscopy and in vitro mineralisation with SBF, micro-CT imaging (chemical analysis), and uniaxial tensile loading and video gauge (VG) imaging (mechanical tests). The results showed there were two distinct regions of mineralisation in old tendons compared to the young tendons which had one region or points of immature mineral. The collagen organisation predetermined the maturity of each mineral region therefore regions furthest proximal were always more mature. Turkey tendons mineralise to balance their weight with locomotive activity. The structural integrity of the tendon was compromised during over-mineralisation resulting in high modulus in overall tendon. The occurrence of right leg dominance was revealed by differences in the right tendon's adaptation for greater mechanical load, the over-mineralisation and the loss of collagen content in remineralisation. The absence of higher signalling components (such as tenocytes in the collagen matrix and proteoglycans present in the ECM) results in a perturbed mineralisation system. Non-mineralised regions of the tendon greatly influenced the mechanical integrity of the collagen. Mineralisation limits the elastic potential of the tendon to provide effective function though predetermined "Never mineralised" regions remained non-mineralised. If tissue that never mineralises can be characterised in a perturbed mineralisation system, it would be possible to control mineralisation thus prolong the longevity of collagenous tissue and open opportunities for new therapeutic agents to target tissues with disrupted mineralisation in a range of metabolic diseases.

Table of Contents

Declaration	2
Acknowledgements	3
Abstract	4
List of Figures	7
1 Introduction	12
1.1 Bone	12
1.1.1 What is healthy bone?	12
1.1.2 Ageing bone	13
1.1.3 Clinical manifestation of ageing	14
1.2 Mineralisation	14
1.2.1 Importance of mineralisation	14
1.2.2 Problems during mineralisation	15
1.3 Tendons	15
1.3.1 Function	15
1.3.2 Mechanical properties of tendons	16
1.3.3 Link between tendon and bone	16
1.3.4 Turkey Leg Tendon (TLT) model	16
1.3.5 Mechanical properties of tendons	17
1.3.6 Raman spectroscopy	17
1.3.7 Tendon spectra	19
1.4 Computational process and analysis	21
1.4.1 Pre-processing	21
1.4.2 Supervised vs unsupervised analysis	22
2 Thesis	23
2.1 Overview	23
2.2 Research hypothesis	23
3 Materials and Methods	24
3.1 Preparation and storage of tendon	24
3.2 Calibrations	24
3.3 Optimisation	25
3.4 Data Collection	28
3.5 Schedule for experiments	28
3.6 Pre-processing	29
3.7 Computational analysis	30
3.8 Bone	30

3.9	Mechanical Testing	30
3.10	Video gauge derived strain measurement using Imetrum imaging	32
3.11	Analysis of Mechanical Testing (Zwick mechanical tester)	33
3.12	Analysis using Imetrum (optical imaging)	33
3.13	Finite Element Analysis - FEA	36
3.14	Remineralisation of tendons in simulating body fluid (SBF)	37
3.14	Micro-computed tomographic (micro-CT) imaging	38
4	Results	39
4.1	Initial Raman analysis of tendons	39
4.1.1	General Differences: Young vs Old	40
4.1.2	Differences in mineralisation between young & old	42
4.1.3	Amide III: Phosphate	44
4.1.4	Amide III: Amide I.....	46
4.1.5	Carbonate: Phosphate	48
4.1.6	Proline: Hydroxyproline	50
4.1.7	Analysis of differences in Young vs Old: Pre- vs Post-mechanical	51
4.1.8	Differences in various region pertaining to their chemical composition.....	53
4.2	Mineral Crystallinity	57
4.3	Mechanical Testing	57
4.3.1	Uniaxial loading from Zwick mechanical tester	57
4.3.2	Determination of the Elastic modulus	58
4.4	Imetrum Imaging	63
4.5	Finite element analysis	66
4.6	Simulating Body Fluid (SBF) experiment	68
4.6.1	Incubation of SBF	68
4.6.2	Analysis of SBF results.....	75
4.6.3	Visualising the effect of SBF.....	79
5	Discussion	81
5.1	Collagen's structural integrity	81
5.2	Collagen's mechanical integrity	83
5.3	Collagen chemistry as related to function	85
6	Strengths and Limitations	88
7	Future works	89
8	Conclusions	90
9	References	91
10	Appendix	96

List of Figures

Figure 1: Example of spectra taken from non-mineralised (never mineralised) regions of tendons in 11-week-old turkey and (fully) mineralised regions in 18-week-old turkey. Also predicted future mineralised and (unmineralised) non-mineralised regions using 11-week-old turkey tendon (1).....	18
Figure 2: Spectral acquisition from flexor hallucis longus (FHL) of 12-week-old turkey; non-mineralised; green vs mineralised region; yellow showing all peaks expected. Setting were used for optimisation of Raman and were used for all subsequent spectra; time [s], power [%] and accumulation [acc].....	19
Figure 3: Example of lipid peaks taken from TLT.....	19
Figure 4: Raman spectra from sample turkey tendon (Right leg, 12 weeks, FHL) used to optimise Raman laser settings; time (s), power (%) and accumulation (acc), a) Initial optimisation – alteration of laser power alone b) Used max power (100%), same number of accumulations + alteration in the total time of each cycle c) Alteration to accumulation alone d) Comparison between the time with most consistent spectra e) Overall comparison between best spectra f) Comparison of spectra in mineralised and non-mineralised region.....	26
Figure 5: Comparisons between various polynomial fittings were applied for baseline correction during pre-processing of spectral data from tendon samples. Polynomial fits were applied at an order of magnitude (°); A) °3 B) °4 C) °5 D) °6 E) °7 displays the Raman spectra produced from the corresponding (°).....	28
Figure 6: Experiment set-up for Imetrum imaging using VG system with tendon sample position within Zwick mechanical tester.....	31
Figure 7: Example of uniaxial tensile stress-strain graph for tendon sample in real-time.....	32
Figure 8: Diagrammatic representation of code written by M. Milad incorporating the delay between Zwick and the Imetrum to produce a real-time measurement. The new defined real-time measurement is combined with the hyperelastic model to produce a stress-strain which corresponds to real-time curve fitting of the uniaxial loading of the tendon. α, β, γ, δ represent subsequent new real time measurements.....	34
Figure 9: Types of modulus of elasticity in the stress-strain curve.....	35
Figure 10: Non-mineralised region vs mineralised region under microscope lens. In a) the non-mineral region the detail of the collagen can be seen on the surface. Under the microscope strands of regular arrangement and almost a successive linear pattern of collagen fibrils is visible compared to b) mineral region where there is high fluorescence and the mineral is uniform over the underlying collagen structure.....	39
Figure 11: Diagrammatic representation mapping difference chemical regions in flexor hallucis longus tendon: A) 15 wks – right tendon and B) 15 wks – left tendon (Min = Mineralised, FM = Future Mineralised). D = distal end, P = proximal end.....	39
Figure 12: Example of spectra from Raman including mineralised and non-mineralised regions from young (12 wks) and old (15 wks) flexor tendon.....	39

Figure 13: PCA plot visualising the distribution of the data from “12 week” young vs “15 week” old tendons. Red circle encompasses cluster of spectra from young tendons which are spectrally similar. Purple circle encompasses high intraclass variation within spectra of the old tendons. Purple compared to green circle reveals interclass variation between old and young tendon thus spectrally different.....40

Figure 14: PCA loadings plot of the contributing factors to the distribution of the spectra relative to PC1 and PC2 from the young and old tendons before tendons were tested mechanically.....40

Figure 15: PCA plot showing the distribution of the level of mineralisation according to the 3 types of regions possible in tendons irrespective of age.....40

Figure 16i: Collagen analysis: Amide III: Phosphate ratio intensity showing the level of mineralisation as a percentage from the distal end before mechanical testing in tendon (A), after mechanical testing in tendon (B) and in untreated tibia (bone) relative to tendon extracted (C). Analysis of mineral per collagen area was determined spectroscopically using Raman by the appearance of chemical bands measured from the maximum peak intensity of amide III ($1240-48\text{ cm}^{-1}$) and phosphate ($955-60\text{ cm}^{-1}$) at various positions along the length of the tendon. Young tendon (RTFHL-12) was compared with old tendon (RTFHL-15) to see how this chemical property changed with age.....43

Figure 16ii: Collagen analysis: Amide III: Amide I ratio intensity showing the collagen organisation as a percentage from the distal end before mechanical testing in tendon (D), after mechanical testing in tendon (E) and in untreated tibia (bone) relative to tendon extracted (F). Analysis of collagen organisation was determined spectroscopically using Raman by the appearance of chemical bands measured from the maximum peak intensity of amide III ($1240-48\text{ cm}^{-1}$) and amide I ($1658-64\text{ cm}^{-1}$) at various positions along the length of the tendon. Young tendon (RTFHL-12) was compared with old tendon (RTFHL-15) to see how this chemical property changed with age.....45

Figure 16iii: Collagen analysis: Carbonate: Phosphate ratio intensity showing the maturity of mineralisation as a percentage from the distal end before mechanical testing in tendon (G), after mechanical testing in tendon (H) and in untreated tibia (bone) relative to tendon extracted (I). Analysis of mineral maturity was determined spectroscopically using Raman by the appearance of chemical bands measured from the maximum peak intensity of carbonate ($1068-73\text{ cm}^{-1}$) and phosphate ($955-60\text{ cm}^{-1}$) at various positions along the length of the tendon. Young tendon (RTFHL-12) was compared with old tendon (RTFHL-15) to see how this chemical property changed with age.....47

Figure 16iv: Collagen analysis: Proline: Hydroxyproline ratio intensity showing the collagen tissue stability as a percentage from the distal end before mechanical testing in tendon (G), after mechanical testing in tendon (H) and in untreated tibia (bone) relative to tendon extracted (I). Analysis of collagen tissue stability was determined spectroscopically using Raman by the appearance of chemical bands measured from the maximum peak intensity of proline ($850-54\text{ cm}^{-1}$) and hydroxyproline ($875-6\text{ cm}^{-1}$) at various positions along the length of the tendon. Young tendon (RTFHL-12) was compared with old tendon (RTFHL-15) to see how this chemical property changed with age...48

Figure 17: Detailed PCA plot relative to age, mineralisation level and transition along the length pre-mechanical testing.....46

Figure 18: Detailed PCA plot of PC1 and 2 relative to age, mineralisation level and transition along the length post-mechanical testing.....46

Figure 19: PCA loadings plot of the contributing factors to the distribution of the spectra relative to PC1 and PC2 from the young and old tendons after tendons were tested mechanically along with average spectrum of data PCA plot (dotted line)	47
Figure 20: LDA plot of LD1 and 2 relative to age, mineralisation level and transition along the length pre-mechanical testing.....	47
Figure 21: PCA-LDA plot of LD1 and 2 relative to age, mineralisation level and transition along the length pre-mechanical testing.....	48
Figure 22: Illustration of direction of mineral converging to highest mineral presence within proximal region of changing mineralisation profile including shoulder peaks along region. Arrow indicating direction of convergence. Arrow indicating direction of convergence	49
Figure 23: Detailed PCA plot of PC2 and 3 relative to age and mineralisation level along the length of the tendon post-mechanical testing. Red circles indicate variance in 12 wks 1st min region.....	50
Figure 24: Mechanical testing of tendon using Zwick mechanical tester in action, a) showing the tendon taught set to an initial pre-load before commencing conditioning cycles b) tendon under tensile load during conditioning cycles.....	52
Figure 25: Viscoelastic behaviour of tendons. Left: Stress-strain curve analytics. Right: Example of stress strain curve from experimental data of young flexor tendon (12 wks)	53
Figure 26: Hysteresis cycles produced from uniaxial loading of various tendons and linear approximation taken from a consistent point in linear elastic region of resulting stress-strain activity for elastic modulus (EM) calculation.....	56
Figure 27: Strain at the start of Zwick mechanical tester induced uniaxial loading (t=0) and the first stress-strain point recorded at 2 seconds detected by the video gauge of the iMetrum imaging system (iMIS).....	58
Figure 28: Various stages of uniaxial tension applied to the tendon (L_FD-15 shown above) using the iMetrum imaging setup. Video extensometer gauge, VG (Imetrum, Bristol, UK) captured surface displacement in a singular plane. 1) Faint outline as tendon snaps 2) Stretched middle region indicated by elongation of marker.....	59
Figure 29: Stress-strain graph from resulting iMetrum imaging setup with real time points of uniaxial tensile stress along the length of A) R_FD-12 and B) L_FD-12 tendon. The derived in-house code (82) accounts for the artefact in the stress-strain graph.....	60
Figure 30: Strain 1 and Strain 2 from iMetrum imaging setup of initial tendon (L_FD-12 tendon).....	60
Figure 31a: FEA model of the possible distributions of elastic properties along the tendon length relative to modulus. The values used were arbitrary.....	61
Figure 31b: FEA model of the possible distributions of elastic properties along the tendon length relative to displacements. The values used were arbitrary.....	62
Figure 31c: FEA model of the possible distributions of elastic properties along the tendon length relative to strain. The values used were arbitrary.....	62
Figure 32a: Average spectra for demineralised tendons – (RFHL-15 and LFHL-15)	63

Figure 32b: Average spectra for remineralised tendons – day 1 (young; LFHL-12 and old; LFHL-15).....	63
Figure 32c: Average spectra for remineralised tendons – day 3 (young; RFHL-12 and old; RFHL-15)	63
Figure 32d: Average spectra for remineralised tendons – day 6 (young; LFHL-12 and old; LFHL-15)	64
Figure 32e: Average spectra for remineralised tendons – day 7 (young; RFHL-12 and old; RFHL-15)	64
Figure 32f: Average spectra for remineralised tendons – day 10 (young; LFHL-12 and old; LFHL-15)	64
Figure 32g: Average spectra for remineralised tendons – day 13 (young; RFHL-12 and old; RFHL-15)	65
Figure 32h: Average spectra for remineralised tendons – day 14 (young; LFHL-12 and old; LFHL-15)	65
Figure 33: Chemical analysis of mineral and collagen changes along length of young and old tendon at various timepoints during the incubation with SBF.....	66
Figure 34: Breakpoints in RFHL-12 tendon found at day 6 of SBF incubation.....	66
Figure 35: Changes in the collagen of the right old tendon along length during incubation with SBF at a) day 3 b) day 7 c) day 13.....	68
Figure 36: Collagen analysis (Amide III: I) in Left old tendon; Day 14.....	69
Figure 37: PCA plot showing distribution of tendons during incubation with SBF relative to PC1 and 2. Blue circle indicates spread of the data in this area of the plot while red circle indicates the clustering of spectra within this region particularly the purple circles within this circle are groups of spectra from day 1 (bottom) and day 14 (top) respectively. The red arrow highlights the days in which spectra begins to become more spread. Data is colour coded according to day of chemical analysis; day 1-14.....	70
Figure 38: PCA plot showing distribution of tendons during incubation with SBF according to region with respect to age relative to PC1 and 2. Blue circle indicates spread of the data in this area of the plot. Red circle identifies the regions of the young tendon which contribute to the variation in day 3. Purple circles identifying the regions of tendons spectra within day 1 (bottom) and 14 (top)	71
Figure 39: PCA plot showing distribution of tendons before SBF incubation with respect to chemical regions and age relative to PC1 and 2.....	72
Figure 40: PCA scores plot of the difference in the level of mineralisation across the plot. Spectra were colour coded according to day of chemical analysis during SBF incubation.....	73
Figure 41: PCA loadings plot identified the mineral phosphate at 960 cm⁻¹ as the main factor contributing to the spread of the data along PC1. PC2 identified a range of structural chemical components as the contributing factors to the collagen organisation as the mineralisation varies through the day to day progression of SBF incubation.....	74

Figure 42: Micro-computed tomographic (micro-CT) imaging of young tendon

Left: Surface rendered 3D model showing mineralised region in the proximal end of RFHL12 tendon
 Right: Reconstructed cross section of RFHL12 tendon with discrimination between densely packed mineralised collagen fibrils (red) embedded under surface of tendon (white) rendered with CTvox.....74

Figure 43: Micro-CT imaging of old tendon

Left: Reconstructed cross section of LFHL15 tendon (distal region) with discrimination between non-mineralised collagen fibrils; brown, embedded under surface of tendon; white, rendered with CTvox (SkySan 1275, Bruker, Belgium). Right: Surface rendered 3D model of proximal end in LFHL15 tendon with detail of density distribution along surface of tendon.....75

Table 1: Raman band assignments for chemical components expected of turkey leg tendons (66)...18

Table 2: Schedule for data collection of chemical analysis for tendons during incubation in SBF using Raman. All tendons were incubated on the same start day and removed from solution by day 14....36

Table 3: Mineral crystallinity assessment indicating level of mineralisation and maturity of tendon using full-width half height (FWHH) with bone for comparison.....51

Table 4: EM of young (FHL-12) and old (FHL-15) flexor tendons (FHL & FD) to 3.s.f. and length of tendons before and after mechanical testing. EM values were calculated at the 95% confidence level.....56

Table 5: EM calculated as chords taken from stress-strain graphs of R_FD-12 and L_FD-12 tendons. Minimum (min) and maximum (max) moduli were calculated from tangents taken from stress-strain activity at these points.....61

Table 6: Schedule for data collection of chemical analysis for tendons during incubation in SBF using Raman (same as Table 2; Chapter 2)63

Table 7: Variation in the weight of the tendons before, during and after incubation in SBF.....70

1 Introduction

1.1 Bone

1.1.1 What is healthy bone?

Bone is a hard composite which makes up the internal biological framework in humans and vertebrates known as the skeleton. This consists of a calcium containing-mineral substance; hydroxyapatite and a flexible organic protein; collagen. Its role is to provide structure, support and protect various organs in the body. The integrity of the skeleton is determined by bone at the cellular level. This involves osteoblasts, osteoclasts and osteocytes. Osteoblasts are derived from the bone lining and are responsible for the bone formation (1). During the bone lifecycle osteoblasts secrete collagen molecules which polymerise and become collagen fibrils. Osteoclasts are responsible for resorption and changes in the morphology during bone growth (2). Both osteoblasts and osteoclasts are present in a balanced system known as remodelling commencing with resorption finally ending with formation. This is a coupling mechanism (3). Effectively a bone turnover is produced where old bone tissue is replaced with new bone tissue. This is the foundation of building the basic multicellular units (BMUs) (4) responsible for various systemic signalling components in bone.

Osteocytes are mostly inactive osteoblast bone cells which become embedded in mineral (2). They are important signalling components for communication and remain in contact with other bone cells. Osteocytes represent 95% of all bone cells and form a canalicular network between themselves and the bone surface (5). The canalicular network consists of cytoplasmic dendrites and possess mechano-sensing roles which can trigger bone remodelling during osteoblast activity and osteoclast resorption (5). During the process of ageing, the resorptive activity of osteoclast recruits the precursors for the bone forming osteoblasts. While the osteoblasts (which become osteocytes) are reinforced during mineralisation, the activity of osteoclasts only acts to maintain Ca^{2+} effective balancing the coupling mechanism between osteoblasts and osteoclasts (3). To initiate mineralisation, osteoblasts secrete vesicles containing alkaline phosphatase (6). These vesicles rupture for crystals to grow at this centre point. After several days of calcium and phosphate deposition on the surface of collagen fibrils they become hydroxyapatite salt crystals. This process occurs regularly during bone turnover.

Healthy bone has an optimum bone mass to density ratio. This is measured via a bone density test which produces a T-score indicating how much of an individual's bone density is higher or lower than the density of a healthy adult at the age of 30. This also gives the probability of breaking a bone. A T-score between -1 and 1 indicates healthy bone (7) which allows optimum function. A study showed peak bone mass is reached around the age of 21 for females and as late as 26 for some males (8). Bone health is maintained when the bone cells can regulate the consistent turnover of bone approaching peak bone mass. Osteocytes are pivotal for the health and longevity of bone. It is predicted that disturbance to the canalicular network particularly to the lining of the cells because of micro-cracks, can activate apoptosis of bone cells. Osteocytes are able to relay the signal to activated apoptosis and induce remodelling of local bone tissue controlling osteoclast and osteoblast function (5). Without these cells remodelling would not be possible however it is questionable whether remodelling leads to an increase probability of micro-cracks.

The make-up of healthy bone spans past the bone tissue cells. Alongside these cells, the extracellular matrix (ECM) also forms part of the organic interface. The ECM consists of both collagenous and non-collagenous proteins. Non-collagenous proteins in the matrix have an important role in the signalling and regulation of mineralisation via cell and mineral interactions within the matrix respectively. The signalling ability of these proteins is age-dependent and decreases with age. Non-collagenous proteins

include sulphated proteoglycans, acidic glycoproteins and the most abundant non-collagenous protein osteocalcin (4).

Collagenous protein (collagen) is arguably the most important component of the organic matrix and provides the flexibility of the bone structure hence the toughness. This enables resistance to load on impact in addition serving as a template for mineral crystal deposition (inorganic phase) (9). Collagen fibrils are organised at the smallest unit of self-associated fibrils gradually becoming a matrix of larger fibres consisting of numerous cross-links. Cross-linking is the most important feature of collagen fibrils which attributes to its strength. There are 2 main types of cross-links; these are enzymatic cross-links characterised by the enzymes lysyl hydroxylase and lysyloxidase and non-enzymatic cross-links formed by a process called advanced glycation end-products (10). The ratios of enzymatic: non-enzymatic cross-links can change with age.

A range of studies using different types of bone have shown similar patterns in changes induced in enzymatic cross-linking and non-enzymatic cross linking with age (11-13). In individuals greater than 70 years old, there is triple the amount of non-enzymatic cross-linking compared to someone half their age (14). These patterns all lead to decreased strength and toughness of bone with age in addition to an increased chance of prolonged cracking. Non-enzymatic cross-links are more likely to affect bone as it matures than enzymatic cross-links. The non-enzymatic cross-links attribute to the reduction in the optima of mechanical properties. Cross-links determine the orientation and the co-alignment of the mineral crystals within the plane of fibres of the collagen (9). The enzymatic cross links attribute to the increased stiffness in collagen however as the collagen matures in age, there is a loss of these type of cross-links. The regularity of arrangement of both non-enzymatic and enzymatic cross-links are also age-dependent (9).

1.1.2 Ageing bone

The 3 main bone cells have their importance when it comes to different stages of the bone lifecycle. It is arguable which is the most important. However, they are all contributors of bone remodelling. They are also key components of ageing in bone. Most bone cells are restricted to a controlled number of replications and external factors. This leads to a progressive decline in their replicative ability and cells become short-lived e.g. osteoblasts (15). Periodically every 10 years, all bones in the body are reformed (16). The mineral content of bone is age dependent. The mineral present in bone is the equivalent of the naturally occurring mineral hydroxyapatite, although during the process of ageing, many constituents within the mineral are substituted for example, the carbonate which occasionally replaces hydroxyl and phosphate groups on the superficial level and within the crystal lattice (17). Shifting to a higher tissue mineral content with age will yield increased stiffness, and therefore more brittle bones (9).

Bone grows in width (appositional bone growth) via expansion of the periosteum, with new bone tissue replacing old bone tissue (9). As bone matures the cortical zone of bone increases due to addition of mineral deposits and stiffening of the bone (18). This is characterised by cortical drift from early bone development. As humans age, bone continues to increase in width and height until around 20 years old (19). Growth plates close around this point and bone is at its peak of strength with maximum bone density (20). Subsequently bone continues to change morphology as it grows following a range of mechanical changes hence the term bone remodelling. This is seen in both animal and human models (21); (22). Overall bone ages during bone turnover and will undergo several cycles of remodelling to help them to adapt to changes and demands placed on them during the lifetime of bone.

Micro-cracks can develop during the process of repair in bone growth (23). The composition of bone is heterogenous which optimises mechanical properties on the bone via redistribution of loads to try and prevent micro-cracks (1). If any microcracks that have developed remain and are not repaired by bone remodelling this leads to failure of the bone (24). This can manifest in the form of major problems within the bone when additional factors come into play. In theory, there are 3 main factors which lead to failure of bone hence diseased bone. These factors are: disruption of early bone mineral crystals, separation of components which make up the mineral organic interface, and disruption of collagen fibrils. It is possible for failure to arise from different combinations of these factors or all factors occurring at once (9).

1.1.3 Clinical manifestation of ageing

As people grow older from birth to 30 years old there are many changes to bone (19). The probability of this increases in the absence of healthy bone. The changes can become very problematic (25). Osteoarthritis is a debilitating joint disease primarily affecting the older generation. It affects around 8.75 million people in the UK accounting for a third of people aged 45 and over needing treatment (26, 27). Osteoarthritis is a painful joint disease caused by the degeneration of joints and underlying bone. Components of the bone become less resilient thus more susceptible to damage. Bone becomes altered and joints become stiffer limiting the range of motion in joints. Limited locomotion of the joint increases the probability of a joint debilitating disease.

Osteoporosis is another disease which can clinically manifest with age characterised by a progressive loss of bone density. Osteoporosis is defined as a decrease in mineral content and mass which subsequently increases the risk of bone fracture (4). Osteoporosis costs the NHS approximately £1.5 billion a year (28). This is characterised as an age-related loss of bone and by around 80 years of age it is believed that total bone mass will be approximately half its peak value (4). Generally, 1/3 women are affected compared to 1/5 of men (29).

In some cases, clinical symptoms can go unnoticed in osteoporosis until a fracture occurs (30). This is characterised in a specific form of osteoporosis known as post-menopausal osteoporosis. It results in an accelerated loss of bone and becomes a prominent state where the rate of resorption surpasses bone formation. This only occurs in woman as it is dependent on the hormone oestrogen. In women, genetics may determine the signals which produce levels of hormone accountable for oestrogen dependent osteoporosis. The exact mechanism by which the hormones control this condition remains unknown (4). If a post-menopausal woman has a sudden fall due to fracture, it is generally accepted that osteoporosis came prior to fracture.

1.2 Mineralisation

1.2.1 Importance of mineralisation

Mineralisation is process whereby mineral deposits within bone to increase the strength and toughness of the bone. It is also the overarching process by which bones are formed from osteoblasts during ossification. This process is very well-organised. Osteocalcin, the most abundant non-collagenous protein as mentioned before has an important role in promoting mineralisation alongside collagen (2). Osteocalcin specifically does this by attracting osteoclasts and direct regulation of bone density (31). There are two phases involved in mineralisation; these are the inorganic and the organic phases. In the inorganic phase, very precise quantities of inorganic salt crystals align within the bone fibrous matrix (32). The organic phase of mineralization involves collagen organised in various units such as fibrils throughout the bone. The composition of the inorganic crystals is mainly hydroxyapatite (9). Hydroxyapatite crystals make up 65-70% of bone (33) containing the key mineral components

calcium and inorganic phosphate components. These minerals are dispersed throughout collagen within and between fibrils (32). Hydroxyapatite mechanical properties confer hardness within bone. Collagen on the other hand accounts for the organic mass constituting 20-25% of bone. Type 1 collagen is the main type of collagen which predominates in bone. In many vertebrates, this governs the energy storage important for locomotion. The remainder percentage accounts for water in bone (5-15%).

1.2.2 Problems during mineralisation

An absence of healthy bone often arises due to changes in mineralisation. As previously mentioned, in osteoporosis a loss in bone density is attributed to a loss of mineral content. The mineral content governs the level of mineralisation. Poor or highly mineralised tissue compromises its composition heterogeneity (34). This leads to a variation of mineral at different points in the bone tissue and can therefore reduce its mechanical integrity (34). Kerns et al. showed collagen may be primed for mineralisation at specific regions (35). Subsequently coupled deformation takes place between collagen and the mineral component and on transfer of load can be altered hence applied forces are not evenly distributed throughout the bone tissue matrix (34). In retrospect, increased mineralisation generally benefits bone quality, however bone that is too highly mineralised leads to problems such as brittle bones. A low turnover of bone means that less highly mineralised older bone is replaced by lower mineralised new bone (14) thus also increasing the likelihood of brittle bones.

1.3 Tendons

1.3.1 Function

Tendon is a dense fibrous connective tissue attached to bone and muscle which acts as the mechanical link to facilitate movement during locomotion via the limbs. The structure of a tendon encompasses a multi-hierarchical system mainly consisting of collagen fibrils. Collagen fascicles runs from proximal to distal end connected via cross-links throughout the tendon. Together groups of collagen fibrils make up the basic microscopic unit of a tendon. This is the main source of tensile strength within a tendon and can be tested mechanically (36). Type 1 collagen dominates making up 95% of the collagen (37). It is made from cross-striated collagen fibrils with a repeating D period 67 nm long (38). Tendons can be grouped according to their function.

There are 2 main types of tendons; these are typically flexor and extensor tendons. Flexor tendons are known as energy storage tendons and are responsible for storage of elastic energy during loading of tendon. They undergo several rounds of deformation (39) and, extend and recoil repeatedly during locomotion to effectively convert this elastic energy to kinetic energy during movement (38). Extensor tendons are known as positional tendons having a smaller proportion of non-collagenous protein mainly proteoglycans compared to flexor tendons which are energy storage (elastic) tendons. Flexor tendons are prone to greater stress and strain by loading of the tendon and therefore have a greater chance of damage.

Studies have typically used tendons to isolate collagen and analyse these properties (35) (39). Tendons have been used particularly to look at collagen mineralisation, with a range of ways tendons can mineralise. This includes calcification and ossification (40). Ossification is the process when new bone material is laid in place during bone tissue formation as previously mentioned. It occurs in regions where fibroblasts are present, an excess of Ca^{2+} ions and a sufficient supply of blood thus possible in tendons (41). Calcification on the other hand is the process where the tendon becomes harden by an excess of calcium salts. This process is dependent on location and mineral balance (41). It is unclear what favours ossification over calcification and the morphological differences that can be used to

determine which process has caused mineralisation. Nonetheless there remains a gap in the literature of the underlying basis of mineralisation. It is necessary to collate the chemical, material and mechanical properties relating to mineralisation to fully understand collagen's significance in the process of mineralisation.

1.3.2 Mechanical properties of tendons

Mechanical properties have been analysed previously using a range of tendons (42). Flexor tendons include the superior tendons which run deep in the limb and have the advantage of exhibiting the greatest amount of strength as they flex a whole limb thus creating the largest movement. Previous experiments have shown the *flexor hallucis longus* known as the thumb flexor which runs deep in the foot of vertebrates to have the highest elastic modulus in comparison to other tendons (42). Other flexor tendons such as the *flexor perforans et perforans digiti 3* (FPPD3) produced high level ultimate tensile strength subject to mechanical stress (42). Extensor tendons e.g. *extensor digitorum longus* are known to have the lowest resilience (42). This is due to their positional and structural function (43).

Overall flexor tendons are more likely to be involved in loading and strength properties of tendons. Due to the mechanical nature of flexor tendons, they are more prone to injury compared to extensor tendons. There is a decline in age with mechanical ability. As a result, this type of tendon is more likely to undergo processes which increase age-related stiffness such as glycation. Glycation of collagen is known to increase strength of tendon as it has done in rabbit Achilles tendon (44). This is to restore the mechanical ability post injury caused by high level of micro-damage. Flexor tendons repair is slower than extensor tendons. This is seen in the case with the superficial digital flexor tendons (SDFT) and common digital extensor tendon (CDET) in horses (45). Slower repair is directly proportional to lower turnover hence the level of resorption of the tendon is greater than formation. Particularly in flexor tendons which have undergone glycation there is a significant amount of partially degraded collagen in the matrix resulting in the substantial decrease in mechanical ability (46).

1.3.3 Link between tendon and bone

Previous literature has classified tendon as 'bone-like' because very much like bone it is mineralised in a particular way (1). Other literature disagree as tendons only become like bone when they mineralise and not all tendons mineralise (38). The shape of the crystals formed during mineralisation are different in tendon compared to bone (47) (48). What is known however is that mineralisation is common in some avian species e.g. *Meleagris gallopavo*; turkey particularly in the feet and leg region of the turkeys. Tendons of the turkey gastrocnemius consist of a composition of soft tissue and mineralised soft tissue in areas spanning the length of the hip joint to ankle joint. Tendons become characteristically bony when mineralised justifying Currey's earlier description of tendons as bone-like (1). They also mineralise quite rapidly compared to bone thus mineralisation is age-dependent. For this reason, the Turkey Leg Tendon model (TLT) is commonly used to investigate mineralisation in bone.

1.3.4 Turkey Leg Tendon (TLT) model

Turkey is one of the only avian species whereby their tendons become mineralised. Turkey Leg Tendon is a well-established model used to investigate mineralisation. A great deal of work has been done previously on turkey tendons (49) (50). It is well known that mineralisation of TLT starts as early as 12 weeks old (51). Regions of turkey tendon prior to mineralisation exhibit chemical changes in collagen. By 18 weeks of age, the chemical properties of the collagen can be very similar to that of bone. Based on previous literature there is a site-specific difference in collagen before mineral deposition (35), this is characterised as the transition zone. The distance between both mineralised and non-mineralised

regions can be as wide as 1-2 mm. Mineralisation results in increased tensile strength and modulus and occurs with age (38).

1.3.5 Mechanical properties of tendons

The elastic modulus for collagen in turkey tendon as a whole was calculated to be approximately 7-8 GPa (52). During mineralisation, there is an increased collagen fibril length to efficiently transfer stress between adjacent collagen fibrils altering the mechanical properties of the turkey tendon (38). It is speculated that there could be more to mineralisation than just a protective mechanism (46). Tendons with collagen fibrils arranged for energy storage thus those which require high mechanical strength have a reduced turnover and a latency to repair/remodel as a mechanism to prevent weakening of the structure. Additionally, the predisposed nature of tendon loading in these tissues may have a greater significance (42). This may explain the increasing likelihood of tendon injury with age. Tendon injury is associated with problems caused by collagen and mineralisation, hence a problem which can occur in bone.

1.3.6 Raman spectroscopy

Raman spectroscopy is a non-destructive vibrational spectroscopy technique used to provide non-ionising chemical analysis of biomolecules. In previous studies, Raman has been used to measure different levels of mineralisation(35) (53) (54). It is a scattering technique which utilises the Raman shift also known as the Raman effect to produce a range of bands of characteristic frequency shifts on a Raman spectrum (55).

Raman spectroscopy involves the excitement of molecules within a sample using a monochromatic incident radiation from a laser. This causes a scattering of radiation. A large proportion of the scattered radiation produced is of equal frequency to the incidence radiation. This is known as Rayleigh scattering. Raman scattering is the small fraction of scattered radiation which lose energy during vibrational motions and is scattered at a different wavelength (56). This is known as inelastic scattering and is responsible for the spectrum produced (57). Raman scattering produced which has a shorter wavelength hence higher frequency than incidence radiation corresponds to a Stokes shift. While the Raman scattering produced which has a longer wavelength and lower frequency corresponds to an anti-Stokes shift (56). About $1 \times 10^{-7}\%$ of photons are scattered at a longer wavelength (55). Stokes bands have greater intensity than anti-Stokes thus used in most conventional Raman spectroscopy techniques. Anti-stokes however is more suited for fluorescent samples as fluorescence can interfere with Stokes spectral bands (56). In most Raman spectroscopy today, this problem has been overcome by using high-powered lasers with longer wavelength. Common lasers for biological applications include diode lasers (532 nm) and near infrared diode lasers (785 and 830 nm) working the near-IR region (57) (58, 59) which can eradicate problems such fluorescence alongside photodecomposition of samples.

A spectrum of a molecule is composed of bands indicative of the active vibrations which take place when a molecule becomes excited. This vibrational spectrum produces Raman band intensities representative of the strength of chemical interactions within a molecule and atomic arrangement (60). This is classified as a molecule's 'fingerprint' with different molecules having different fingerprints. These vibrations can be defined by their change in polarisability which determines how easily distorted a molecule's electron cloud is thus, the greater the change of polarisability the greater the intensity of the Raman band (60).

Although Raman spectroscopy is very adequate for detecting vibrations thus changes in the polarisability of molecules within bone (61) there are some sensitivity issues which can make it difficult

to analyse some components of bone which include the important non-collagenous proteins for mineralisation. This is due to their lower abundance and very similar spectroscopic nature to collagen making them harder to detect. A highly sensitive instrument is required as the Raman signal can sometimes be masked by background photoluminescence thus background noise can be integrated in the spectra (62). Although there is a range of pre-processing and statistical methods designed to help eliminate this, it remains an issue as the processing of data may be subjective. Samples may overheat and potentially burn especially if the sample is very thin or dry (57). Typically, when looking at bone or tendon, samples are soaked in an aqueous bath solution e.g. phosphate buffer saline (PBS) which will function to maintain hydration of the sample. Reducing the power of the laser is another alternative however the quality of the spectra may suffer (63). Nonetheless the advantage of Raman spectroscopy is that it is possible to measure the main compositional factors which attribute to potential changes in bone quality. These include mineral: matrix and carbonate: phosphate ratios, mineral crystallinity (55), and amide regions characteristic of collagen (64).

Not only does this technique provide information about chemical and spectral analysis of so-called "fingerprints" via functional groups, using Raman allows for the qualitative and quantitative analysis of chemical substances in a sample (65). Furthermore, Raman is used because it offers minimal sample preparation and several ways of imaging samples (64). Thus, a relatively accurate measure of both mineral (inorganic) and protein (organic) components of bone is possible. This is usually followed by univariate and multivariate analyses of the of spectral bands (53).

1.3.7 Tendon spectra

Table 1: Raman band assignments for chemical components expected of turkey leg tendons (66).

Raman shift (cm ⁻¹)	Peak Assignment
822	V _{C-C} - Collagen
850/875	V _{C-C} - Hydroxyproline
938	C-C stretching, alpha-helix - Collagen
955	V ₁ PO ₄ ³⁻ - Mineral phosphate (immature)
959-62	V ₁ PO ₄ ³⁻ - Mineral phosphate (mature)
1220-1280, 1340	Amide III - Collagen amide
1448	CH ₂ CH ₃ - Organic content
1620-1700	Amide I - Collagen amide (C=O)

Previous literature has confirmed there are a range of peaks expected from spectral acquisition of turkey tendons. Kerns et al. showed the mineral phosphate which appears in mineralised regions of older tendons (**Figure 1**) to be caused by stretching vibrations (V₁ PO₄³⁻) at 960 cm⁻¹ (**Table 1**) (35). This peak can sit anywhere between 959-962 cm⁻¹ depending on the carbonate (CO₃²⁻) and monohydrogen phosphate (HPO₄²⁻) content in the mineral (67). It was possible to obtain similar kind of spectra in turkey tendons of younger age (**Figure 2**).

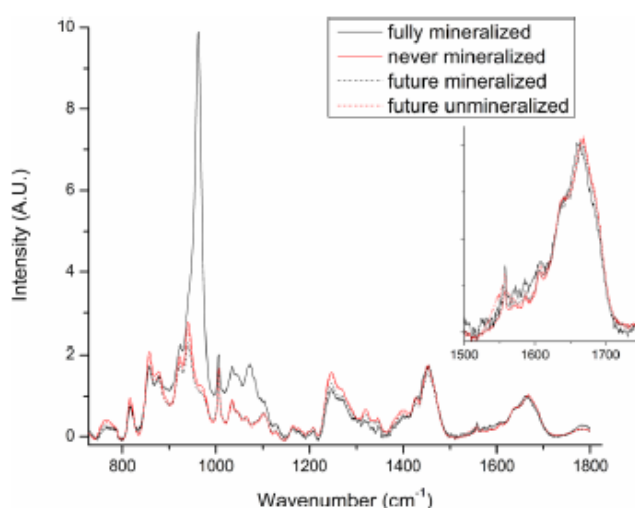


Figure 1: Example of spectra taken from non-mineralised (never mineralised) regions of tendons in 11-week-old turkey and (fully) mineralised regions in 18-week-old turkey. Also predicted future mineralised and (unmineralised) non-mineralised regions using 11 week-old turkey tendon (35).

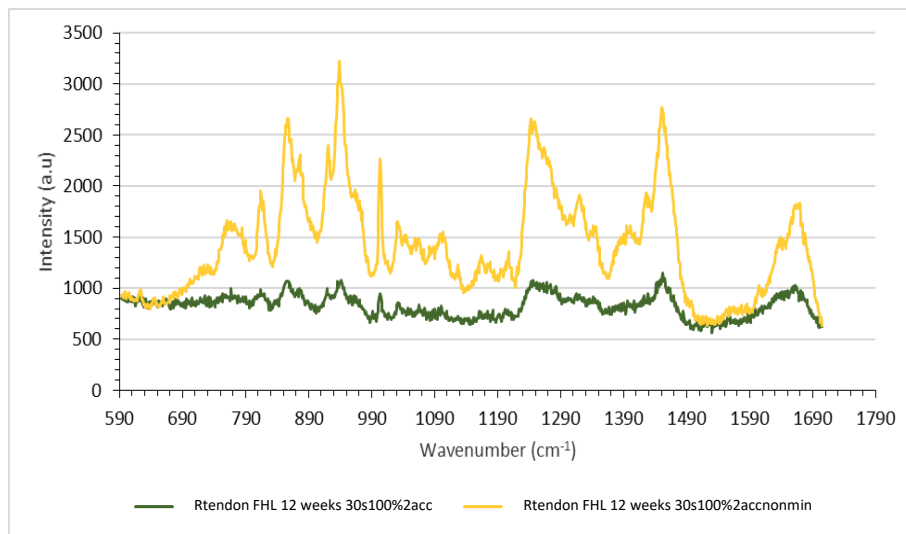


Figure 2: Spectral acquisition from flexor hallucis longus (FHL) of 12 week old turkey; non-mineralised; green vs mineralised region; yellow showing all peaks expected. Setting were used for optimisation of Raman and were used for all subsequent spectra; time [s], power [%] and accumulation [acc]

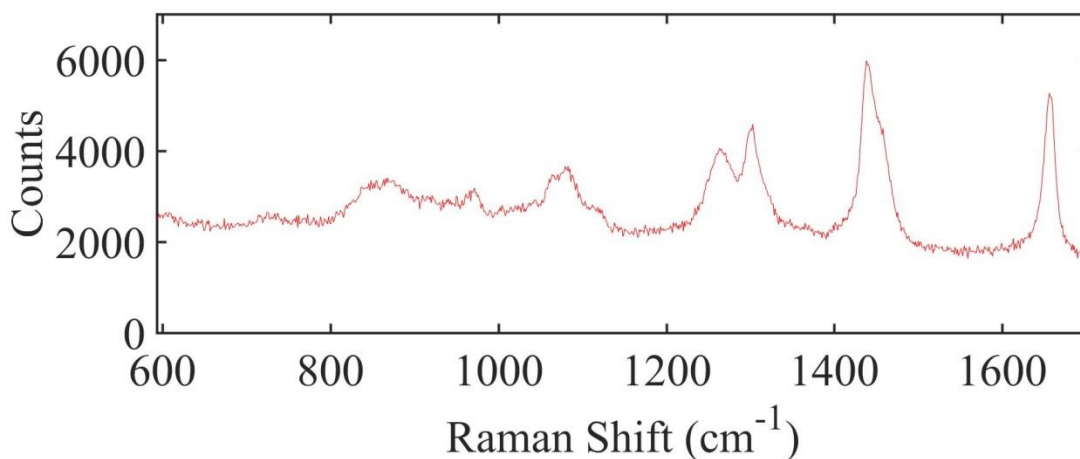


Figure 3: Example of lipid peaks taken from TLT.

The 960 cm^{-1} mineral peak is present in mineralised tendon (**Figure 2**). The larger the height of this peak relative to the collagen peaks the higher the mineral content, thus usually indicative of an older tendon which is more maturely mineralised. The 960 cm^{-1} mineral peak is absent in non-mineral regions, although presence of $937/938\text{ cm}^{-1}$ peak in non-mineral band indicative of a collagen parameter, specifically stretching vibrations of $-(C-C)$ proline and hydroxyproline (68). Shifts in the peak to 941 cm^{-1} is common due to variations in skeletal mode of surrounding polysaccharides, amylose mostly related to this peak (66). During spectral analysis it is possible to obtain data which may resemble collagen related peaks under the Raman microscope but are in fact peaks indicative of lipids. Characteristic lipid band around 1660 cm^{-1} (**Figure 3**) have a distinctive narrower shape at indicative of $\nu-(C=C)$ stretching vibrations of group (*cis*, *cisidene*) of olefinic molecules ($RCH=CHR$) (69). If it appears closer to 1670 cm^{-1} is usually the *trans* isomer of this lipid. Other lipid bands include $1440-1445\text{ cm}^{-1}$ caused by $\alpha-(C-H)$ deformation vibrations, 1310 cm^{-1} ; $\alpha-(C-H)$ deformation vibrations, 1275

α -(=C-H) deformation vibrations from *cis* RCH=CHR (**Figure 3**). These are all so close to peaks which appear in tendon relating to collagen; 1220 (amide III) 1448 (CH₂CH₃) and 1620-1700 cm⁻¹ (amide I) (**Table 1**) respectively. Because of the fingerprint spectral region of tendon other corresponding lipid peaks higher than 1800 cm⁻¹ are not present. The fingerprint region for lipids lies between (1200-700 cm⁻¹). This region has a range of ν -(C-C) vibration thus these peaks alone cannot be used to distinguish between lipid and collagen parameters (69). Lipid peaks can usually be eliminated using this rationale as they appear visibly narrower and usually at very high counts in the spectra. Though this rationale is reasonable it can become subjective thus removing too many peaks can introduce an unwanted bias in the spectral data acquired. An alternative solution would be removal after pre-processing as lipid peaks usually stand out amongst the rest of the spectra and have a substantial effect on the skewness of the data.

1.4 Computational process and analysis

1.4.1 Pre-processing

After spectral acquisition data must undergo some computational processes to be suitable for analysis. Before processing, it is possible to assess the spectra and identify clear outliers e.g. spectral contamination with fluorescence through visual inspection. However, in a circumstance where it is unclear whether bands correspond to a potential lipid band it is best to leave and remove this outlier after pre-processing. Initially a polynomial fit is added to the data. This is a corrective pre-processing technique which aims to fit a baseline to eradicate estimated unknown background noise prior to other pre-processing steps (57). This usually can be applied as an order of magnitude ($^{\circ}$) and this value is chosen according to the type of spectra points in the data. It is important to choose the right magnitude, so this baseline can effectively remove the appearance of any potential oscillatory baselines without loss of initial Raman spectrum intensity (68). Some literature say using an order polynomial fitting 5 $^{\circ}$ or below is most useful to avoid overfitting and loss of spectral components of the data (70), however there is evidence showing the use of polynomial fitting with higher magnitudes. This is entirely dependent of the type of sample being analysed. Particularly high order polynomial fitting are advantageous for large datasets and can eradicate spectral contamination by fluorescence (71). Other baseline correction techniques include first or second-order differentiation however using a polynomial fit has the advantage of maintaining the conventional appearance of Raman shifts correlating to spectral bands (57).

Following baseline correction, the data may need to be normalised to eliminate systemic differences caused by differences in focussing depth and regions of different thickness along the sample. For example, the surface of the tendon is not completely flat as it has different chemical characteristics in different regions, (mineralised vs non-mineralised). There are 2 main methods of normalisation; vector and min-max normalisation. Vector normalisation is based on centring the intensity of all the chosen spectra at one point. Therefore, the centred intensities are equated to a spectrum vector of 1 (72). Studies have shown a small decrease in variance between classes using this technique compared to prior computational processing (57).

Min-max normalisation is where normalisation is done comparing peaks by selecting a minimum and maximum. For biological samples, occasionally, this can be done using the phenylalanine peak (73). The overall idea is that the most consistent peak within the spectra is used so for many studies in tendon and bone, amide I/III is used. Although in some studies amide III is chosen over amide I as amide I is an absorptive peak (74). Nonetheless, spectra are normalised this way thus 1000 or more variables scaled down to 1 producing values between 0-1. The most consistent peak is scaled down to

1 as a maximum, then within this region another peak which forms a natural baseline around this area is used as the minimum; 0.

For this study a min-max normalisation was adopted. This is advantageous as it allowed for comparison between chemically similar peaks by scaling them down for volume. The technique chosen depends on the spectral components of the data and which fits the data well but both techniques are ideal because they do not cause drastic changes to the spectral features of the Raman spectra. It is important that baseline correction takes place before normalisation to eradicate a sloping baseline. Other pre-processing steps such as smoothing can be used additionally however this technique is the most subjective and can result in loss of some important spectral features. Overall the number of pre-processing steps should be chosen wisely to avoid biased results.

1.4.2 Supervised vs unsupervised analysis

Computational analysis encompasses a range of multivariate techniques. The main difference between most of these techniques is whether they are supervised or unsupervised. Principal component analysis (PCA) is an unsupervised analysis technique. PCA does not consider which class each spectrum falls into, but any differences will be visible on a score plot. A principal component (PC) is a linear uncorrelated variable and PCA attempts to separate the data using a natural variance picked out from the group of data. This reduces spectra to principal components which constitute a large amount of spectral variance. It has the advantage of removing background noise and simultaneously conserving the most important spectral data hence variability (75). In a typical dataset up to 1000 spectral variables nearly all the variance (100%) is captured within 10-20 PC's. PC1 has the greatest variance followed by subsequent PC's in a descending order. Through mathematical calculations, it is possible to see if there is more than the assigned number of classes in a collection of spectral variables (72) (76). This can be displayed visually in a loadings and scatter plot.

Linear discriminant analysis (LDA) on the other hand is a supervised technique and it will minimise the variance within each group and maximise the variance between groups. Therefore, this can identify the best linear combination of the spectral variables for discrimination (57). A linear discriminant (LD) is a linear combination to separate two or more classes resulting in a reduction of dimensionality. LDA can be applied in a stepwise manner without the influence of PCA or after PCA (PCA-LDA). The latter is used over the former with highly dimensional data and prevents the common problem of LDA easily overfitting the data (76). PCA-LDA is displayed in loading plot where the difference between groups can be identified from the pseudospectrum from PCA-LDA i.e. LD1 and 2. The heights of peaks in this plot indicate how this chemical peak contribute to the variance. It is good to have a combination of both supervised and unsupervised methods to provide an all-round data analysis approach.

2 Thesis

2.1 Overview

Collagen governs the biomechanical properties of all connective tissue involved in tensile strength and structural integrity (77). Using a TLT model enables collagen to be isolated so that the parameters of collagen mineralisation can be assessed. Mineralisation is a physiological process that occurs in these tendons as a means of preserving/maintaining elastic energy during increased load-bearing activities such as locomotion in turkeys. However, it can be very abruptly disrupted by the onset of certain metabolic bone diseases in the absence of healthy ageing (51). Assessing the tendon/bone quality provides a very useful tool in exploring disease-related changes in collagen.

2.2 Research hypothesis

Distinct regions where mineralisation occur is accompanied by a change in biomechanical properties of collagen. The collagen fibrils with the collagen becomes more aligned and adapted to the mechanical demand of the tendon. This study aims to:

- Identify the stages of mineralisation process & associated Raman spectral signatures using the TLT as a model.
- Determine changes in collagen chemically and mechanically that lead to mineralisation in the maturing turkey leg tendon (TLT).
- Identify the links between mineralisation and potential problems which can arise leading to unhealthy ageing of collagenous tissue.

3 Materials and Methods

3.1 Preparation and storage of tendon

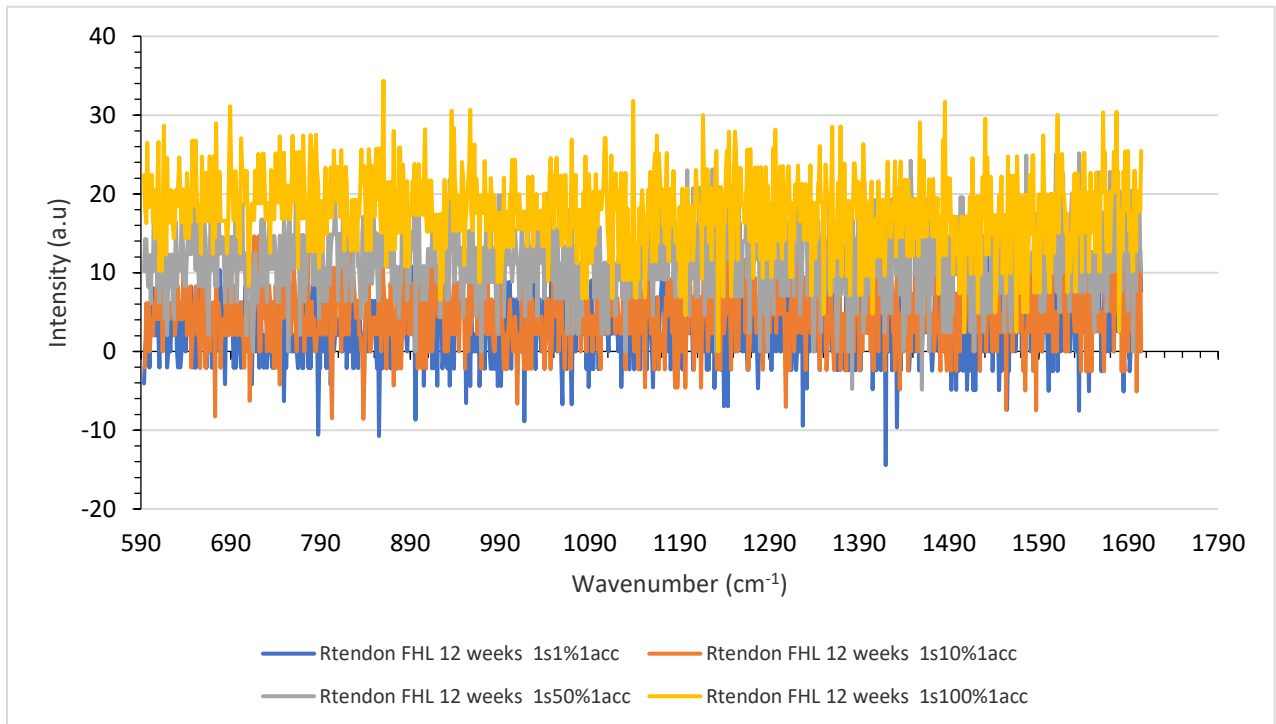
2 slaughtered turkeys from the age range of 12-15 weeks were acquired from a local farm (Lancashire, UK). Tendons were removed from left and right leg of each turkey with the aim to extract the main flexor tendons, *hallucis longus* and *digitorum longus*. A total of 7 tendons were removed successfully for this study (**Table 2**). Tendons were taken along the length of the leg and blunt dissected from the point of origin at the hip joint to the bifurcation point near the ankle. All extracted tendons were washed, wrapped in phosphate buffer saline (PBS) and stored, fresh frozen at -80°C . Freeze-thaw cycle were kept to a maximum of 5 to prevent damage to the microstructure of tendon (78).

3.2 Calibrations

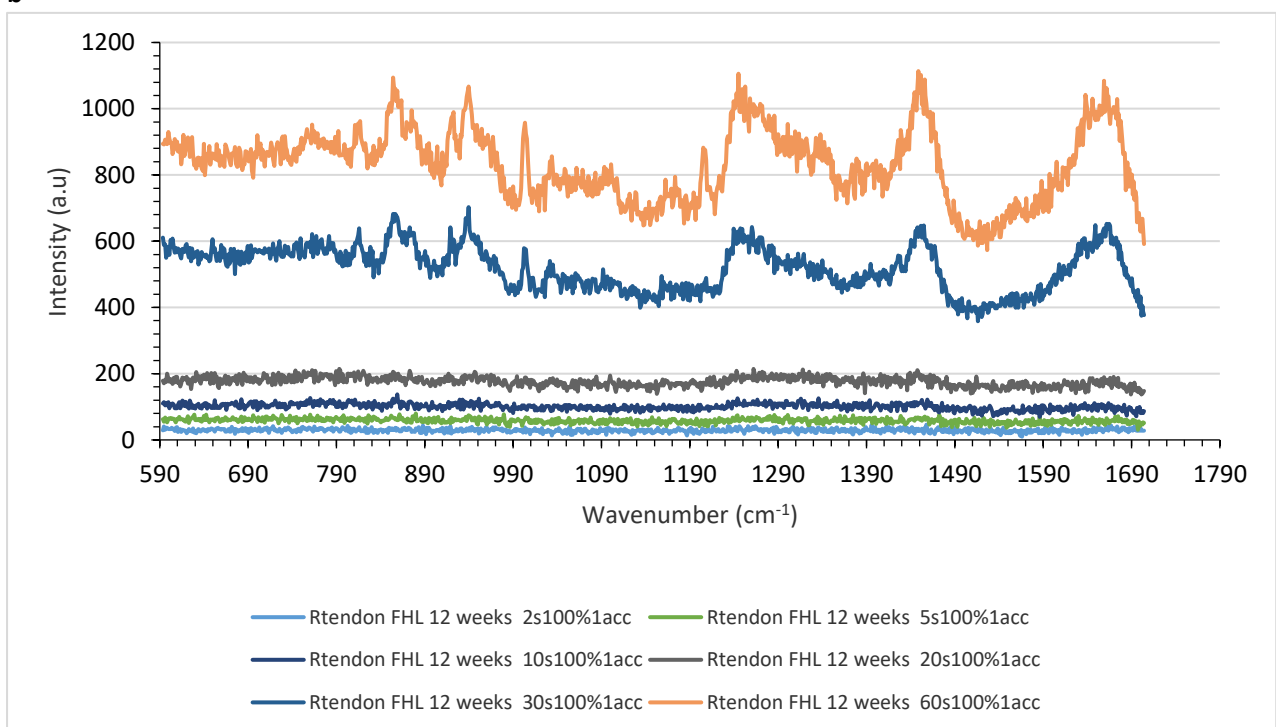
Prior to Raman spectral acquisition, tendons were thawed at room temperature (approx. 25°C). A Raman spectrometer (Renishaw plc, Gloucestershire, UK), 785 nm diode laser with a X50 long working distance objective was used to analyse tendons. Before use of the Raman instrument several daily checks were made ensuring the correct laser alignment and stabilisation of the laser for 30 mins. A silicon measurement was taken at 10% laser power with peak achieved at 520.5 cm^{-1} . Whenever there was a shift and a peak at 520.5 cm^{-1} was not achieved, a calibration offset was made. A further calibration was made measuring polystyrene under the microscope to identify the peaks in the biochemical fingerprint range. 2 large peaks at approximately 1001 cm^{-1} and 1031 cm^{-1} should be achieved indicative of the maximum height/intensity ratio. It was expected that intensity of the peak achieved at 1001 cm^{-1} was 4 times greater that of the intensity at 1031 cm^{-1} . Regardless there should always be a 30 cm^{-1} difference between the two peaks.

3.3 Optimisation

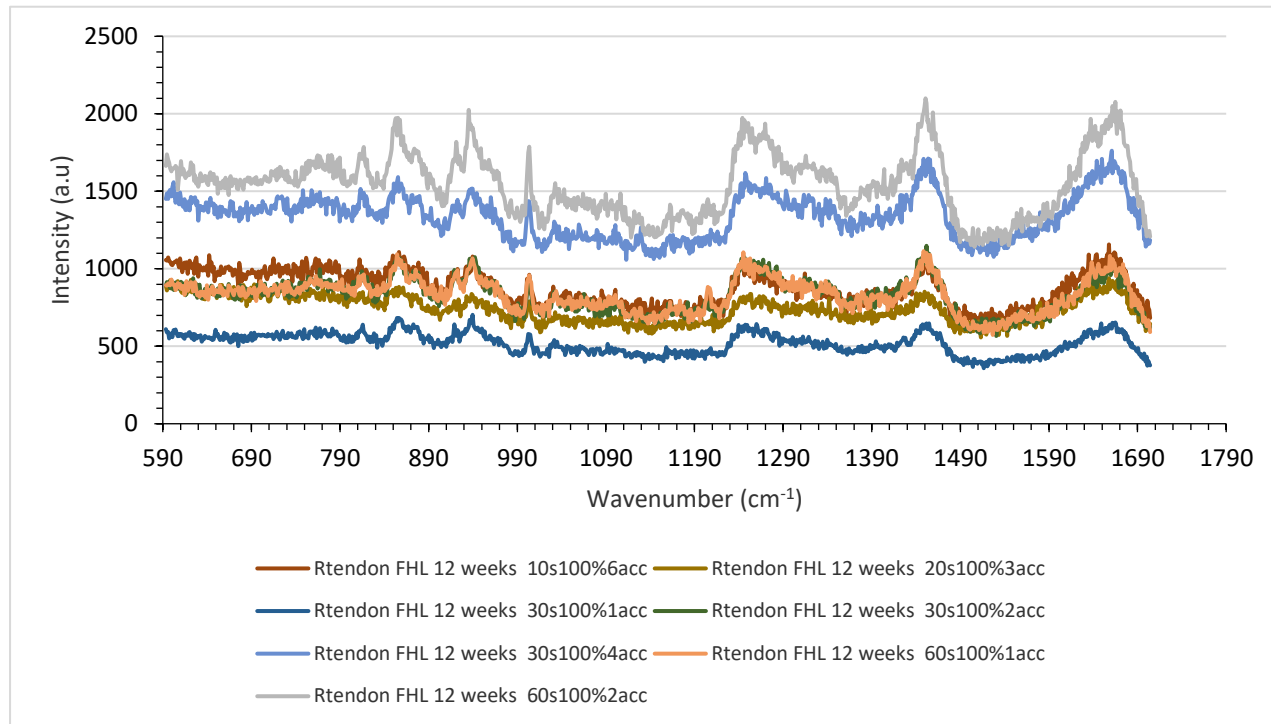
a



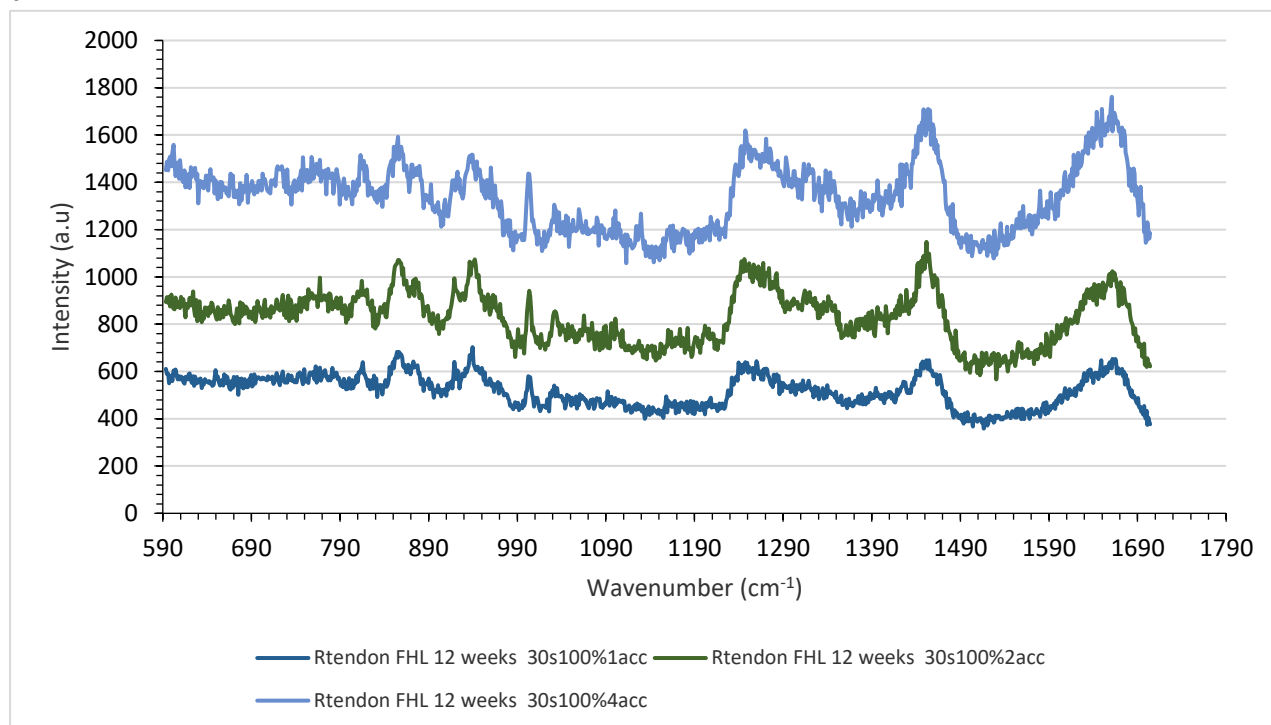
b



c



d



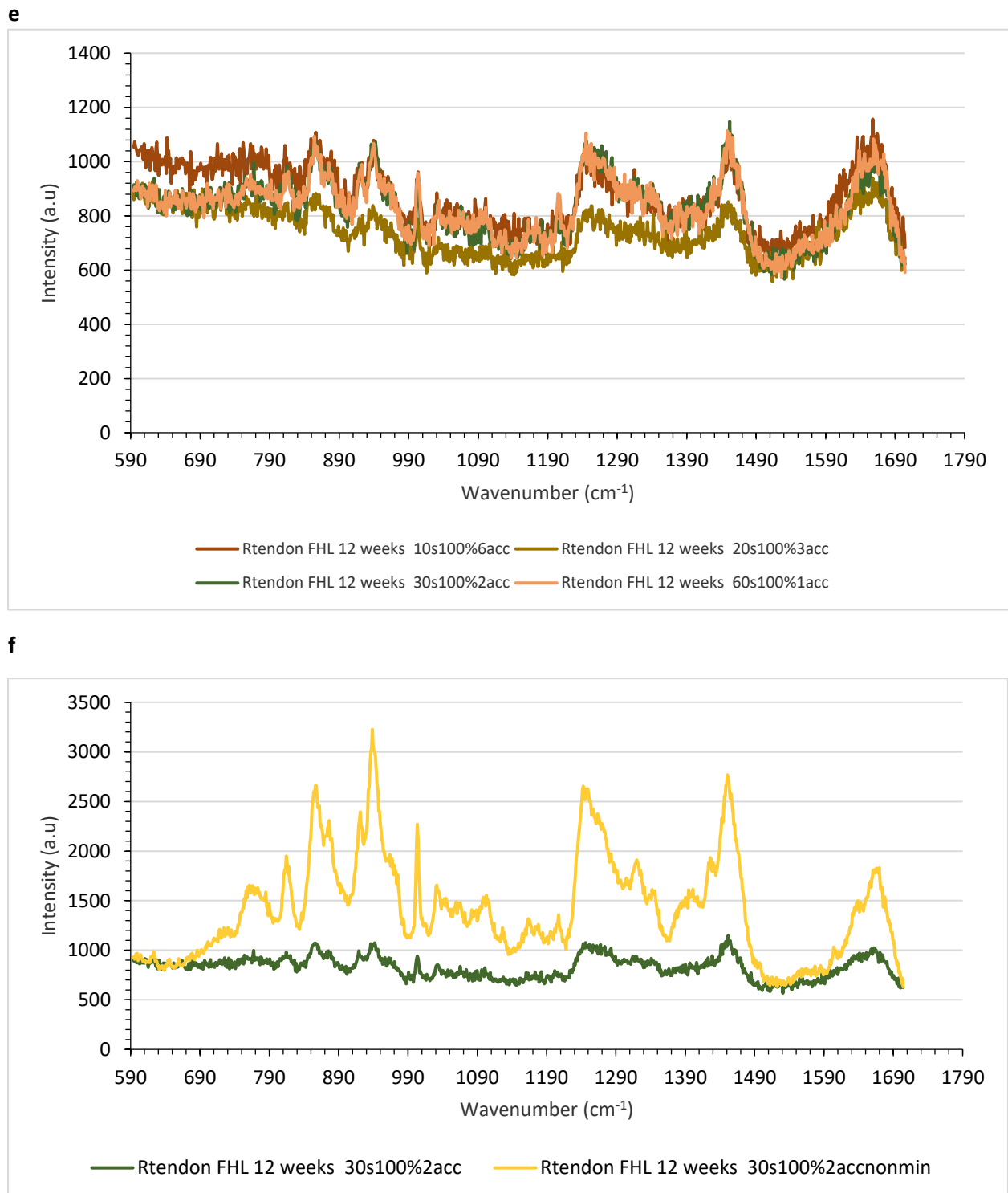


Figure 4: Raman spectra from sample turkey tendon (Right leg, 12 weeks, FHL) used to optimise Raman laser settings; time (s), power (%) and accumulation (acc), a) Initial optimisation – alteration of laser power alone b) Used max power (100%), same number of accumulations + alteration in the total time of each cycle c) Alteration to accumulation alone d) Comparison between the time with most consistent spectra e) Overall comparison between best spectra f) Comparison of spectra in mineralised and non-mineralised region.

Optimisation was used to produce the best spectra possible in under 3 mins (79). The different peaks from a mineralised and non-mineralised region were laid against each other in the same plot for

comparison following optimisation. Non-mineralised regions were defined as regions where a phosphate band ($959\text{-}962\text{ cm}^{-1}$) was absent. Mineralised regions were defined as regions with a phosphate band present ($959\text{-}962\text{ cm}^{-1}$). An initial phosphate peak appearing at start of this region distinguishing when a non-mineralised region transitioned to a mineralised region. Peaks corresponding to tendons (**Table 1: Chapter 1**) are easily identifiable. The settings; 2 accumulations, 30 seconds per accumulation, 100% laser power ($\sim 20\text{ mW}$) were used for all subsequent spectral acquisitions thereafter.

3.4 Data Collection

Data was collected from the tendons in the same orientation taking spectra from distal to proximal end. An origin was set 1 cm away from the bifurcation point (distal end) of the tendon. A range of time/accumulation/laser power settings were tested on a sample tendon to achieve an efficient data set. Data was therefore collected every 0.5 cm using settings above (**Figure 4f**) producing the clearest spectra and reduced background noise. During the process tendons were kept completely parallel to the laser and hydrated in PBS to prevent drying of the sample under the laser without compromising the data. A dataset of up to 70 spectra was recorded for each tendon depending on its length.

3.5 Schedule for experiments

Table 2: Schedule for experiments which were conducted on each tendon, bone and order of experiments. The number represents the type of experiment conduct. Experiments are listed below:

1. Initial Raman analysis; Pre-processing, Computational analysis
2. Mechanical Testing
3. Post-Mechanical Raman analysis; Pre-processing, Computational analysis
4. VG analysis
5. Demineralisation with EDTA
6. (Re)mineralisation with SBF
7. Post-SBF Raman analysis; Pre-processing, Computational analysis
8. Micro-CT analysis

Tendon	Type of tendon/bone	Age (weeks)	Experiments conducted
RFHL-12	<i>Flexor hallucis longus</i>	12	1, 2, 3, 6, 7, 8
LFHL-12	<i>Flexor hallucis longus</i>	12	1, 2, 3, 6, 7
RFHL-15	<i>Flexor hallucis longus</i>	15	1, 2, 3, 5, 6, 7
LFHL-15	<i>Flexor hallucis longus</i>	15	1, 2, 3, 5, 6, 7, 8
RFD-12	<i>Flexor hallucis longus</i>	12	1, 2, 3, 4
LFD-12	<i>Flexor Digitorium</i>	12	1, 2, 3, 4
RFD-15	<i>Flexor Digitorium</i>	15	1, 2, 3
LBone-12	<i>Tibia (Left)</i>	12	1, 2, 3
RBone-15	<i>Tibia (Right)</i>	15	1, 2, 3
LBone-12	<i>Tibia (Left)</i>	12	1, 2, 3
RBone-15	<i>Tibia (Right)</i>	15	1, 2, 3

3.6 Pre-processing

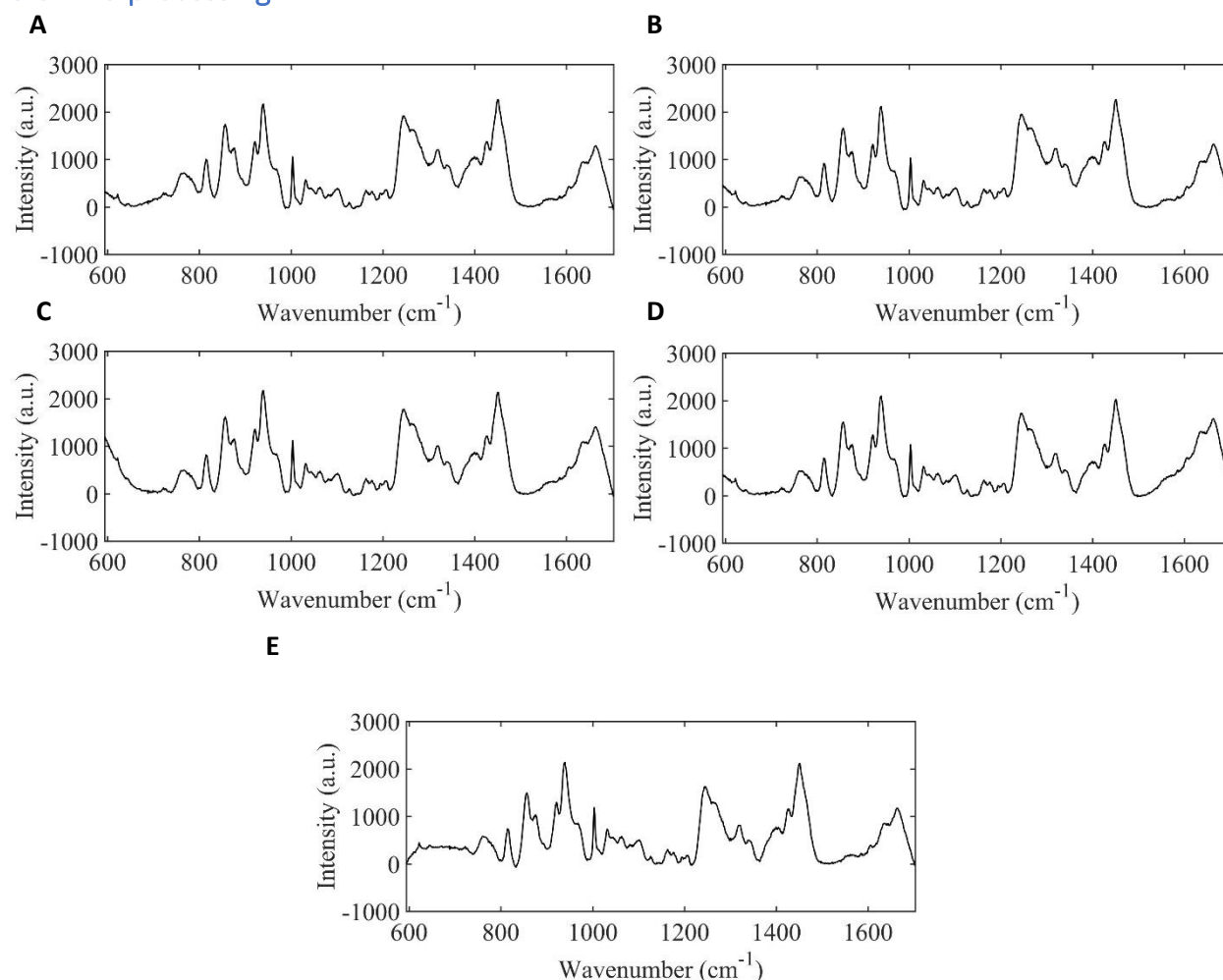


Figure 5: Comparisons between various polynomial fittings were applied for baseline correction during pre-processing of spectral data from tendon samples. Polynomial fits were applied at an order of magnitude ($^{\circ}$); A) $^{\circ}3$ B) $^{\circ}4$ C) $^{\circ}5$ D) $^{\circ}6$ E) $^{\circ}7$ displays the Raman spectra produced from the corresponding ($^{\circ}$).

Once spectra were acquired from tendon samples, data underwent a range of (supervised) pre-processing steps. All spectra underwent the same pre-processing. A range of comparisons were made to decide the degree of polynomial fitting used. The data were baseline corrected using a polynomial fitting to a magnitude order 7 ($^{\circ}7$) (**Figure 5E**) because this fitting created a natural baseline while retaining most of the important spectral features which are particularly lost at the lower and high wavenumber ends in $^{\circ}3$ - 6 (**Figure 5A-E**). Adding a polynomial fit remove any noise in the spectra due to fluorescence of sample while the baseline was corrected for any skewed baseline (80). Using this effectively maintains a natural Raman appearance (57). This was followed by normalisation of the data. Two approaches were tested: min-max and vector normalisation. Min-max normalisation was more appropriate and used to normalise the data with amide III as the maxima for normalisation. The maximum peak intensity was measured from 1240-48 cm^{-1} . This was done to scale the spectra and remove any inconsistencies in the data due to tendon thickness at different areas (mineralised regions would have a different consistency in comparison to non-mineralised regions). Amide III was used for this purpose due to stability of this peak and consistency in all spectra.

3.7 Computational analysis

Univariate analysis made comparisons between specific chemical components/groups within the region of interest in the biochemical cell fingerprint (approx. 500-1800 cm^{-1}). This included full-width half height (FWHH) calculations to assess the mineral crystallinity of mineral regions. A mixture of both univariate and multivariate techniques was employed. This was done to account for the consideration of statistical dependencies between wavenumbers where univariate analysis could not singlehandedly outperform multivariate analysis. Principal component analysis (PCA; using an in-house written Matlab script, MATLAB, The Math-Works, Inc.), a form of multivariate analysis was performed with the spectra classed according to the percentage along the length of the tendon from the distal end. This was compared with spectra classed according to age. All the data was captured within 10 principal components (PCs) with PC1 having the most variance followed by PC2 etc. A factor rotation was applied to force the data through maximum variance during orthogonal linear transformation which mathematically defines PCA (76). Scatter plots were produced to visualize the spread of the data and help analyse trends in the variance between groups and within groups. Loadings plots were subsequently used to characterise the chemical peaks within the spectra in order of their contribution to the variance seen in a particular PC axis. This was done in PC1 and PC2 because they contained data with the most variance. Following this, linear discriminant analysis (LDA) was considered and compared with PCA and PCA-LDA to see if there was any additional spectral information that could be identified.

3.8 Bone

Data was also collected from the tibia bone relative to the tendons taken from the turkey. These bones underwent the same preparation, pre-processing and Raman analysis as the tendons defined in (Table 2).

3.9 Mechanical Testing

A Zwick/Roell testing machine was used to test the mechanical integrity of the tendon in correspondence to the ISO 527 Determination of tensile properties standards (81). This enabled a crude measurement of the Young's/elastic modulus of the tendon. The tendon was loaded uniaxially following unloading displaying characteristic elastic hysteresis in a force/displacement graph. Hysteresis is the energy dissipation produced after several cycles of loading and subsequent unloading of tendon. All samples underwent 10 conditioning cycles immediately prior to the test cycle. Consistency was maintained by calculating the Young's modulus for each tendon only during the test cycle.

The Zwick machine used the TestXpert II software and initiated a self-test start up routine. A protocol was set up for tensile strength testing of the tendon. A 'Tensile testing with Conditioning cycles' template was opened via the test program/program series. This template allowed testing over several cycles with a pre-determined pre-load and percentage strain. The test type was selected for 'Plastic'. As the tendon is a biological sample and this machine is generally used for engineering materials, the 'plastic' test type was the closest matching template. After this the series layout and graph were checked ensuring a graph of force (N) against distance travelled (mm) was produced with all cycles displayed on a single graph. The data collected produced a series of stress-strain curves. A test tendon was loaded manually into the clamps of the Zwick machine (with proximal end at the top clamp and distal at the bottom). Blue roll was sufficient enough to provide friction and prevent slippage at both proximal and distal ends of the tendon. It was wrapped in small amounts around the tendon before clamping the tendon securely in the Zwick machine.

Following this several test parameters were set. This included parameter settings for test definition, start position, the test phase up to pre-load, specimen data, conditioning cycles, test phase and end of test, results. The test was already defined as a 'tensile' test by the template chosen prior. The speed the crosshead travelled to the starting position was set to 200 mm/min. This was the value at which the test begins after reaching pre-load value in addition to the speed at which the crosshead travelled to pre-load value. A pre-load of 1N was set at a pre-load speed of 50 mm/min with 60 s to reach pre-load. No holding time in pre-load was set therefore immediately pre-load was reached test could begin. The specimen shape and cross-section were inputted as 'round' shape specimen, with a specimen diameter (estimated with a ruler). On average, this was 2 mm for the tendon but should be measured and inputted prior to testing. The test length was determined by the length of the corresponding tendon. This was measured before and after the cycles of uniaxial loading with the Zwick machine and was used to see the effect mechanical testing had on the length of each tendon.

Within conditioning phases, the tendons were loaded with a 5% strain per cycle and a speed of 1 mm/s. The testing phase would run a simple test cycle with the same parameters as the conditioning phase. A displacement is applied to the crosshead of the mechanical tester at a constant rate so that it increases monotonically. The corresponding strain results in a proportional, albeit, nonlinear stress which is manifested as a force registered by the force transducers. As the displacement is increased monotonically, so the force increases. However, as the displacement and corresponding strain increases beyond a point where the tendon begins to fail, the rate of increase of force decreases until the force reaches a maximum and starts to decline with continuing increasing strain. This maximum force is indeed the maximum force registered during the test and denoted F_{max} . At the end of the test, the break investigation ran decreasing the maximum force by 30 % and prevented the tendon from breaking. It was important to stand clear of the machine when testing any specimen. This protocol was loaded up for testing of all tendons.

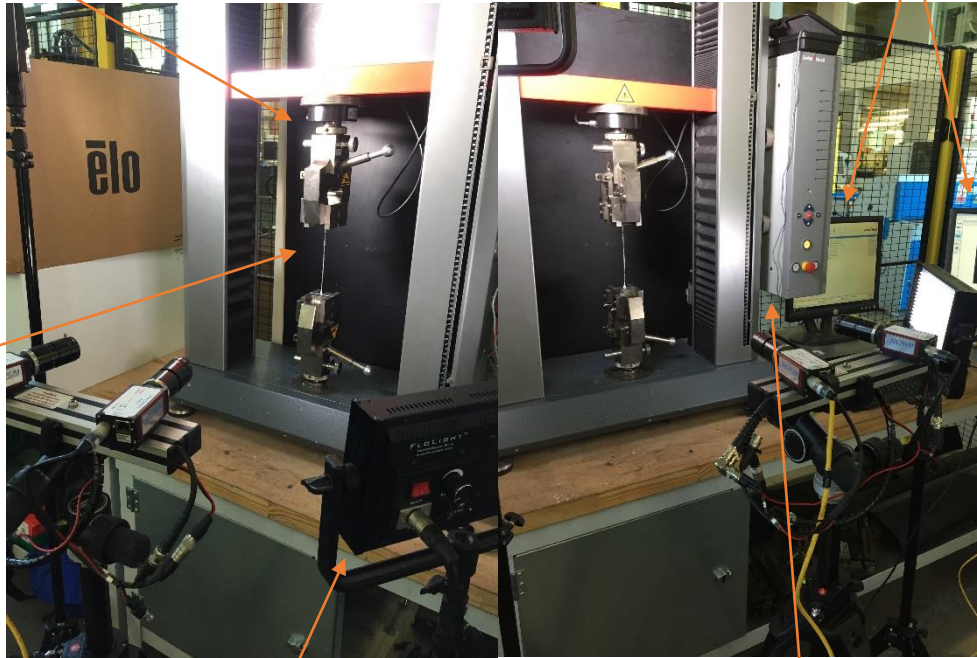
The mechanical tester registered displacement of the crosshead and the force acting on the force transducers at each time step. All other aspects, i.e. stress, strain, strength etc. are calculated from these values. Data was acquired at the sampling rate of 50 samples a second. The results from uniaxial loading were collated in a table including elastic modulus, strain at elastic modulus, strain at maximum stress, coefficient of determination, and length pre- and post-mechanical testing (**Table 4: Section 4**). After mechanical testing, tendons underwent Raman analysis thus examination of the chemistry of the tendons post mechanical testing. Regions were defined in the same manner as there were before mechanical testing.

3.10 Video gauge derived strain measurement using Imetrum imaging

Gauge with 1N
preload

Data acquisition
system

Tendon (sample)



Lighting
equipment

Zwick mechanical
tester

Figure 6: Experimental set-up for Imetrum imaging using VG system with tendon sample positioned within Zwick mechanical tester.

A non-contact optical technique including a video extensometer gauge, VG (Imetrum, Bristol, UK) was used to capture the behaviour of the tendon applied in uniaxial tension and planar shear test format. The tendon surface was marked in a recognisable dotted pattern using a black semi-permanent marker to gauge the area of interest and detectable by the VG system. The system captured multiple strain measures (multiple regions of interest up to 100 points) from the surface of the sample during testing. The results reported in this study were confined to 2-D measures of surface displacement in plane and were acquired using a single camera focused on the sample surface with an illuminated background from lighting equipment during testing (**Figure 6**). The VG image analysis system uses state of the art Digital Image Correlation technology (63), commonly used to provide an optical measurement (82).

3.11 Analysis of Mechanical Testing (Zwick mechanical tester)

All data collected from mechanical testing was analysed and imported into Python (in house code, Python; Enthought Canopy USA). For analysis of data any true stress in tendon was converted to engineering stress which assumed the area of the tendon remained constant. The purpose of this was to allow consistency when the elastic modulus was extracted from each tendon data. The integral of the stress with respect to strain provided the energy dissipation during tendon loading and unloading under the conditioning cycles. Upper and lower limits for strain were identified from the force registered by the force transducers. A straight line was fitted to these limits which provided the gradient of the data therefore the elastic modulus could be extracted. Following this the co-variance of the fit was calculated in the form of standard error using a student t-test. This provided the confidence intervals for each data set. The co-efficient of determination was subsequently used as a final justification to see how close the straight-line approximation matched the line of best fit.

3.12 Analysis using Imetrum (optical imaging)

All data collected from the Imetrum optical imaging was analysed using a real-time excel spreadsheet derivation (in-house code). This was based on 3 principles which included difference between the start and the end time (duration) of the uniaxial loading of the tendon unveiling a new measurement defined as real-time measurement and the number of points which was desired during this duration (100 points). Subsequently a line of best fit was plotted to the hyperplastic behaviour at these points and displayed a highly accurate representation of the stress-strain activity at these specific points in the tendon.

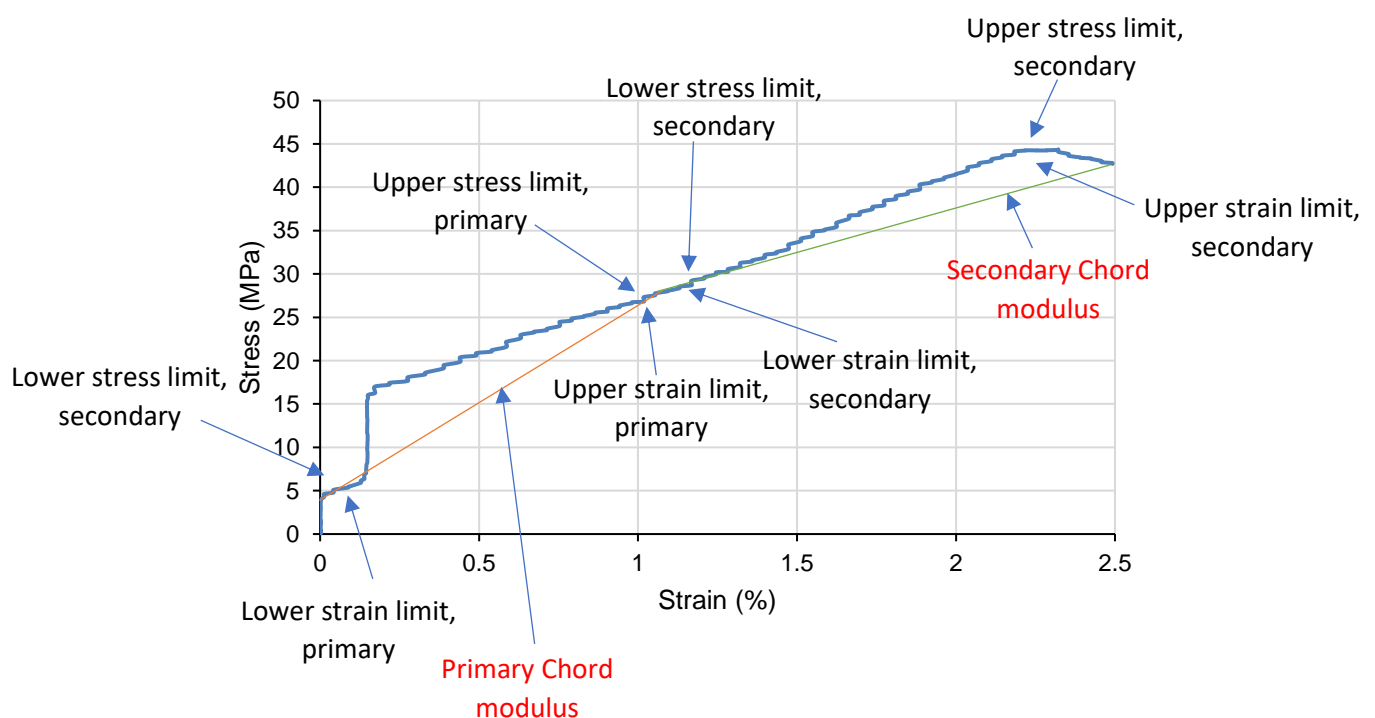


Figure 7: Example of uniaxial tensile stress-strain graph for tendon sample in real-time

The hyperelasticity model can be composed as a function of strain energy based on either principal stretches (λ) or invariants (I) of the strain tensor. Invariants can be written as a function of principal

e.g. $I_1 = \lambda^2_1$. The two are interchangeable with a different hyperelasticity models using either one (83) (84).

The common component is that strain is directly proportional to the sample's stress strain response depending on a series of constant parameters within the material. To use a hyperelastic model, the constants must be calculated through curve fitting to the stress-strain data obtained from the experimental data (**Figure 7**). The amount of energy stored in the hyperelastic material; W , at a specific strain point within the tendon is a function of three strain invariants from the Green deformation tensor defined as I_1 , I_2 and I_3 thus $W = W(I_1, I_2, I_3)$ (82).

An excel spreadsheet (in-house code) derived by M. Milad using a combination of the main constraints of a hyperelastic model and a new defined real-time measurement to produce real-time measurement of stress-strain which corresponds to the tendon as it is stretched therefore obtaining a real-time curve fitting of the uniaxial loading (**Figure 8**) (82).

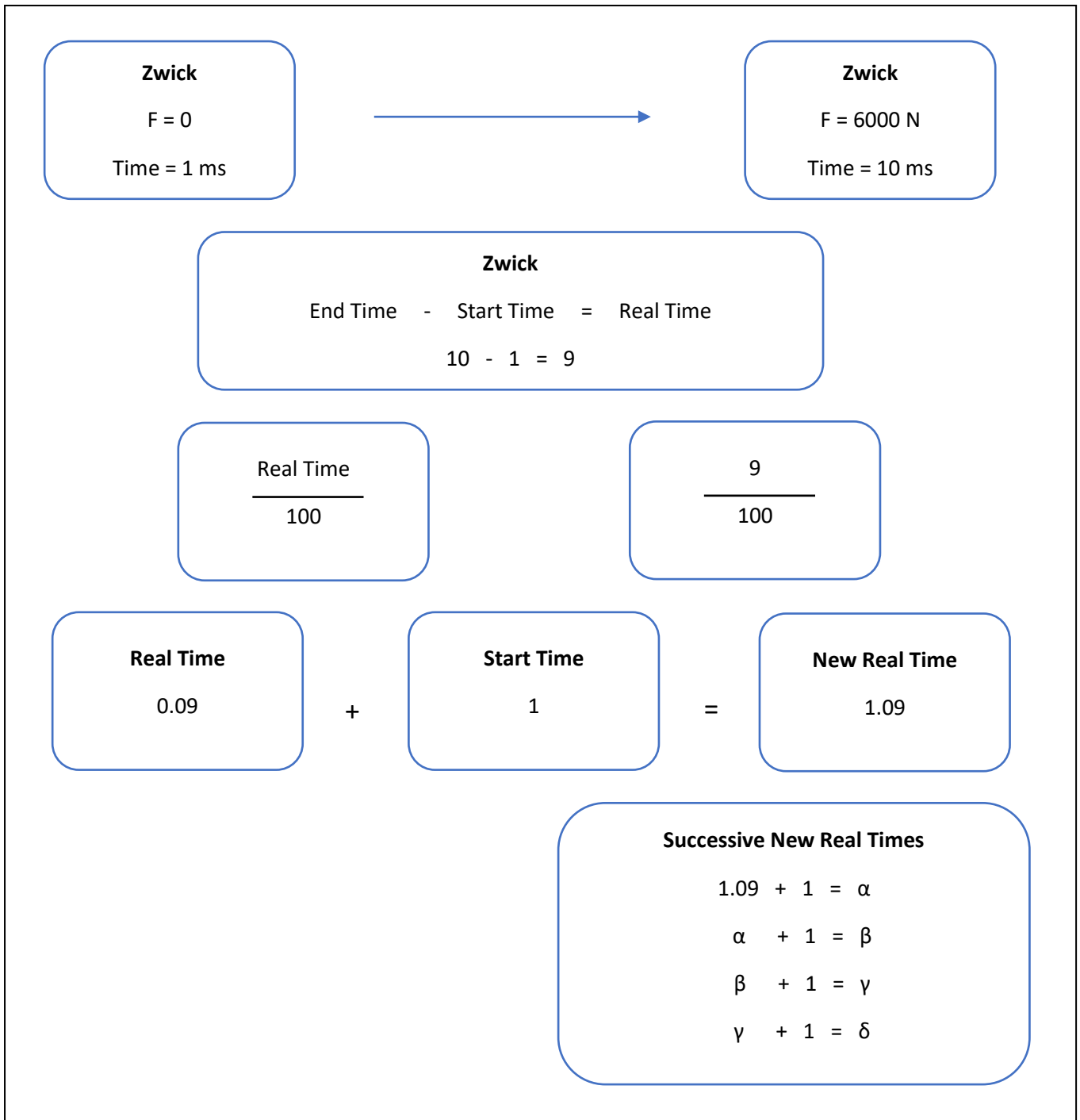


Figure 8: Diagrammatic representation of code written by M. Milad incorporating the delay between Zwick and the Imetrum to produce a real-time measurement. The new defined real-time measurement is combined with the hyperelastic model to produce a stress-strain which corresponds to real-time curve fitting of the uniaxial loading of the tendon. α , β , γ , δ represent subsequent new real time measurements.

The Imetrum imaging system (**Figure 6**) is started after the Zwick mechanical tester because there is a delay between the first stress-strain point and a visual image detected by the video gauge, this needs to be accounted for. This delay is usually few seconds and produces ‘invalid’ data set. The excel

spreadsheet in-house code adopts a new measurement in real-time. For the newly defined time, a set number of points can be determined to calculate a range of stress-strain values within this time. Choosing 100 points, this would be done by dividing real time by the number of points there are producing 100 new points of real-time measurement between at given start and end time (**Figure 8**). The resulting stress strain points are taken from a region of smooth increase rather than a fluctuation of stress-strain. A range of suitable methods can then be used to take the elastic modulus upon mechanical testing on TLT.

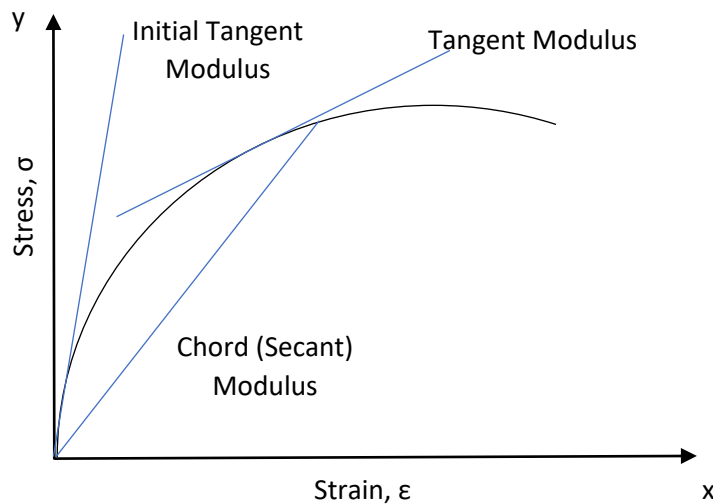


Figure 9: Types of modulus of elasticity in the stress-strain curve

There are 3 different ways to calculate the modulus from a stress-strain curve (**Figure 9**). The tangent modulus is used to work out the modulus at any specified stress/strain point. When a tangent is taken from a linear elastic region this is also known as Young's modulus, thus the initial tangent modulus taken from the initial linear elastic region of the stress-strain graph. This is defined by Hooke's law (85). The chord (secant) provides the modulus constructed from a range of stress-strain points (from a start and end-point) and can be used to work out the modulus at maximum stress intensity (86). It is also possible to calculate a primary and secondary modulus depending on whether the modulus before and/or after the linear region in the curve is required (**Figure 7**).

3.13 Finite Element Analysis - FEA

Finite Element Analysis - FEA was used to model the tendon as a structure with distributed elastic properties along the length of tendon. Different strain distributions were compared to determine the trend seen if the modulus was constant, varied linearly or exponentially along the length of tendon due to variations in the level of mineralisation.

3.14 Remineralisation of tendons in simulating body fluid (SBF)

Table 3: Schedule for data collection of chemical analysis for tendons during incubation in SBF using Raman. All tendons were incubated on the same start day and removed from solution by day 14.

Tendon	Chemical analysis (Raman)
LFHL-12	Day: 1, 6, 10, 14
RFHL-12	Day: 3, 7, 13
LFHL-15	Day: 1, 6, 10, 14
RFHL-15	Day: 3, 7, 13

FHL tendons underwent a demineralisation and remineralisation process to access the *in vivo* bioactivity of the mineral (87). This was done by incubating tendons using SBF over a period of 2 wks in a staggering treatment in the manner shown here (**Table 3**). The young tendons (12 wks) were incubated in SBF while the old tendons (15 wks) were first demineralised (10% EDTA pH 7.5) to remove the current mineral, then incubated in SBF to drive mineral formation via remineralisation.

The following reagents were used to make SBF:

- [1] sodium chloride, NaCl (8.035g) [Sigma Aldrich]
- [2] sodium hydrogen carbonate, NaHCO₃ (0.355g) [Sigma Aldrich]
- [3] potassium chloride, KCl (0.225g) [Sigma Aldrich]
- [4] di-potassium hydrogen phosphate trihydrate, K₂HPO₄ (0.231g) [Fisher Scientific]
- [5] magnesium chloride hexahydrate, MgCl₂.6H₂O (0.311g) [Sigma Aldrich]
- [6] hydrochloric acid, 1M-HCl (39 ml) [Sigma Aldrich]
- [7] calcium chloride, CaCl₂ (0.292g) [Sigma Aldrich]
- [8] sodium sulphate, Na₂SO₄ (0.072g) [Sigma Aldrich]
- [9] Tris-hydroxymethyl aminomethane, (HOCH₂)₃CNH₂ (6.118g) [Sigma Aldrich]

SBF was prepared from powder reagent grade chemicals except for hydrochloric acid (HCl) which was in liquid form. 1000 ml of SBF was prepared by dissolving each reagent fully (before addition of the subsequent reagent) in 700 ml of ion-exchanged and distilled water in the order; [1-8] (87). Solution was made in a clear plastic beaker using a magnetic stirrer, water bath and a heat plate to maintain the temperature at 36.5 ± 0.5 °C and adjust pH. Hygroscopic reagents [1]-[6] were added in the shortest period possible to minimise exposure to air. Prior to the addition of [9] (HOCH₂)₃CNH₂, if solution was less than 900 ml it was made up to this mark using ion-exchanged and distilled water while the pH was measured at 2.0 ± 1.0 °C. [9] was added in small quantities and alternated with a further 2.5 ml of 1.0 M HCl until all (HOCH₂)₃CNH₂ had dissolved in solution adjusting pH cyclically to arrive at the conditions pH 7.40 at 36.5 °C. Solution was made up to a final 1000 ml and cooled to room temperature (25 °C) assuming that rate of solution temperature decrease (approx. 0.1 °C/min) of the SBF solution will have a pH of 7.42 ± 0.01 (87).

SBF solution was stored in clear plastic bottle with tight lid and kept between 5-10 °C to be used within 30 days. Tendons were incubated in an air-tight zipper eco-friendly plastic bag at 36.5 °C with SBF, making sure each tendon was fully immersed in solution with no bends in the tendons. Raman spectra were collected from tendons in a staggered manner (**Table 3**) and analysed in the format used for previous experiments (**Section 2**). Data was collected this way due to the length of examination of each tendon making it only possible to examine no more than 2 tendons daily. Thus, for consistency

on a particular day both 12 wks and 15 wks of the same side was compared. Solution was changed every 4-6 days with tendon measured at half-way mark (1 wk) to measure progress.

3.14 Micro-computed tomographic (micro-CT) imaging

Tendons were scanned under a micro-CT using an aluminium filter at 8 μm resolution, 50 kV, 181 μA after incubation in SBF. The micro-CT visualised the differences structurally from changes to the tendon chemistry. Prior to scanning tendons were cut to approximately 8 cm per piece and positioned in a 15 ml falcon tube with no contrasting agents. The falcon tube fitted adequately into the micro-CT. Polystyrene in addition to small amount of blue roll soaked in PBS in the falcon tube was used to prevent tendon samples from drying out. The polystyrene also helped to position the tendons up right from furthest distal end to furthest proximal end and would not be detected by the micro-CT. Micro-CT imaging was used to make surface rendered 3D models and reconstructed cross-sections of regions along the length of the tendon with CTvox software (SkySan 1275, Bruker, Belgium). This differentiated mineral from non-mineral regions. It also showed the density of the tissue indicative of the organisation of the collagen within tendon at these regions. After this no further testing took place on tendons.

4 Results

4.1 Initial Raman analysis of tendons

The aim of this chapter was to identify the stages of mineralisation process & associated Raman spectral signatures using the TLT as a model. Initially Raman analysis was conducted on the tendons to identify their inherent structural chemistry. Tendons were then subjected to uniaxial loading, imitating the tendons' physical capacity under strain. This was a test of their strength. Literature has shown pushing the tendons to the limits of their physical capacity can reveal a detail of information on potential problems which may arise during ageing of the tendon (38). The results emphasize the importance of Raman analysis for detecting changes in the underlying chemistry of the tendon which may affect its structural integrity.

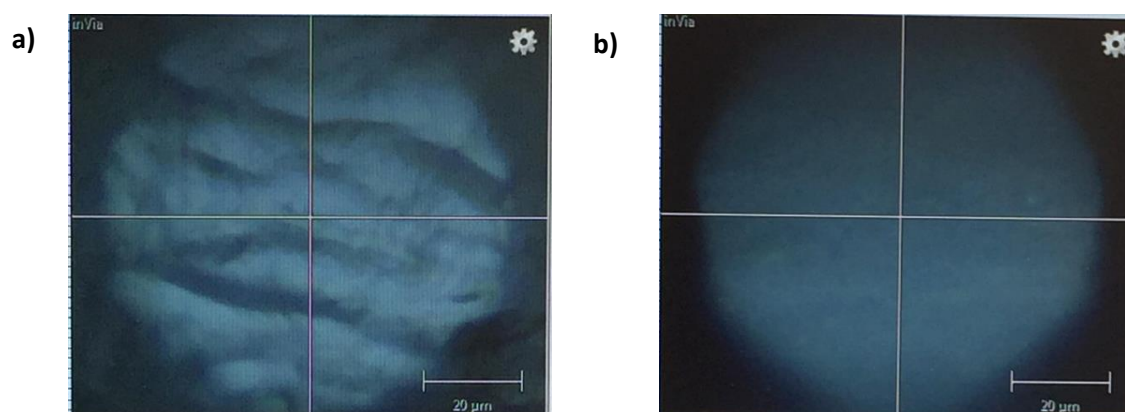


Figure 10: Non-mineralised region vs mineralised region under microscope lens. In a) the non-mineral region the detail of the collagen can be seen on the surface. Under the microscope strands of regular arrangement and almost a successive linear pattern of collagen fibrils is visible compared to b) mineral region where there is high fluorescence and the mineral is uniform over the underlying collagen structure.

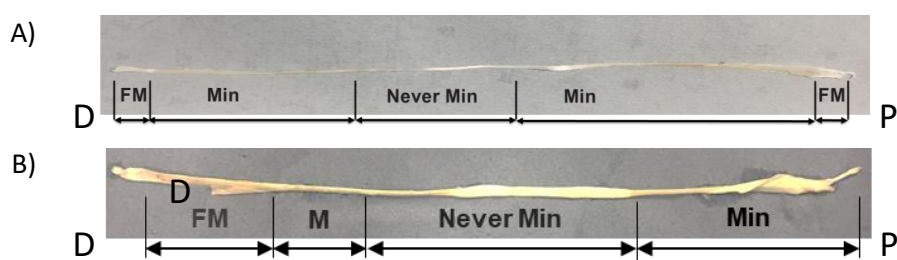


Figure 11: Diagrammatic representation mapping difference chemical regions in flexor hallucis longus tendon: A) 15 wks – right tendon and B) 15 wks – left tendon (Min = Mineralised, FM = Future Mineralised). D = distal end, P = proximal end.

Chemical regions were determined as displayed in the (Figure 11). The origin was set as 1 cm away from the bifurcation point (distal end) and the first region was defined as non-mineralised tissue due to the absence of phosphate peak ($959-62\text{ cm}^{-1}$). Data was collected every 0.5 cm along the length of the tendon during the initial Raman analysis and after mechanical testing. Tendons transitioned from non-mineralised tissue to mineralised tissue by the onset of a sharp phosphate peak ($959-62\text{ cm}^{-1}$) indicative of mineral (Figure 11).

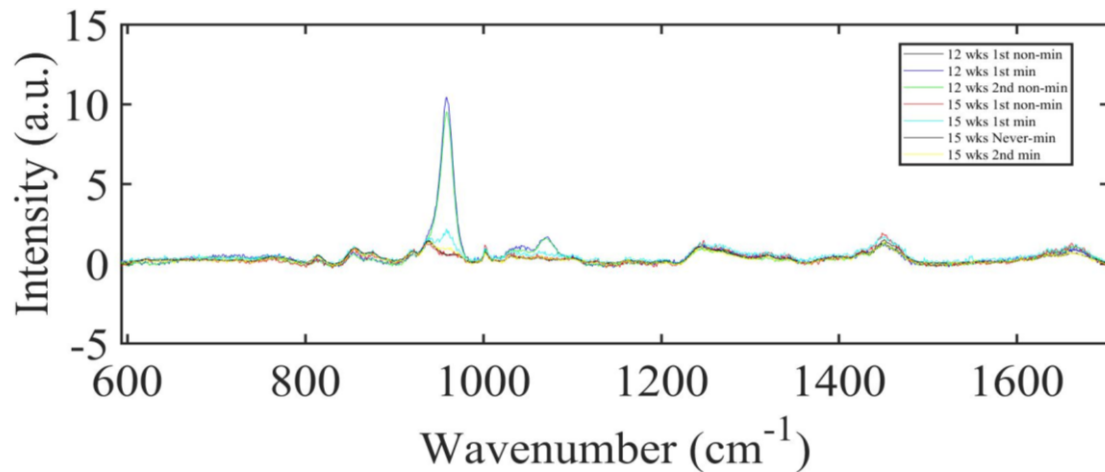


Figure 12: Example of spectra from Raman including mineralised and non-mineralised regions from young (12 wks) and old (15 wks) flexor tendon.

In regions with greater levels of mineralisation the peak is larger and narrower particularly seen in first mineral region of young tendon and second mineral region of old tendon. Other peaks which are identifiable in the TLT above are as shown in **Table 1; Chapter 1** with expected chemical components in TLT.

4.1.1 General Differences: Young vs Old

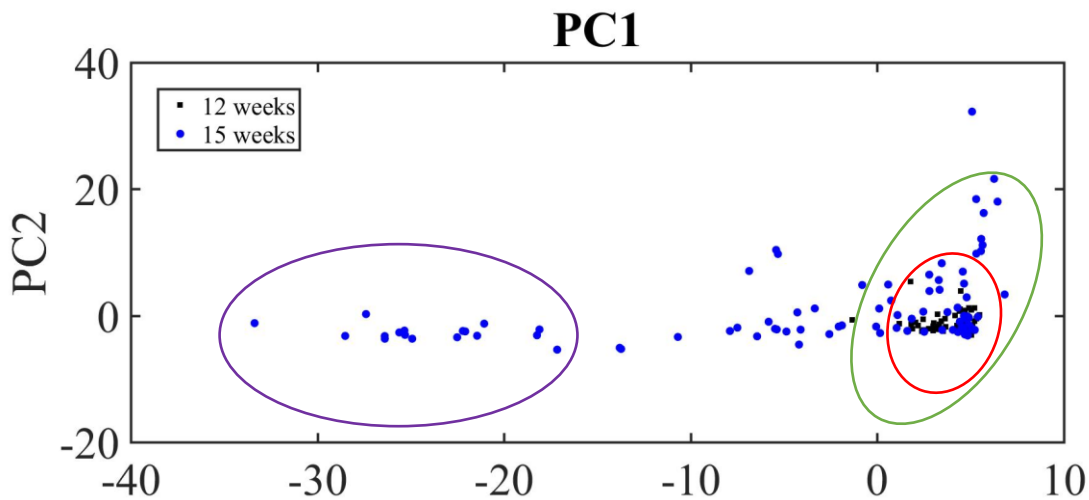


Figure 13: PCA plot visualising the distribution of the data from “12 week” young vs “15 week” old tendons. Red circle encompasses cluster of spectra from young tendons which are spectrally similar. Purple circle encompasses high intraclass variation within spectra of the old tendons. Purple compared to green circle reveals interclass variation between old and young tendon thus spectrally different.

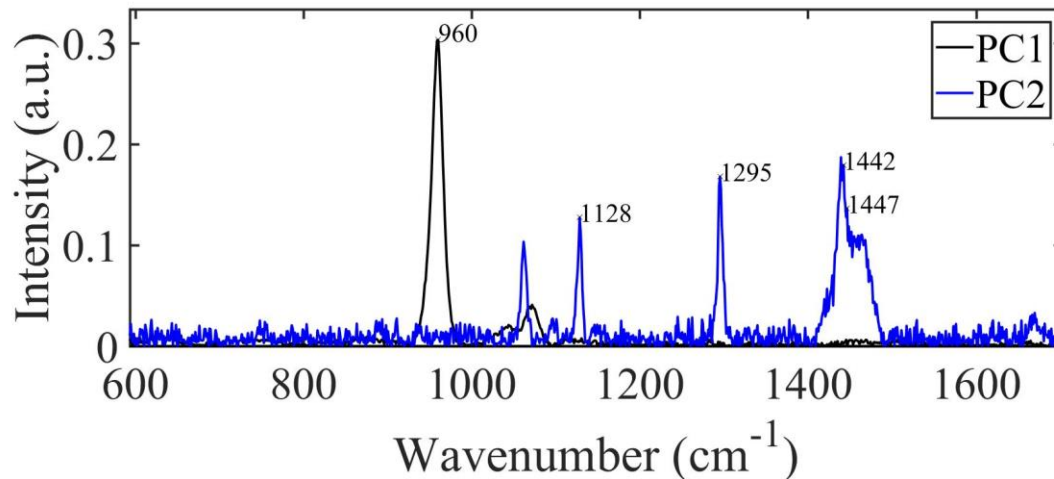


Figure 14: PCA loadings plot of the contributing factors to the distribution of the spectra relative to PC1 and PC2 from the young and old tendons before tendons were tested mechanically.

Initially comparisons were made between 2 major types of flexor tendons: FD and FHL irrespective of whether they were right or left tendons. The distribution of the spectra along PC1 correlated the data according to the greatest variance. The most contributing factor to this difference was the 960 cm⁻¹ V₁ PO₄³⁻ peak (**Table 1**). This was indicative of the level of mineralisation because mineral phosphate is the main component of the hydroxyapatite crystals which form during mineralisation. High mineral was confirmed in old tendons compared to the young tendons (**Figure 16i**) therefore the interclass variation seen between young and old tendon. The old tendons acquired most of the spread in this axis also presenting the greatest intraclass variation while most young tendons spectra were clustered in one area (**Figure 13**). The most contributing factors to the difference visualised along PC2 were structural protein features; 1442-1447 cm⁻¹; CH₂ collagen assignment, 1295 cm⁻¹; CH₂ deformation and 1128 cm⁻¹ related to C-N stretching in the tissue (66). This suggests features related to the collagen of the tendon (**Figure 14**). PC2 revealed intraclass variation between both young and old tendons which confirmed differences in the mineral alongside the collagen components of the tissue. There was also some overlap indicating similarities in the chemical properties of the mineral and collagen in both age groups. (**Figure 13**).

4.1.2 Differences in mineralisation between young & old

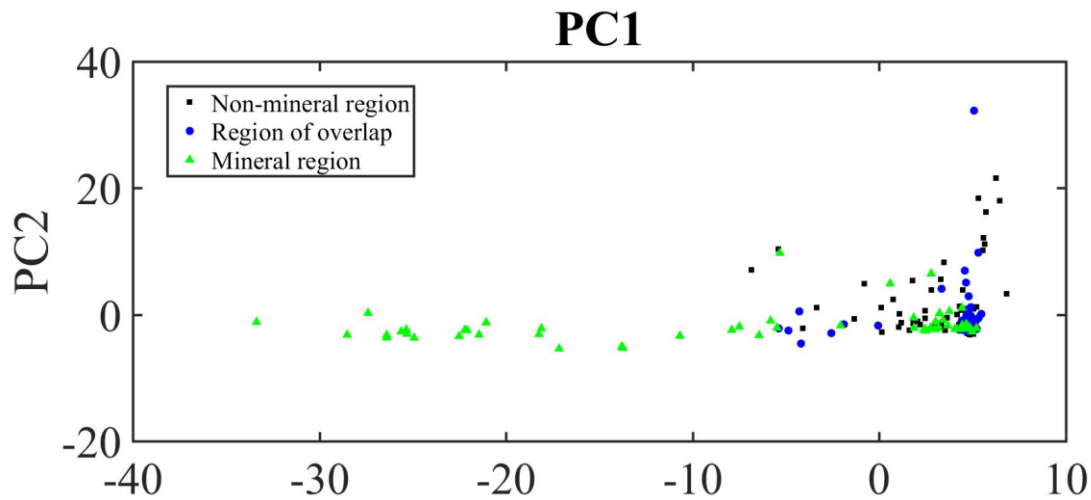


Figure 15: PCA plot showing the distribution of the level of mineralisation according to the 3 types of regions possible in tendons irrespective of age.

Simple analysis techniques lead to objectively mapping the changes along the length of the tendon with the differences seen between age groups. These revealed differences in the level of mineralization were caused by multiple mineral regions effectively making it possible to split the tendons up into 3 regions (**Figure 15**). This included a mineral region, a non-mineral region and a region of overlap containing both mineral and non-mineral components. This also enabled different ratio intensities to be compared from previously defined chemical parameters (**Table 1**) which are known in the literature to contribute to properties present in tendon (50). These are the amide III: phosphate, amide III: amide I, carbonate: phosphate and proline: hydroxyproline comparison ratios. Previous literature has revealed no significant difference between types of tendon FD and FHL (42). For this reason, it was only necessary to compare one group of flexor tendons. FHL was slightly advantageous being the longer tendon therefore the magnitude of the trend that would occur post-mechanical testing was enhanced providing easier comparison between age groups

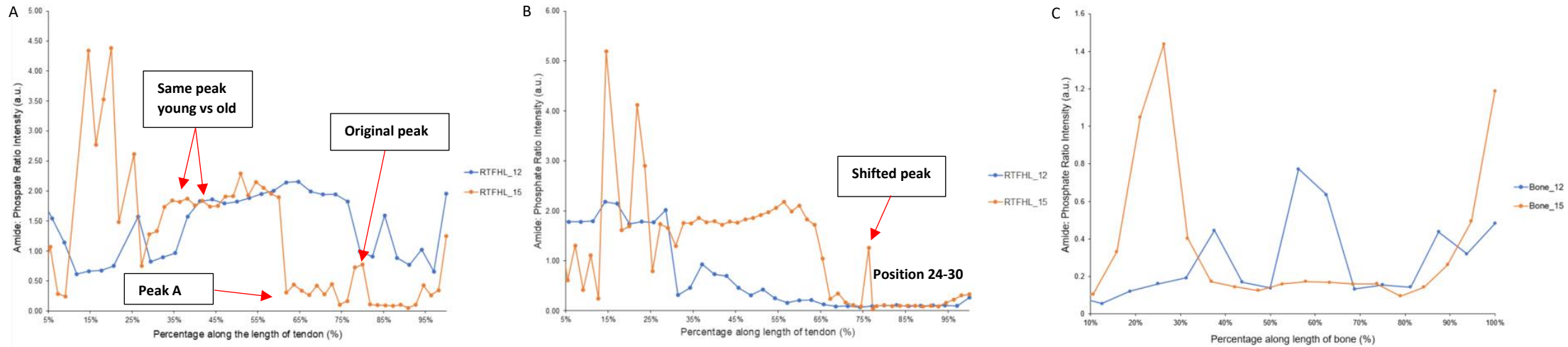


Figure 16i: Collagen analysis: Amide III: Phosphate ratio intensity showing the level of mineralisation as a percentage from the distal end before mechanical testing in tendon (A), after mechanical testing in tendon (B) and in untreated tibia (bone) relative to tendon extracted (C). Analysis of mineral per collagen area was determined spectroscopically using Raman by the appearance of chemical bands measured from the maximum peak intensity of amide III ($1240-48\text{ cm}^{-1}$) and phosphate ($955-60\text{ cm}^{-1}$) at various positions along the length of the tendon. Young tendon (RTFHL-12) was compared with old tendon (RTFHL-15) to see how this chemical property changed with age.

The results for both left and right tendon comparisons for each group were very similar. For this reason, it was only necessary to compare tendon from one side as you would expect the same characteristics from left and right tendon since both were acquired from the same turkey.

4.1.3 Amide III: Phosphate

Pre- and post-mechanical testing, the graph comparing the amide III: phosphate (amide: phosphate) ratio particularly in the old tendon (**A; RFHL-15 - Figure 16i**) possesses a similar shape up to 60% along the length of the tendon. This suggests that there were minimal changes to the mineral content after uniaxial loading of the tendons. The major difference was seen further proximally along the length of the tendon after 60%. From this point onward until the proximal end of the tendon the amide: phosphate ratio plateaued with one peak at 76% along the length post-mechanically. Although the amide: phosphate generally plateaued both pre- and post-mechanical, in pre-mechanical there were still several regions where this region increased fluctuating more compared to post-mechanical. Looking closely at the graph it seems that the peak at 76% along the length of the tendon post-mechanically had been shifted from a position of around 79% along the length of the tendon (**A & B; RFHL-15 - Figure 16i**). This peak is also narrower suggesting partial displacement of the mineral post-mechanical testing to acquire a greater percentage of the region closer to the proximal end of the tendon. The young tendon follows a similar shape as the old tendon but regions of peak amide: phosphate shifted more proximally for example the peak at 33% along the tendon in FHL-15; old is at 38% along the length of the tendon in FHL-12; young. Overall the region closest to the distal end has higher amide: phosphate in the old tendon compared to the young tendon. The reverse trend is seen in the proximal end with amide: phosphate ratio being higher in the young tendon. A large proportion of the young tendon displays an amide: phosphate ratio between 1 and 2 which indicates a large proportion of this tendon having low or no mineral content. Post-mechanical shows a different outcome with much of the young tendon displaying a ratio which would be suggestive of mineralised tissue. This is because much of the tendon at this age remains non-mineralised before mechanical testing. Points along the tendon which displayed low mineral contain newly formed or immature mineral revealing regions that will become mineralised with increasing age. After mechanical testing it was clear there was a change to the collagen structural arrangement that would have caused a decrease in the amide III thus altering the amide: phosphate intensity ratio overall producing one that was suggestive of increased mineralisation.

The higher the amide: phosphate ratio intensity, the lower the mineral and the lower the collagen organisation so it would seem towards the proximal and distal end there is greater mineral than the central regions of the tendon. This is expected (according to literature) (35). Amide III: phosphate ratio is essentially an indication of the mineral to matrix dynamic (67). This depicts the level of mineralisation with a low ratio of amide III: phosphate being equivalent greater mineral per collagen unit. Compared to the related bone these tendons were taken from the change in intensity ratios was more gradual moving proximally (**C - Figure 16i**). There were also distinct regions of high amide: phosphate ratios in the tendon with young showing an opposite trend to old tendon (**A & B- Figure 16i**).

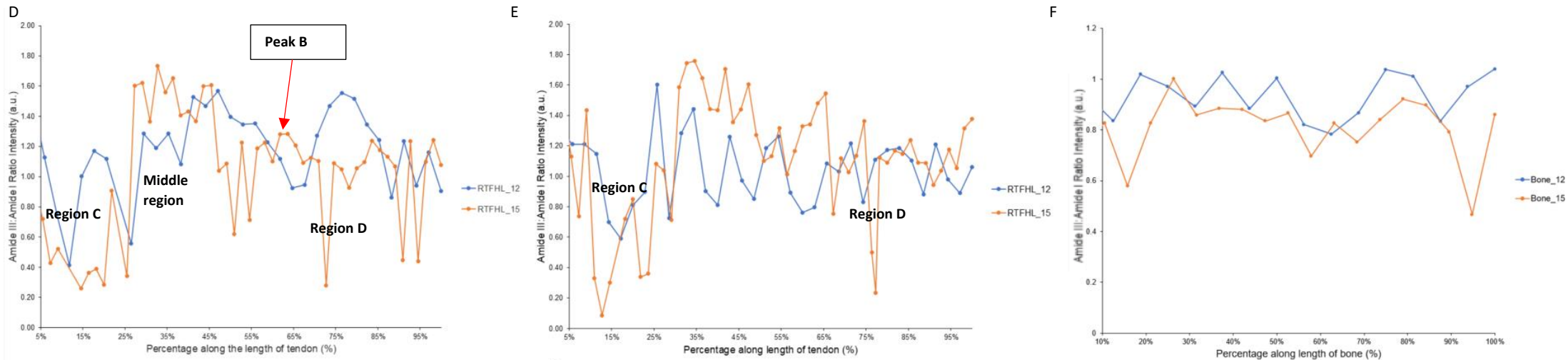


Figure 16ii: Collagen analysis: Amide III: Amide I ratio intensity showing the collagen organisation as a percentage from the distal end before mechanical testing in tendon (D), after mechanical testing in tendon (E) and in untreated tibia (bone) relative to tendon extracted (F). Analysis of collagen organisation was determined spectroscopically using Raman by the appearance of chemical bands measured from the maximum peak intensity of amide III ($1240-48\text{ cm}^{-1}$) and amide I ($1658-64\text{ cm}^{-1}$) at various positions along the length of the tendon. Young tendon (RTFHL-12) was compared with old tendon (RTFHL-15) to see how this chemical property changed with age.

4.1.4 Amide III: Amide I

The ratio of amide III: amide I (amide III:I) is a big contributor to the properties expressed within the collagen of the tendon. Changes in the amide III: phosphate coincide with specific changes in amide III: I. On initial comparison it is clear both young and old tendon maintain a relatively similar shape before and after mechanical testing. Comparing mineral content with amide III:I there are no sporadic changes to maintain the integrity of the collagen along the length of the tendon with varying mineral content. On closer examination, subtle changes can be seen in the distribution of amide III: I moving proximally along the length of the tendon. Much of the young tendon is affected by uniaxial loading compared to its old counterpart (**D & E; RFHL-12 - Figure 16ii**). On average the amide III: I ratio intensity is higher at the proximal end compared to distal. Regions of high amide III: amide I ratio e.g. **peak B** corresponds to regions of high mineral content (low amide III: phosphate; **peak A**). This suggests a conformational change in the structure of collagen whereby in regions of higher mineral content amide I is almost replaced with amide III or at least these regions amide III becomes precedent over amide I. Literature has shown this chemical change is indicative of changes to the structural organisation of the collagen particularly the alignment of the collagen fibrils (35). Mineralised regions tend to have increased alignment of collagen fibrils. The **middle region** (27-45%) of the tendon show ratio intensity close 1. This coincides with regions of lower mineral and suggestive of the balance within the underlying collagen chemistry in lower mineral regions.

Subsequently the major difference pre- and post-mechanical testing is seen in the peak in **region C** (13-27%) and **region D** (68-87%) along the length of the young tendon (**D & E; RFHL-12 - Figure 16ii**). After mechanical testing, **region C** is shifted further proximally along the length of the tendon while the **region D** had a reduced amide III: I ratio intensity. Subsequently the area of the tendon influenced by this amide III: I ratio intensity is reduced (**D; RFHL-12 - Figure 16ii**). Nonetheless it is shown therefore the young tendon (FHL-12) is more susceptible to changes in the structure and more so in these regions relatively close to distal and proximal ends respectively. Overall pre-mechanical testing the ratio intensity of this collagen property drops as low as 0.3 while after testing the ratio intensity stabilises between 0.6 – 1.6. Like the amide: phosphate, the bone shows a similar profile to amide III: I chemistry of the tendon but with a more gradual change which is expected because the collagen chemistry of bone is quite like tendon. Bone varies because it consists of fully mineralised tissue and displays both homogeneous and heterogeneous properties while tendon are heterogeneous (88).

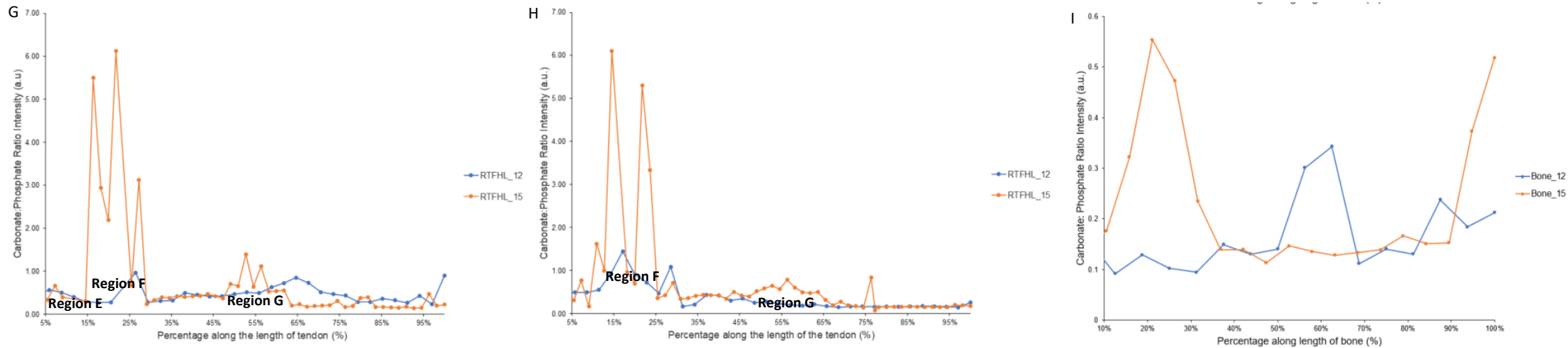


Figure 16iii: Collagen analysis: Carbonate: Phosphate ratio intensity showing the maturity of mineralisation as a percentage from the distal end before mechanical testing in tendon (G), after mechanical testing in tendon (H) and in untreated tibia (bone) relative to tendon extracted (I). Analysis of mineral maturity was determined spectroscopically using Raman by the appearance of chemical bands measured from the maximum peak intensity of carbonate ($1068-73\text{ cm}^{-1}$) and phosphate ($955-60\text{ cm}^{-1}$) at various positions along the length of the tendon. Young tendon (RTFHL-12) was compared with old tendon (RTFHL-15) to see how this chemical property changed with age.

4.1.5 Carbonate: Phosphate

Carbonate: phosphate ratio intensity is relatively stable for the young aged tendons and shows a similar ratio throughout the length of the tendon from proximal to distal end. **Region E** near the distal end of ratio splits into 2 peaks post-mechanical testing. The high region of carbonate: phosphate around 65% decreases levelling out to the similar ratio intensity to the adjacent regions along the length of the tendon (**G & H; RFHL-15 - Figure 16iii**). After uniaxial loading the 3 peaks in the old tendon **region G** had a decreased carbonate: phosphate ratio.

The carbonate: phosphate ratio depicts the maturity of mineral within the tendon. As mineral matures phosphate group becomes more prominent replacing the carbon thus lower carbonate: phosphate ratio overall in the old tendon (**G & H; RFHL-15 - Figure 16iii**). **Region F** along the length of the tendon particularly in the old age group show the high intensity peaks in carbonate: phosphate ratio suggested that there are areas along the length of the tendon whereby there is a chemical transition of carbonate to phosphate as tendons moving from mineralised to non-mineralised regions tendon (**G & H; RFHL-15 - Figure 16iii**). On the other hand, the relatively stable ratio of carbonate: phosphate ratio remains reflecting the smaller number of mineralised regions in the young tendon. The carbonate: phosphate ratio almost mirrored the amide: phosphate ratio. This was due to C=O and C=N involvement in amide chemistry. This was also reflected in bone to a higher degree.

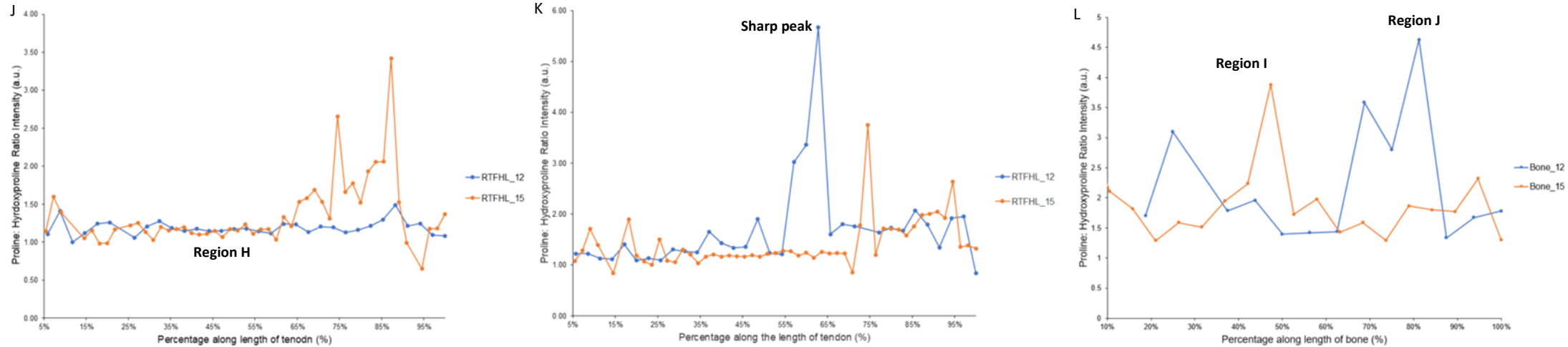


Figure 16iv: Collagen analysis: Proline: Hydroxyproline ratio intensity showing the collagen tissue stability as a percentage from the distal end before mechanical testing in tendon (G), after mechanical testing in tendon (H) and in untreated tibia (bone) relative to tendon extracted (I). Analysis of collagen tissue stability was determined spectroscopically using Raman by the appearance of chemical bands measured from the maximum peak intensity of proline ($850-54\text{ cm}^{-1}$) and hydroxyproline ($875-6\text{ cm}^{-1}$) at various positions along the length of the tendon. Young tendon (RTFHL-12) was compared with old tendon (RTFHL-15) to see how this chemical property changed with age.

4.1.6 Proline: Hydroxyproline

This ratio identifies changes in this collagen specific bands moving proximally from the distal end of the tendon. Overall the old tendon seems to maintain the same graph shape pre- vs post-mechanical testing however major peaks in the graph were shifted further proximally (**J & K; RFHL-15 - Figure 16iv**). **Region H** (middle) which shows a relatively maintained proline: hydroxyproline ratio of 1 became more greatly distributed post-mechanically. This region spanned around 35-70% from the distal end which then increased to 20-75% after mechanical testing. A major difference is seen in the proline: hydroxyproline ratio of the young tendon pre- vs post-mechanical testing. This is the appearance of a sharp peak in the young tendon 62% from the distal end. Regardless of age the proline: hydroxyproline ratio stayed relatively the same up until 59% from the distal end of tendon. Post-mechanically this area was reduced to 35% (**J & K; RFHL-15; Figure 16iv**). This ratio is dependent on hydroxylation of the enzymatic cross-links in hydroxyproline or a decrease in proline. Hydroxyproline is collagen specific and a unique biomarker of collagen (67). It is also directly proportional to collagen cross linking. A reduced rate of hydroxylation leads to a decrease in the collagen stability of the tissue and the ability for cross-links to form in collagen become impinged (89). Moving proximally from the distal end there is a high rate of hydroxylation thus an increase in the formation of cross-links within the collagen (**J & K; RFHL-15; Figure 16iv**). However, in the young age (**J; RFHL-15 - Figure 16iv**) for much of the length along the tendon the ratio of proline to hydroxyproline is almost level at 1 which would suggest there is an almost equal amount of proline and hydroxyproline thus collagen specific crosslinking in the tendon is occurring at a constant rate. Comparing this ratio to bone although there are similarities in the overall shape there are some major differences particularly in the appearance of large peak in **Regions I**; old and **J**; young.

4.1.7 Analysis of differences in Young vs Old: Pre- vs Post-mechanical

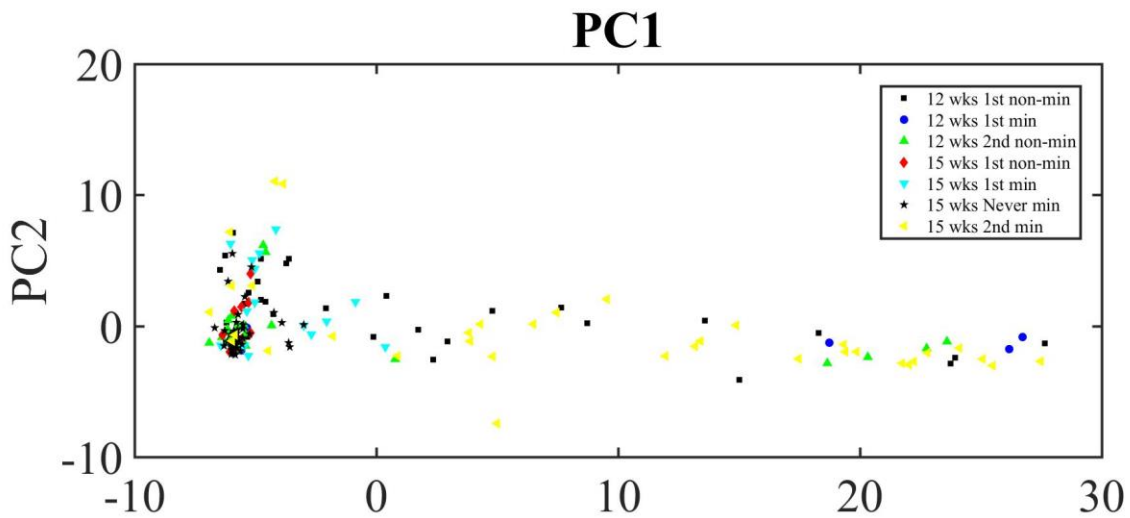


Figure 17: Detailed PCA plot relative to age, mineralisation level and transition along the length pre-mechanical testing.

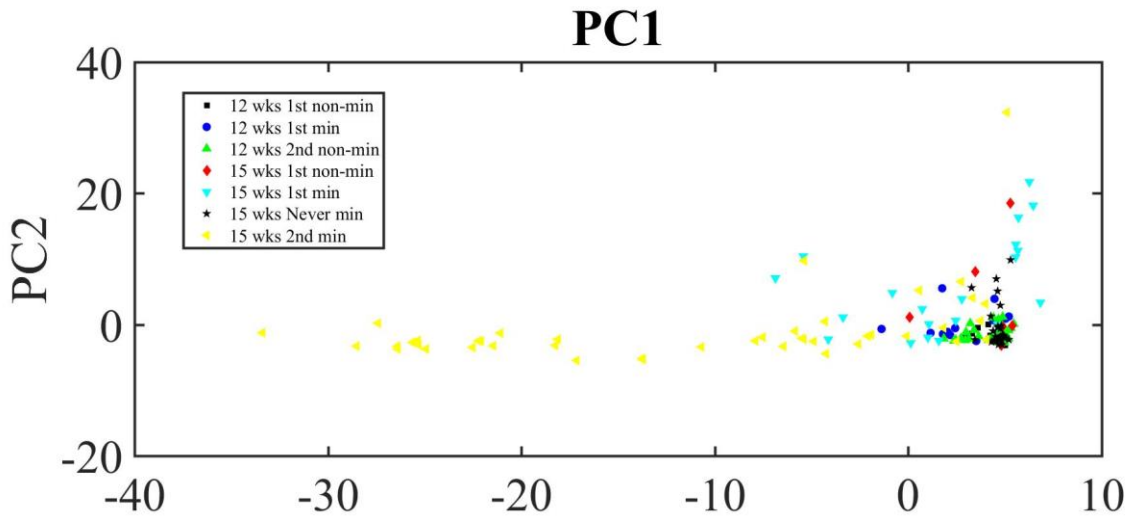


Figure 18: Detailed PCA plot of PC1 and 2 relative to age, mineralisation level and transition along the length post-mechanical testing.

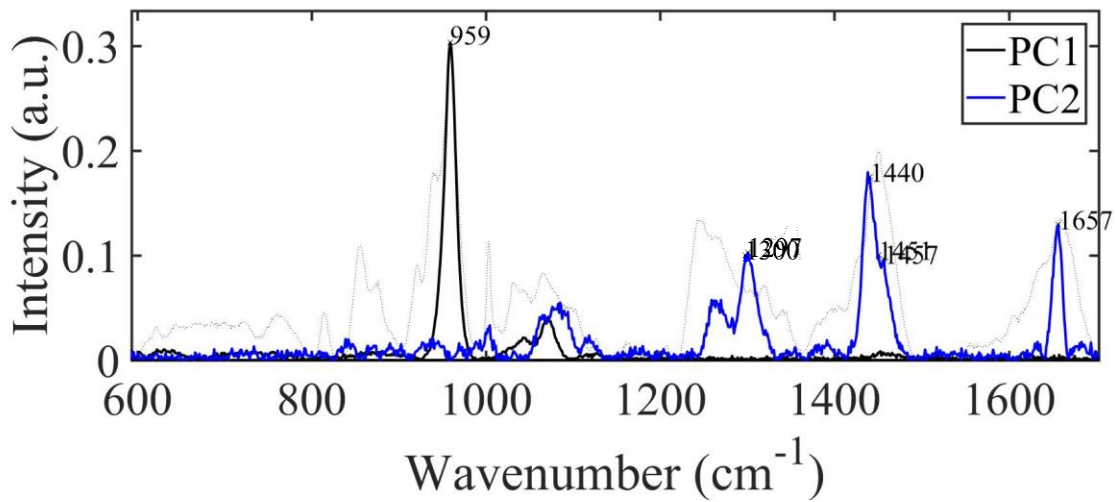


Figure 19: PCA loadings plot of the contributing factors to the distribution of the spectra relative to PC1 and PC2 from the young and old tendons after tendons were tested mechanically along with average spectrum of data PCA plot (dotted line).

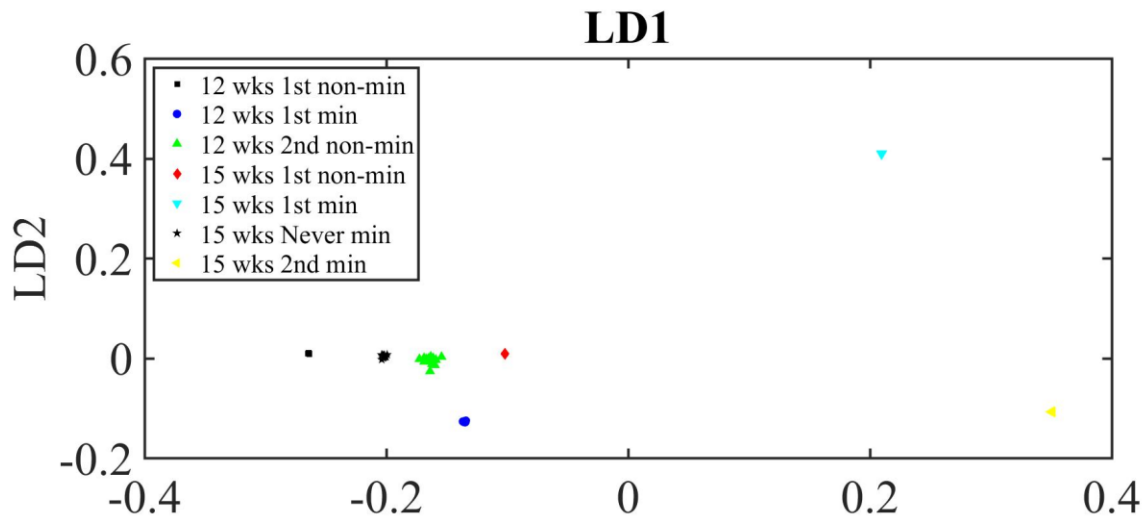


Figure 20: LDA plot of LD1 and 2 relative to age, mineralisation level and transition along the length pre-mechanical testing.

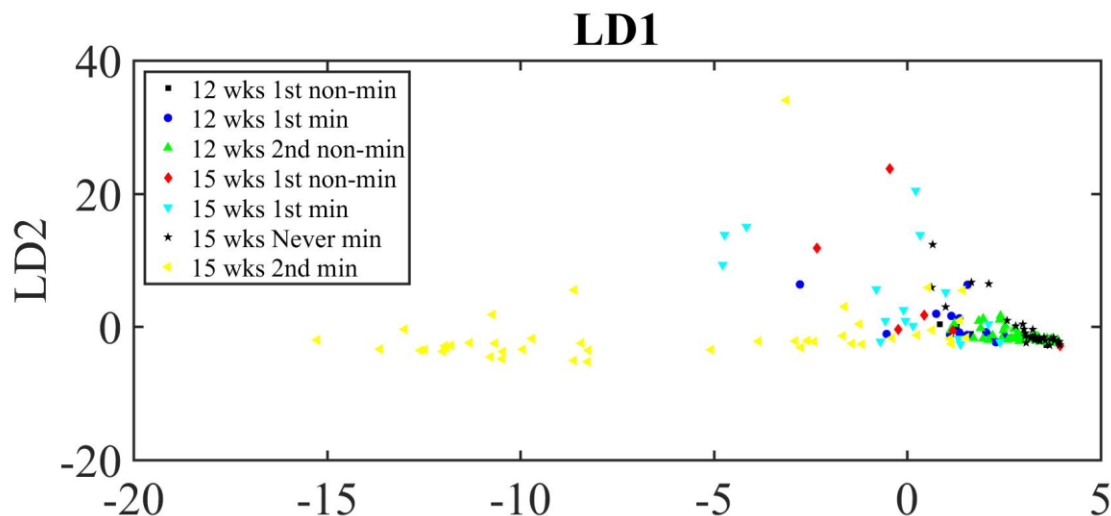


Figure 21: PCA-LDA plot of LD1 and 2 relative to age, mineralisation level and transition along the length pre-mechanical testing.

Initially a difference was seen in the mineral peak contributing to the distribution of the data along the PC1 axis. There was a slight shift in the wavenumber values. Pre-mechanical testing the mineral peak was caused by the 960 cm^{-1} band (**Figure 14**). Post-mechanical testing this changed to a 959 cm^{-1} peak (**Figure 19**). These are both classified mineral phosphate peaks. Usually newly deposited mineral containing high HPO_4^{2-} shifting this peak to a lower wavenumber (67). Although this suggests newly deposited mineral this may be caused by displacement of HPO_4^{2-} during uniaxial loading. Elongation of the tendon under tensile load mimicked the appearance of increased HPO_4^{2-} by increasing the amount per unit area of collagen fibril. This trend continued when comparing the cause of the spread in PC2 after mechanical testing. The amide I; 1657 cm^{-1} peak became one of contributing factors (**Figure 19**). This trend was confirmed in the univariate analysis as amide I dominated over amide III causing the amide III:I ratio intensity to decrease in **regions C and D** after post-mechanical testing (**E; Figure 16ii**). On average this peak was also a contributing factor in PC2 before mechanical testing, but its contribution increased after uniaxial loading suggesting changes to the collagen alignment in this region. Other differences include a shift in contribution factors such as $1442\text{-}1447$ (pre-mechanical) to $1440\text{-}1457\text{ cm}^{-1}$ (CH_2 stretching/ CH_3 asymmetric deformation post-mechanical) due to the physical stretching of the tendon under mechanical load. The 1128 cm^{-1} peak became absent post-mechanical testing hence a potential replacement in a C-N stretching component within the collagen of the tendon (**Figure 14**).

4.1.8 Differences in various region pertaining to their chemical composition

It was possible to visualise the differences in the relative chemical composition per length of tendon from distal end. Moving proximally along the tendon there were 35 different points determined by the number of spectra collected from young tendon (12 wks) compared to the 55 spectra collected from the old tendon (15 wks). The 12wks 1st non-min region became more spread post-mechanically which corresponded to changes related to amide I previously seen (**Figure 18**). There was an increase in the number of spectra which composed the 1st non-min region of the 12 wks (43% increase on average). At position 24 – 30 spectrally along the length of the tendon small developing peaks at 959 cm^{-1} (shoulder peak) were present (**B; Figure 16i**) (**Figure 23**). Inherently displaying mineral characteristics this suggested

possible breaking of the mineral in mineralised regions thus an increase of regions previously classified as mineralised prior to mechanical load becoming non-mineralised. This region correlated with high intraclass variation seen post-mechanically compared to its clustered appearance originally seen pre-mechanically testing in PC1 and PC2.

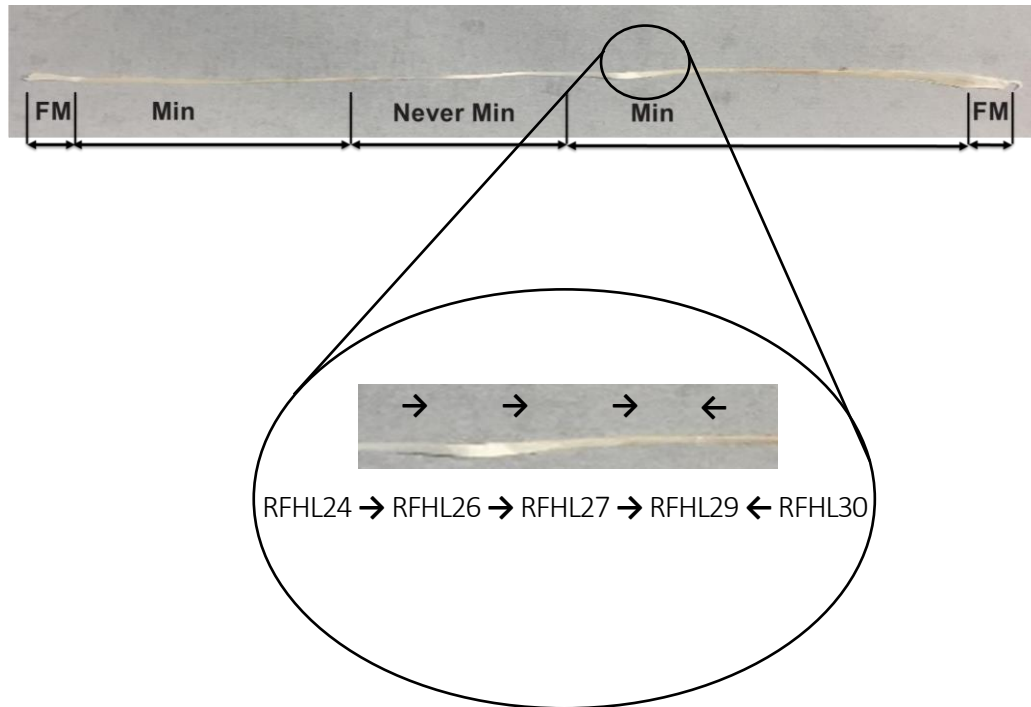


Figure 22: Illustration of direction of mineral converging to highest mineral presence within proximal region of changing mineralisation profile including shoulder peaks along region in old tendon. Arrow indicating direction of convergence. RFHL 24 = 24th position from the distal end of the right FHL tendon.

Both pre- and post-mechanical, the '15 wks Never min' region remains clustered in the PC1 and PC2. In PC1, 15 wks 2nd min region (old tendons) with more mature mineral contributed to most of the variation (**Figure 17**). This remains a contribution factor post-mechanical testing. After comparing the mineral crystallinity at these 2 regions the first mineral region of 15 wks had less mature mineral than the 2nd mineral region in this age group. In PC2, the 1st and 2nd min region 15 wks remain to have the most variance throughout both stages with 1st min region becoming more spread after mechanical testing (**Figure 18**). This suggests components of both mineral (PC1) and collagen properties (PC2) in 1st mineral region which caused it to have a greater variance than the 2nd thus young mineral being more greatly affected to changes in collagen after tendon loading hence more easily influenced due to greater alignment of collagen in old tendons which made it harder for these chemical properties to be altered.

Moving towards the proximal end of the tendon between 68-88% along the length pre-mechanical testing there is sharp increase in the amide III:I ratio intensity (**D; Figure 16ii**). In the same region post-mechanically (**E; Figure 16ii**) the intensity drops and this peak therefore a decrease in amide III. This corresponds with a transition zone between mineral and non-mineral and indicative a change in the collagen alignment to adapt for the transitioning to mineral (**Figure 22**).

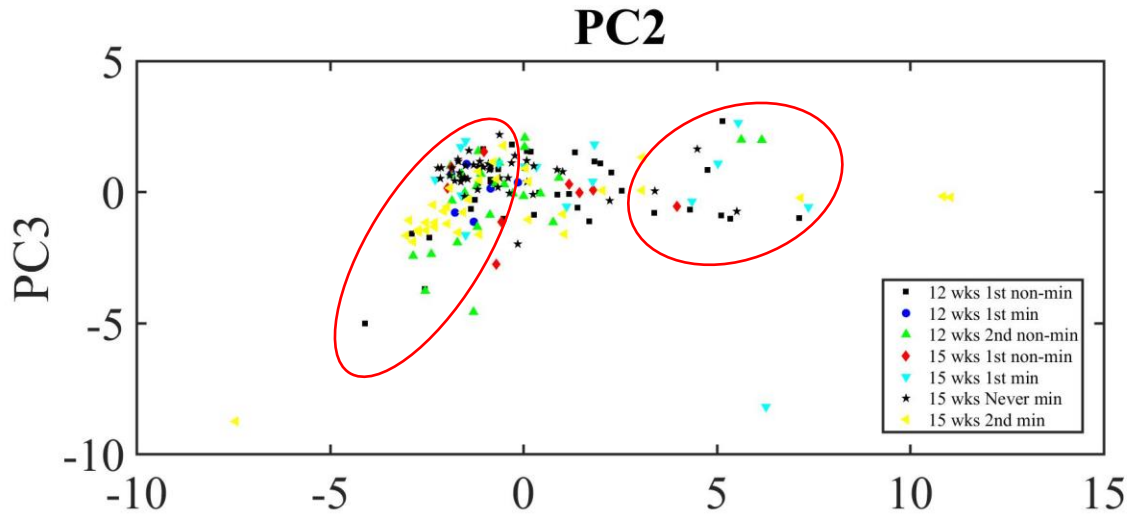


Figure 23: Detailed PCA plot of PC2 and 3 relative to age and mineralisation level along the length of the tendon post-mechanical testing. Red circles indicate variance in 12 wks 1st min region.

In attempt to see if there was any separation in PC2, a scatterplot compared PC2 and PC3. The corresponding loading plots showed that in the axis of 2nd and 3rd most variance, the data was separated due to collagen related peaks (**Table 1**). In PC2, 12wks 1st non-min region stood out again, being amongst one of the groups with the most intraclass variation. The group which clustered the most was the 15 wks 'Never min' region (**Figure 22**). However, it was clear that there were spectra from each group which displayed variation intraclass. Most groups were more clustered in the PC3 than PC2. This was expected due to the degree of variance along these axes although there were a few stray spectra from 12 wks 1st and 2nd non-min groups, 15 wks 1st non-min group.

4.2 Mineral Crystallinity

a	% from distal end of tendon			
		33%	67%	100%
	L15 – FHL			0.062
	R15 – FHL			0.055
			0.042	

b	% from distal end of tendon	33%	67%	100%
		Bone 13 weeks (R)	0.062	0.034
	Bone 15 weeks (R)	0.045	0.057	0.052

Table 4(a): Mineral crystallinity assessment indicating level of mineralisation and maturity of tendon using full-width half height (FWHH) b) Comparison of mineral crystallinity with bone

The full-width half height (FWHH) was used as an assessment of the mineral crystallinity. A narrower phosphate bandwidth is indicative of increased mineral crystallinity (55). This is also accompanied by a reduced carbonate: phosphate ratio as carbonate is less readily substituted with phosphate. This is seen particularly in old tendons with a high FWHM ratio. Comparison was only possible in old tendons as most spectra along the length of tendon presented with a mineral peak at 960 cm^{-1} . The results show that the second and the final third along the length of the RFHL (R15 – FHL) tendon, and the final third of the LFHL tendon present a ratio indicative of its mineral crystallinity level. LFHL (L15 – FHL) has the highest and narrowest peak thus high mineral crystallinity while the lowest and widest peak was between the regions 33.3%-66.7% along the length of the same tendon (**Table 4a**). These values are lower than bone which is expected as bone is a very highly mineralised structure (**Figure 16**).

4.3 Mechanical Testing

Tensile strength is an indication of the structural adaption made by the tendons to carry a certain mechanical load. Tendons increase in stiffness due to mineralisation affecting their capacity to store elastic energy during locomotion (50). Using this property, it was possible to imitate the typical function of tendons via uniaxial loading thus providing an insight into potential compromises in the mechanical integrity of tendons due to age. The aim of this chapter was to determine changes in collagen mechanically that led to mineralisation in the maturing turkey leg tendon (TLT). By comparing a range of techniques, it is possible to determine the tensile strength of the tendon as a function of stress/strain activity. Accessing both non-linear and viscoelastic components to tendons' behaviour attempted to provide effective moduli which are ill-defined due to the non-trivial complex nature of TLT.

4.3.1 Uniaxial loading from Zwick mechanical tester

Tendons were stretched via uniaxial loading of tendon via a Zwick mechanical tester as demonstrated in **Figure 24**. This ran conditioning cycles set to a constant strain throughout the cycles. Strain of 5% was used originally but when tendon failed this test, the strain was decreased to 2.5%. This occurred in the older tendons because of their elastic capacity. From these cycles the elastic modulus was calculated as an indication of the tensile strength of the tendons. The results show a range of trends giving an insight on the structural integrity of the tendons.



Figure 24: Mechanical testing of tendon using Zwick mechanical tester in action, a) showing the tendon taut set to an initial pre-load before commencing conditioning cycles b) tendon during conditioning cycles of uniaxial loading.

4.3.2 Determination of the Elastic modulus

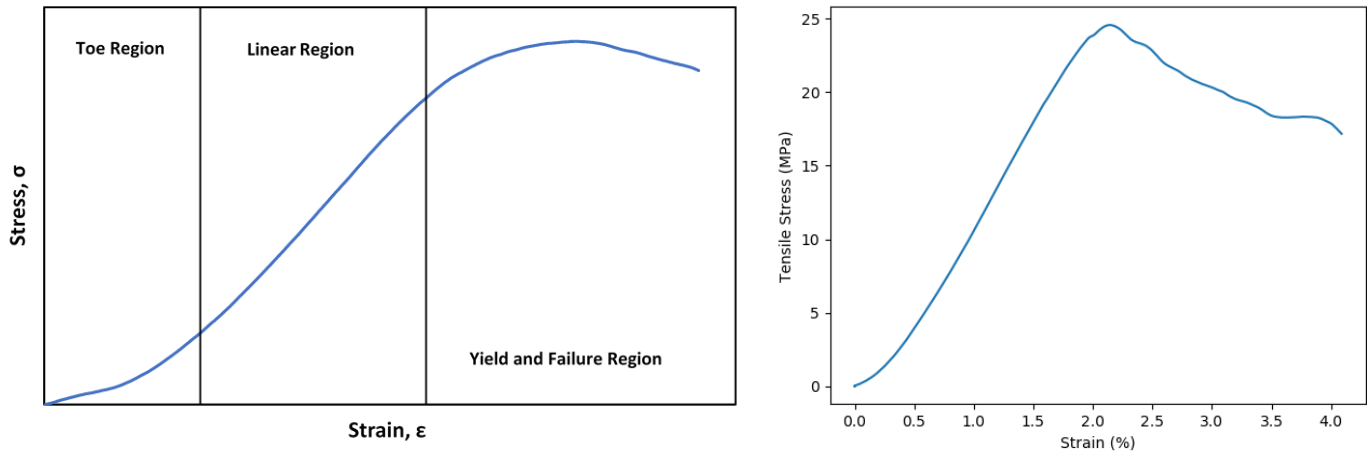
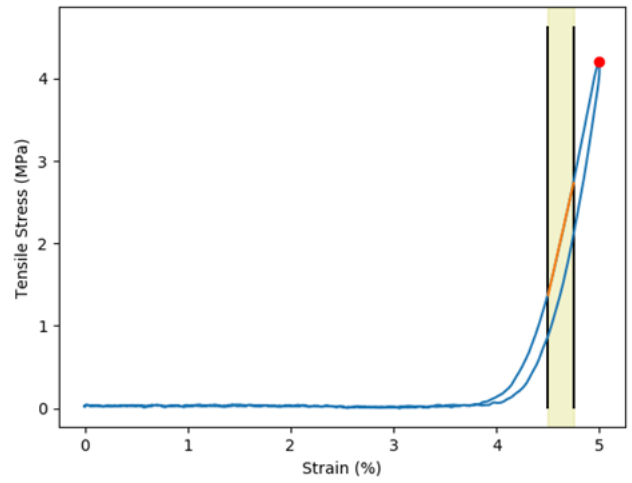
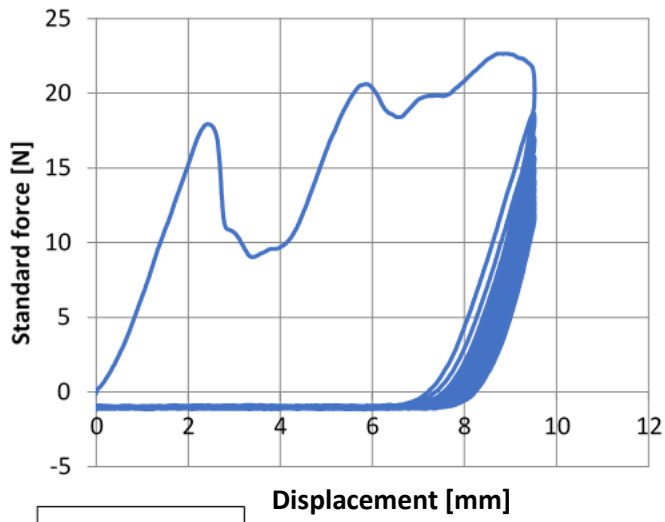


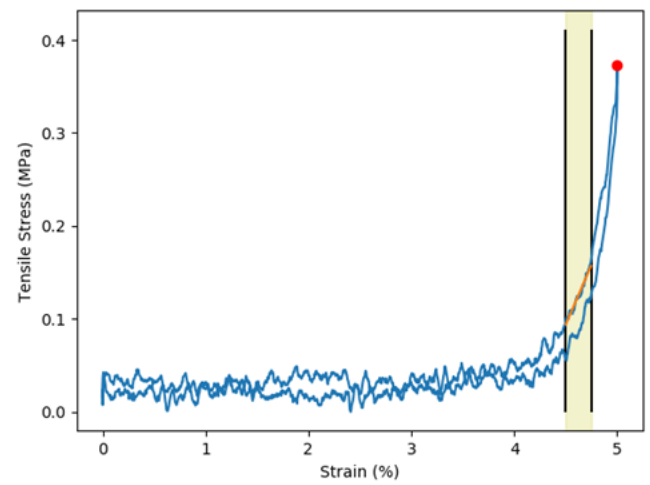
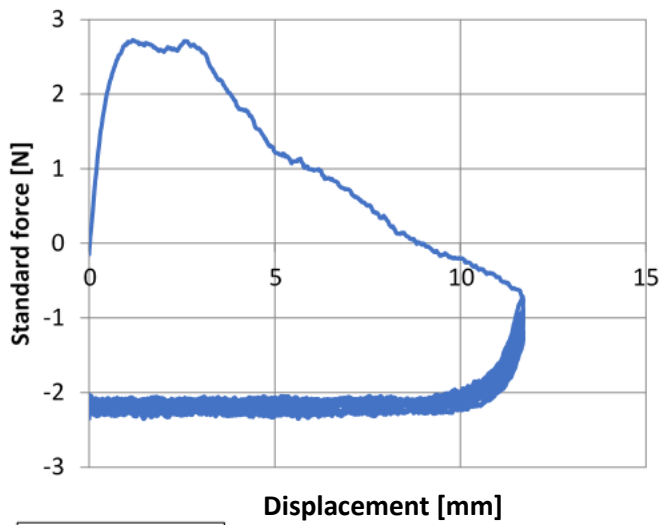
Figure 25: Viscoelastic behaviour of tendons. Left: Stress-strain curve analytics. Right: Example of stress strain curve from experimental data of young flexor tendon (12 wks).

The beginning of the stress-strain curve starts with the toe region, this is usually the non-linear region of the curve where a low mechanical load respective to the strength of the tendon is applied (left) (**Figure 25**). In the experimental data this region occurs over a short period of time due to the length of the tendon. Stretching of crimps in collagen fibrils attribute to relatively low stiffness. When the crimps in the collagen fibrils become fully elongated the linear region is entered. This is also known as the linear elastic region. The Young's modulus can be calculated from this region provide an effective modulus for the strength of the tendon. Collagen fibrils orient themselves in the direction of the tensile load and begin to physically stretch. As the fibrils are stretched the tendon begins to change its structure to withstand the mechanical load increasing the stiffness of the tissue. This region is very steep in the experimental data (right) and can increase the tissue stiffness even further if mineralisation is present (**Figure 25**). At the end of the linear region the tendon's physiological upper limit is reached. The 'yield and failure' region is entered, this includes the upper and lower yield stress point of the tendon. At yield, the ultimate tensile strength (UTS) of the tendon can be calculated. Subsequently tissue encounters microfailure. At a structural level the cross-links between collagen fibrils start to fail. The slope of the hysteresis loop increases with displacement and this is seen in the hysteresis cycles below (**Figure 26**) (90). They cannot return to their original shape and break in over a few seconds.

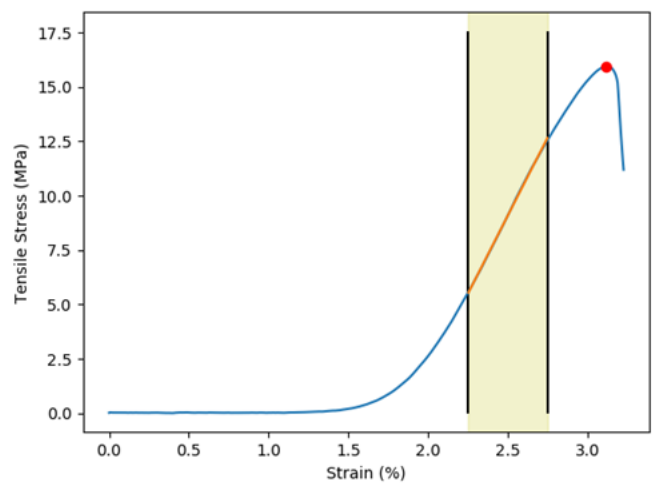
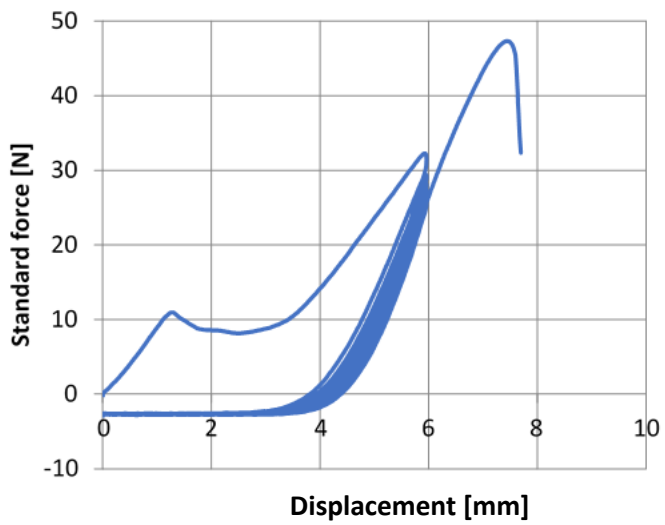
R_FHL-12



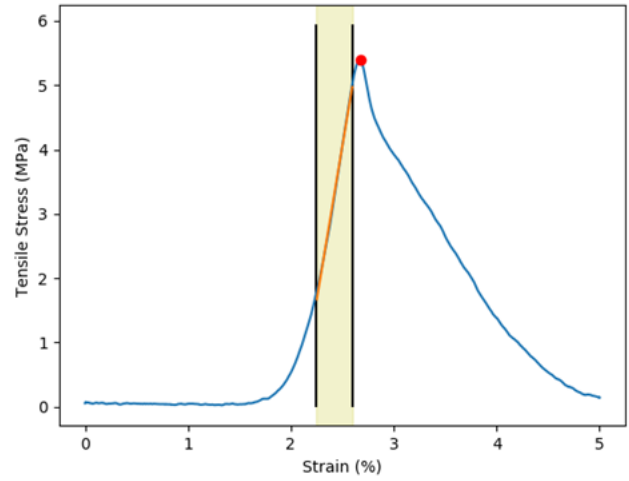
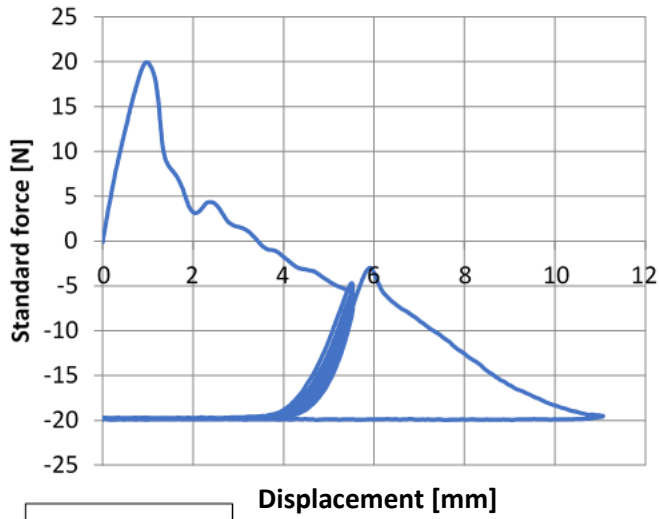
L_FHL-12



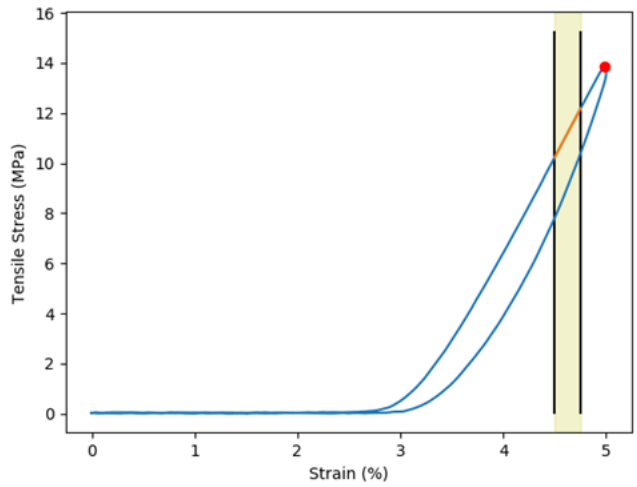
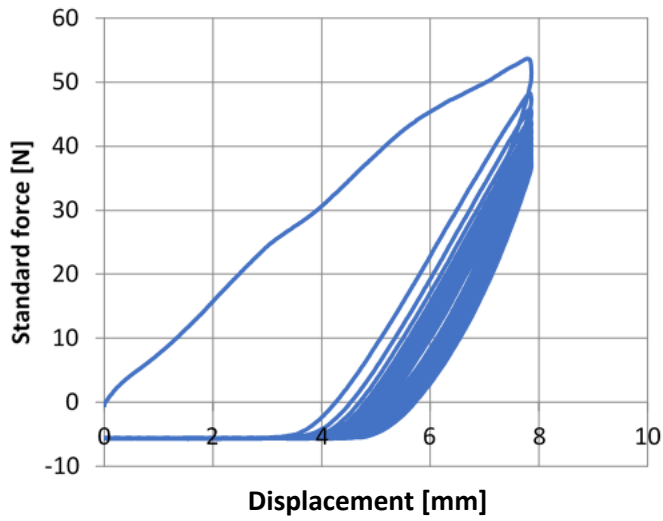
R_FHL-15



L_FHL-15



R_FD-12



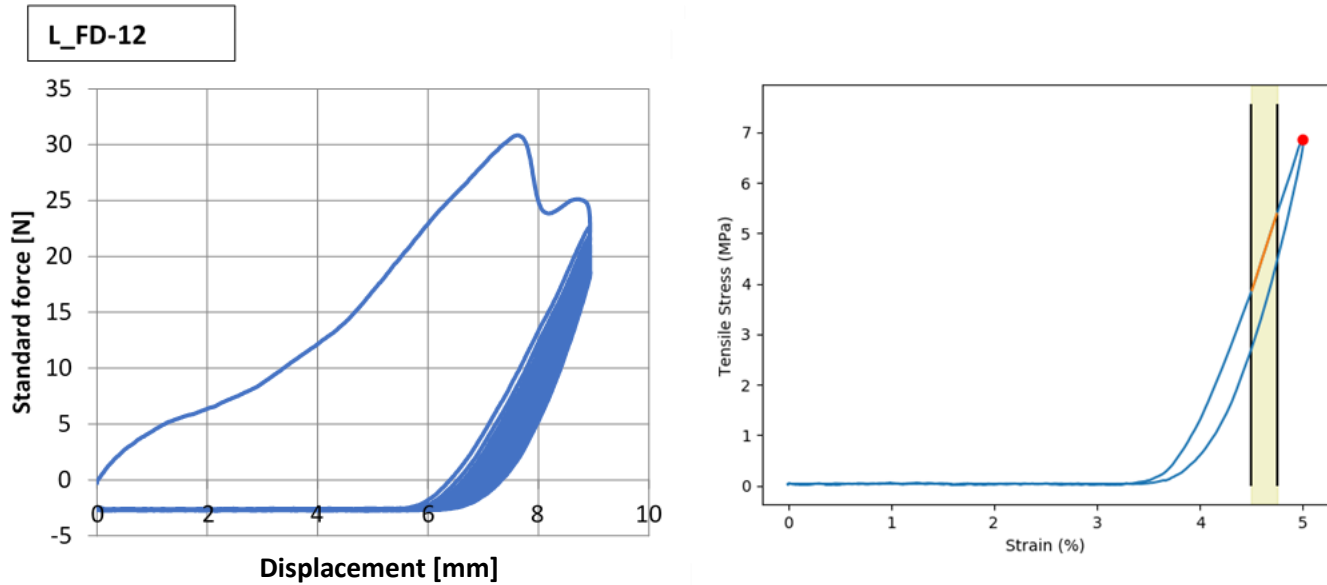


Figure 26: Hysteresis cycles produced from uniaxial loading of various tendons and linear approximation taken from a consistent point in linear elastic region of resulting stress-strain activity for elastic modulus (EM) calculation.

Table 5: EM of young (FHL-12) and old (FHL-15) flexor tendons (FHL & FD) to 3.s.f. and length of tendons before and after mechanical testing. EM values were calculated at the 95% confidence level.

Tendon	EM (MPa)	Strain, EM was taken from (%)	Strain at Max Stress (%)	Coefficient of determination	Length (Pre-mechanical) cm	Length (Post-mechanical) cm
R_FHL-12	26	4.5-4.75	4.9996	0.96658	19.5	21.6
L_FHL-12	550	4.5-4.75	4.9966	0.99963	23.4	25.1
R_FHL-15	1435	2.25-2.75	3.1182	0.99967	23.8	31.2
L_FHL-15	959	2.25-2.6	2.6726	0.99756	22.1	28.7
R_FD-12	773	4.5-4.75	4.9882	0.99997	15.7	21.5
L_FD-12	628	4.5-4.75	4.9953	0.99983	17.9	22
R_FD-15	733	4.5-4.75	4.9956	0.99796	19.0	26.4

From the results produced by the Zwick mechanical tester, the EM was taken as the Young’s modulus. Over a short period of stress/strain the tendons followed Hooke’s law when subjected to uniaxial loading, therefore EM taken from this period correlated with the linear response exhibited by the tendon when a constant strain rate was applied thus proportional to the applied force (stress) (91).

The strength of the FD tendons were quite similar compared to the FHL tendons which varied in EM (**Table 5**). FD tendons were also shorter than FHL tendons. This may suggest the compromise in elastic capacity in the FHL tendons as they increased in age hence reduction in strain (from 5 to 2.5%) to complete the cycle. The initial curve produced by the right old tendon (R_FHL-15) reaches UTS and the cycle breaks. An Fmax in the mechanical tester setup broke the cycle and assumed that strain beyond 5% would cause the

tendon to reach its physiological limit of elasticity; yield and field region (**Figure 25**) before hitting inelastic plastic deformation followed by ultimate failure.

From **Table 5** it is clear the old tendons (15 wks) had a greater tensile strength capacity (EM) compared to the young tendons (12 wks). When using a strain of 5% all values of elastic modulus were measured between 4.5 and 4.75% strain and when using a strain of 2.5% for the old tendons with a weak elastic capacity the elastic modulus measured between 2.25 and 2.6/2.75% strain. From these ranges, the elastic moduli were taken in all plots. The co-efficient of determination was very close to 1 (**Table 4**). Therefore, the straight-line approximation matched the line of best fit.

On initial examination the elastic modulus of the right young (R_FHL-12) tendon was very low compared to all other tendons (**Table 5**). However, the strain rate that the EM was calculated from was consistent with the other tendons and the strain rate at maximum stress was similar to tendons of the same age region. This suggests another factor could have influenced this result as the hysteresis cycle displays a different pattern compared to the other tendons (**Figure 26**). The left old FHL tendon (L_FHL-15) displayed a negative stress-strain graph although this did not affect the outcome of the elastic modulus calculation as the cycle was still completed.

4.4 Imetrum Imaging

The prior model determined the EM via hysteresis cycles. A new alternative approach is to compare the modulus over a range of strain (%). In this test the tendon exhibited non-linear elastic stress-strain behaviour. This was expected due to the nature of this non-trivial material for mechanical testing. Thus, using the chord modulus produced an estimate of the change in strain for a specified range in stress (ASTM E111-97). These tendons looked at a range of strain between 0-3% (**Figure 29**).

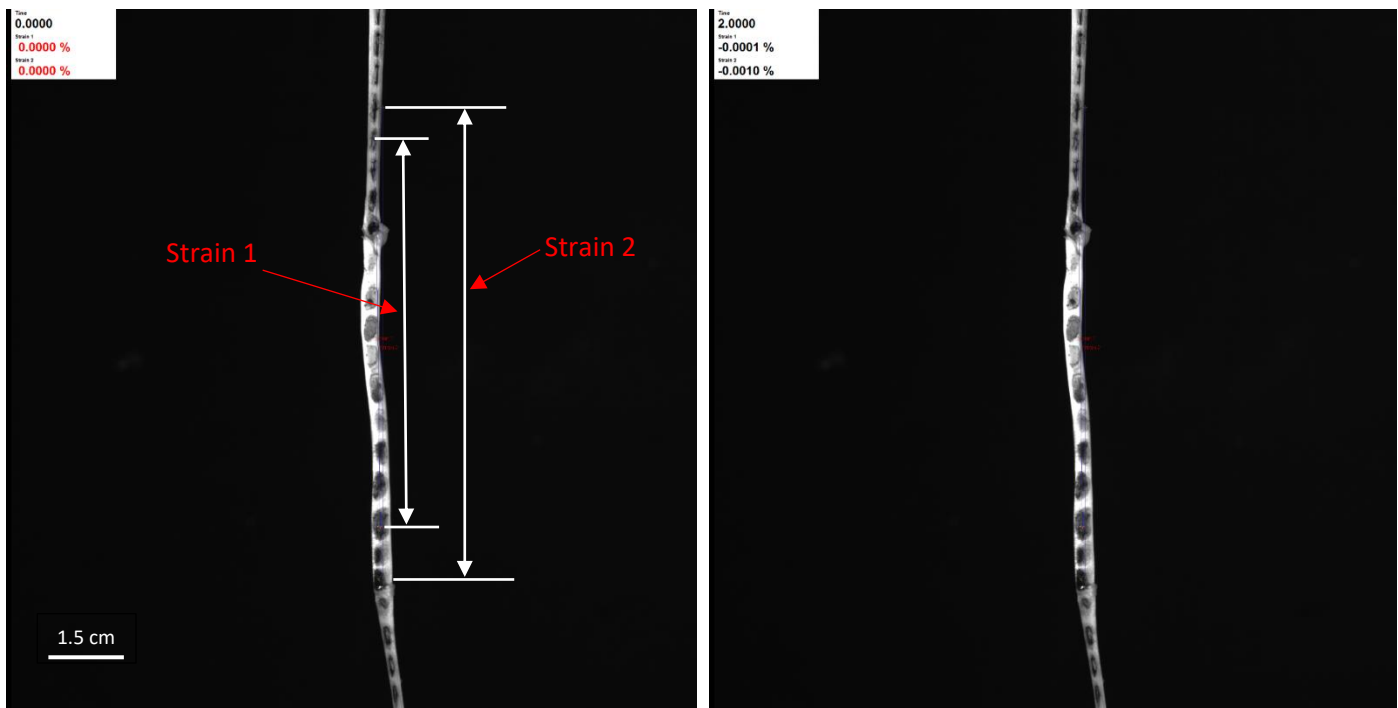


Figure 27: Strain at the start of Zwick mechanical tester induced uniaxial loading ($t=0$) and the first stress-strain point recorded at 2 seconds detected by the video gauge of the Imetrum imaging system (iMIS).

The iMIS was able to record 2 strain; Strain 1 and Strain 2 respectively corresponding to the lower and upper limits of strain (**Figure 6; Methods**). This was only possible because of the markers that were made in a continuous pattern recognisable by the video gauge allowing it to pick up differences in strain over time during loading (**Figure 27**). At 2 seconds when the iMIS detected the first stress-strain point succeeding $t=0$, Strain 1 is = -0.001 % while Strain 2 = -0.0010 %. This property is present in both left young FD (L_FD-12) and right young FD (R_FD-12) tendon, but for visually representation it is only necessarily to show one tendon therefore only left young FD tendon was chosen.

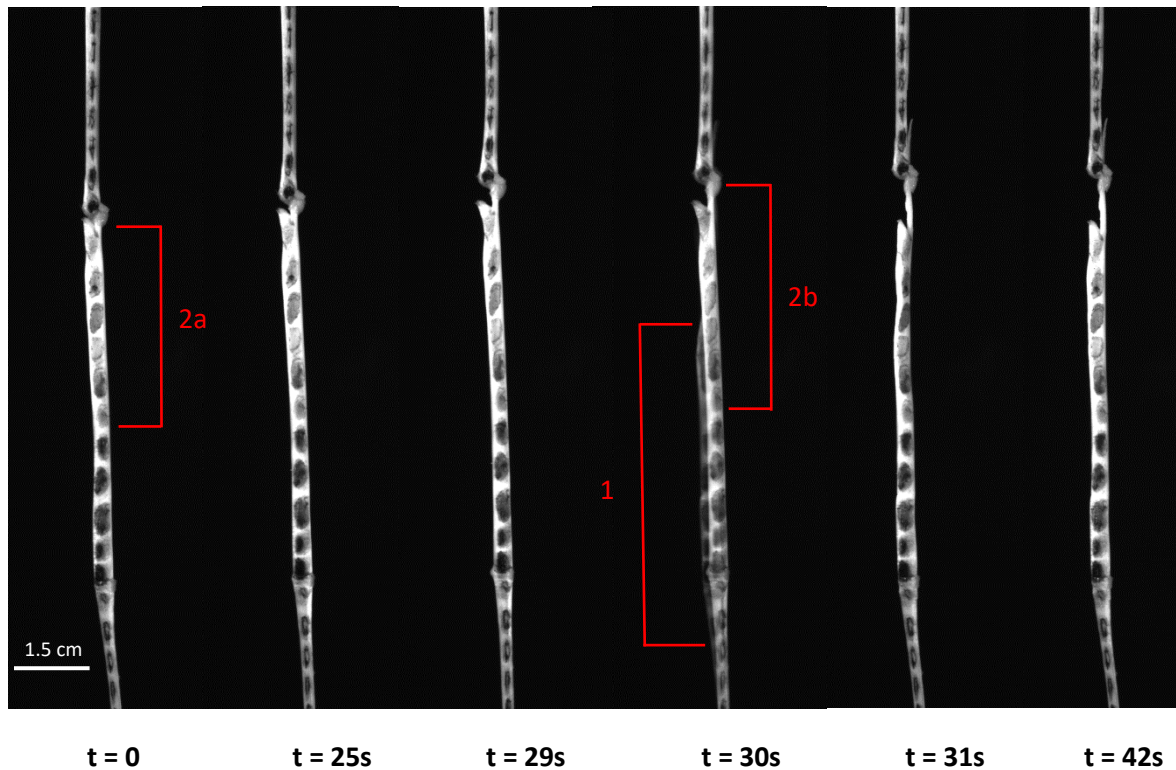


Figure 28: Various stages of uniaxial tension applied to the tendon (L_FD-15 shown above) using the Imetrum imaging setup. Video extensometer gauge, VG (Imetrum, Bristol, UK) captured surface displacement in a singular plane. 1) Faint outline as tendon snaps 2) Stretched middle region indicated by elongation of marker.

As the loading gradually transitions from the first stage to the last stage ($t = 0 - 42s$), the middle region of the tendon is mostly affected. The tendon is stretched, and the marker points begin to elongate. At exactly $t = 30s$ the tendon snaps. This is seen as a faint outline in the 4th visual ($t = 30s$) from the snapping process and the orientation of the tendon becomes slightly twisted after this. At the breaking point, just before the tendon snaps the middle region is stretched to its maximum length. The middle marker becomes longer (2b) than its original length at the start of the test (2a) (**Figure 28**). Prior tests of uniaxial loading using the Zwick mechanical tester confirmed the limit that right young FD tendon should have been stretched was 5.8 cm at which point it would reach the ultimate tensile strength however was stretched to 7.7 cm before breaking at max stress. The limit for left young FD tendon was 4.1 cm but was stretched to 5.9 cm therefore breaking (**Table 5**).

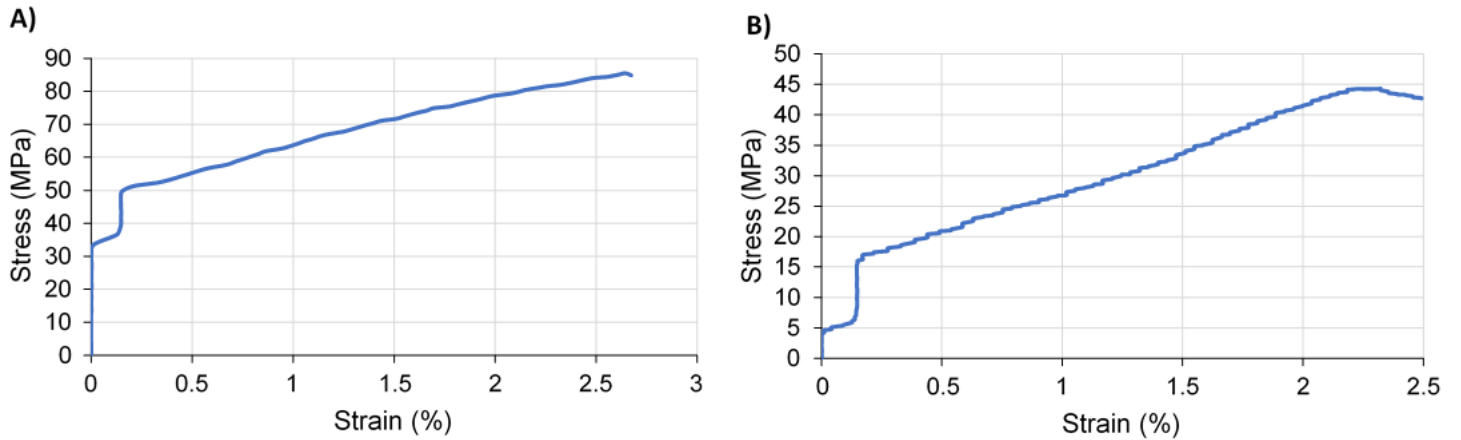


Figure 29: Stress-strain graph from resulting iMetrum imaging setup with real time points of uniaxial tensile stress along the length of A) R_FD-12 and B) L_FD-12 tendon. The derived in-house code (82) accounts for the artefact in the stress-strain graph.

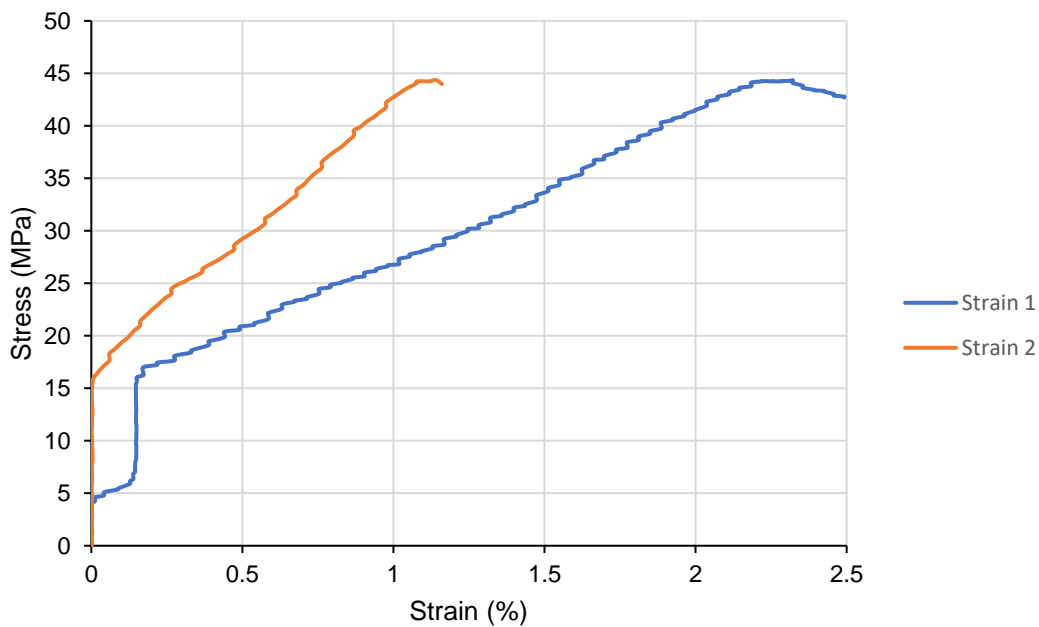


Figure 30: Strain 1 and Strain 2 from Imetrum imaging setup of initial tendon (L_FD-12 tendon).

The curve for each strain displays the stress-strain activity over 100 points using the Imetrum setup. It is expected that Strain 1 and Strain 2 should be equal if the material is homogeneous. Strain 1 and Strain 2 for the same tendon are different characteristically displaying inhomogeneous properties (**Figure 30**).

Table 6: EM calculated as chords taken from stress-strain graphs of R_FD-12 and L_FD-12 tendons. Minimum (min) and maximum (max) moduli were calculated from tangents taken from stress-strain activity at these points.

Tendon	EM (MPa)	Modulus at min strain	Modulus at max strain
R_FD-12	15.0	32.6	322.8
L_FD-12	13.4	19.6	96.9

As previously seen in the results from the hysteresis cycles (**Figure 26**) using the Imetrum system shows a higher modulus in the right tendon (**Table 5, 6**). This adds evidence to suggest a right leg dominance with these tendons (**Chapters 1,2**). The modulus at the min and max strain (%) provided a single effective modulus for these specific points. For both right and left tendons, the chord modulus values are lower than the modulus at the max strain (%) and even the min strain (%) (**Table 6**). Also compared to the results calculated using the Young’s modulus (**Table 5**), the EM via the chord modulus is a fraction of those results. It is expected that using the chord modulus method, the modulus would be lower as this is essentially fitting a local modulus to the entire tendon therefore an average over low and high stress/strain. Further work is required to ensure the data is consistent with the other experimental strategies in this novel technique (**Table 5**). Nonetheless it showed inhomogeneous properties of the tendon.

4.5 Finite element analysis

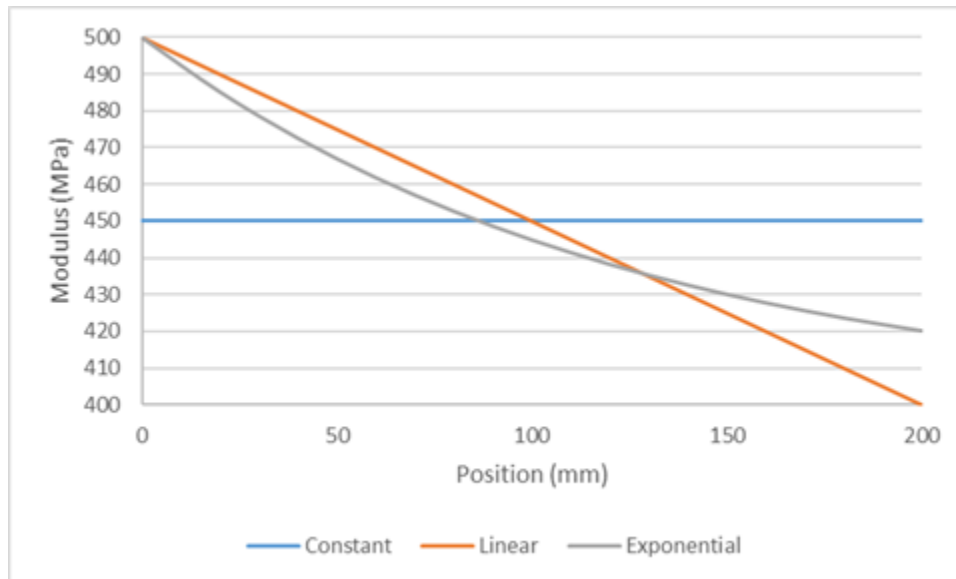


Figure 31a: FEA model of the possible distributions of elastic properties along the tendon length relative to modulus. The values used were arbitrary.

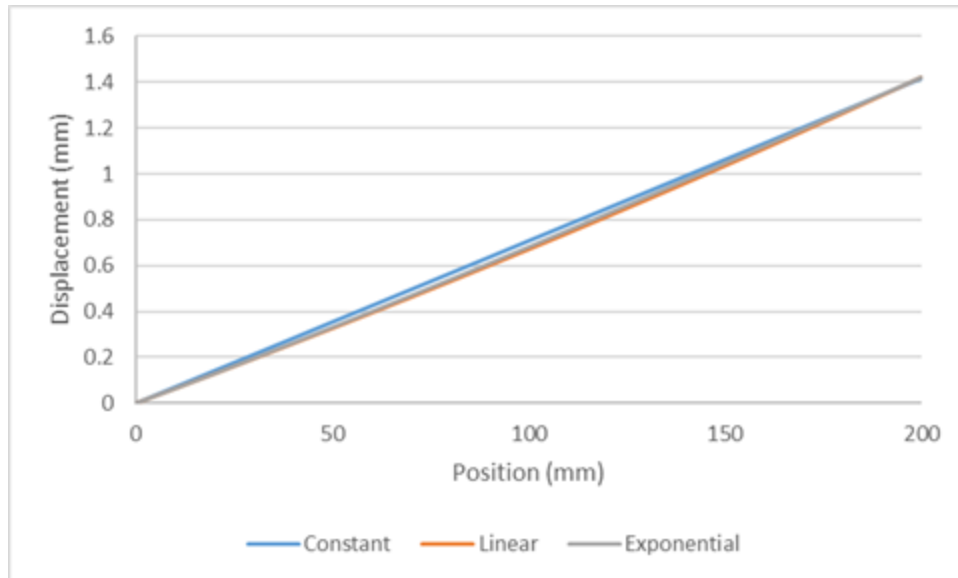


Figure 31b: FEA model of the possible distributions of elastic properties along the tendon length relative to displacements. The values used were arbitrary.

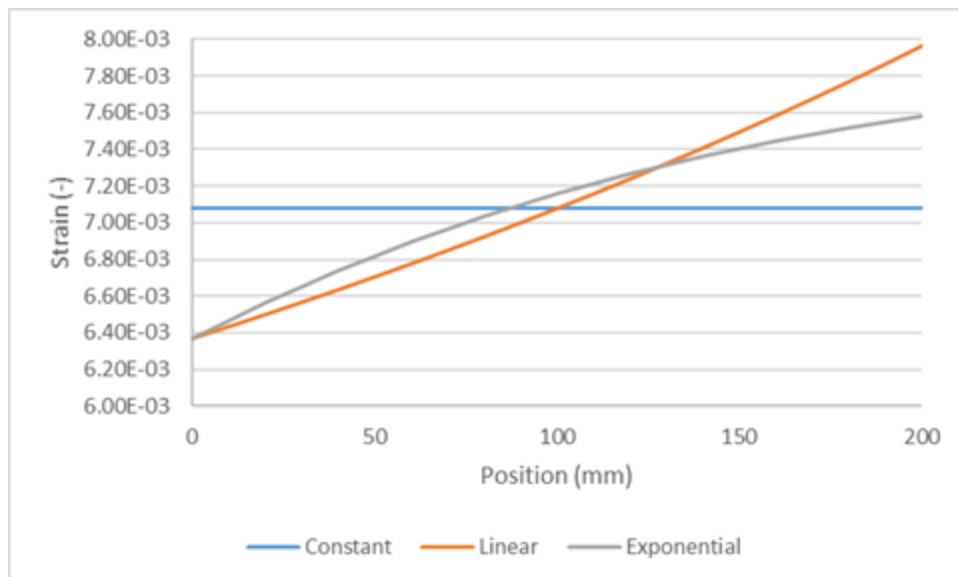


Figure 31c: FEA model of the possible distributions of elastic properties along the tendon length relative to strain. The values used were arbitrary.

Considering the graphs above, FEA shows the possible distributions of elastic properties along the tendon. These include a constant, linear and exponential rate of change. Note the average modulus is the same in all cases; area of intersect shown in **Figure 31a**. Looking at the displacement along the length of the tendon there is not much difference between the 3 types of moduli trends (**Figure 31b**). When the strains were calculated relative to each distribution there was a difference in each modulus trend (**Figure 31c**). This would be a feasible new model to see how well the experimental values fit into one of the distributions.

4.6 Simulating Body Fluid (SBF) experiment

4.6.1 Incubation of SBF

Simulating body fluid (SBF) is known for its ionic similarity to human blood plasma and its ability to drive apatite formation. It is a good indicator of tissue bioactivity (87). Through a new strategized testing method, SBF provided a measure of the collagen bonding ability of tendons in the process of mineralisation. By comparing this between young and old tendon, it was also possible to characterise the effect age had on the chemical changes occurring within the tendons in the remineralisation process. Thus, the aim of this chapter was to identify the links between mineralisation and potential problems which can arise leading to unhealthy ageing of this collagenous tissue.

After successful demineralisation when all mineral content was removed from the old tendons (**Figure 32a**), both young and old tendon where incubated in SBF with ion concentrations very similar to human blood plasma (87). Staggering the treatment in the manner shown below (**Table 7**) allowed for comparison of young vs old tendon on a day to day basis. The results show how chemical composition of the tendon particularly the mineral content and the collagen related components change ex vivo over a period of 2 weeks.

Table 7: Schedule for data collection of chemical analysis for tendons during incubation in SBF using Raman (same as Table 2; Chapter 2)

Tendon	Chemical analysis (Raman)
LFHL-12	Day: 1, 6, 10, 14
RFHL-12	Day: 3, 7, 13
LFHL-15	Day: 1, 6, 10, 14
RFHL-15	Day: 3, 7, 13

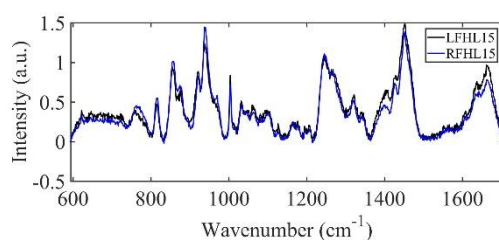


Figure 32a: Average spectra for demineralised tendons – (RFHL-15 and LFHL-15)

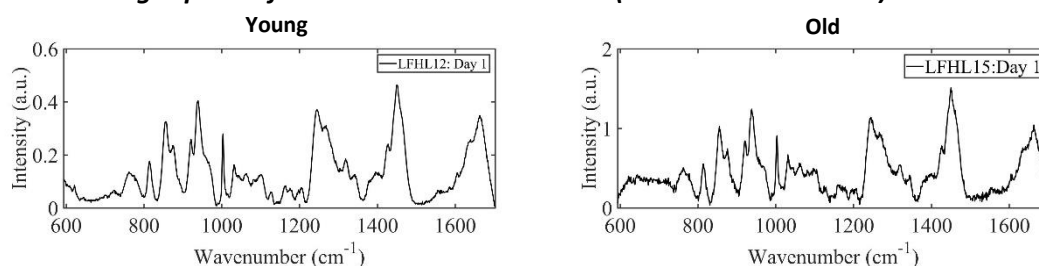


Figure 32b: Average spectra for remineralised tendons – day 1 (young; LFHL-12 and old; LFHL-15)

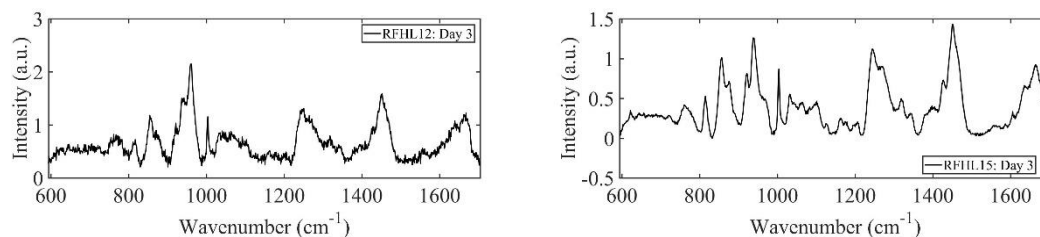


Figure 32c: Average spectra for remineralised tendons – day 3 (young; RFHL-12 and old; RFHL-15)

The progression of changes that occurred chemically within each tendon was monitored by acquiring spectra daily. After 1 day of incubation, there were very minimal changes to the chemistry of the tendons (**Figure 32a**). There was no evidence of a mineral profile however overall intensity of collagen related peaks; amide I band – 1620 cm^{-1} compared to the demineralised samples had increased slightly (**Figure 32b**). The organic content (CH_2) peak – 941 cm^{-1} had a reduced average intensity after the first day of remineralisation (decreased from 1.36 to 1.16). Within the amide III region there is not much change (1.03 to 1.06) in intensity of the largest peak (between $1220\text{--}1340\text{ cm}^{-1}$), however there is a slight decrease in the peak around 1320 cm^{-1} (0.55 to 0.47). The slight fluctuation between these chemical components is expected as the tendons make an adjustment acclimatizing to the new ionic environment before initiating the remineralisation process.

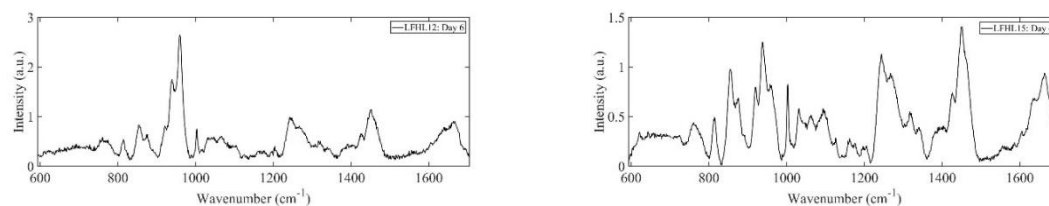


Figure 32d: Average spectra for remineralised tendons – day 6 (young; LFHL-12 and old; LFHL-15)

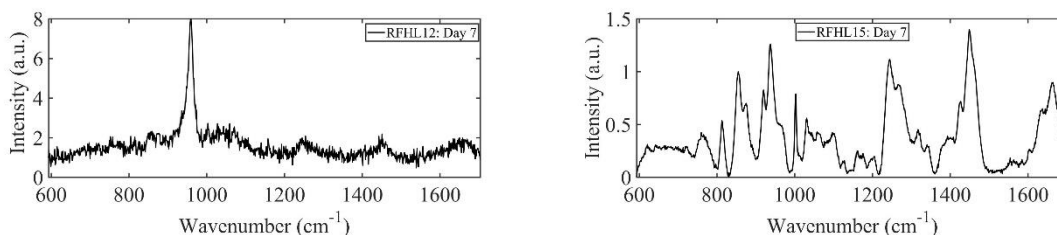


Figure 32e: Average spectra for remineralised tendons – day 7 (young; RFHL-12 and old; RFHL-15)

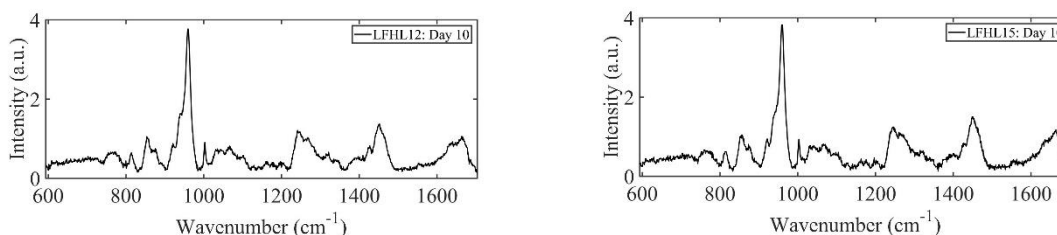


Figure 32f: Average spectra for remineralised tendons – day 10 (young; LFHL-12 and old; LFHL-15)

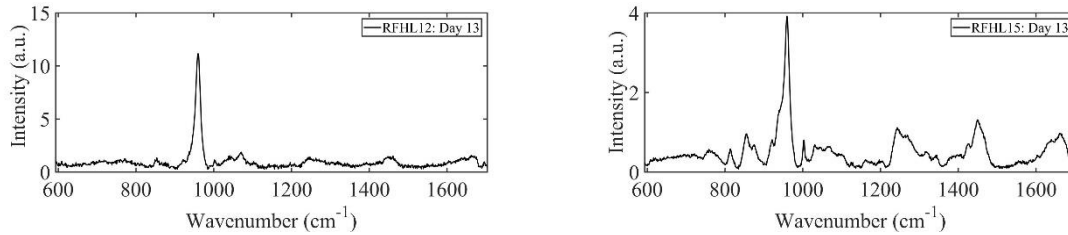


Figure 32g: Average spectra for remineralised tendons – day 13 (young; RFHL-12 and old; RFHL-15)

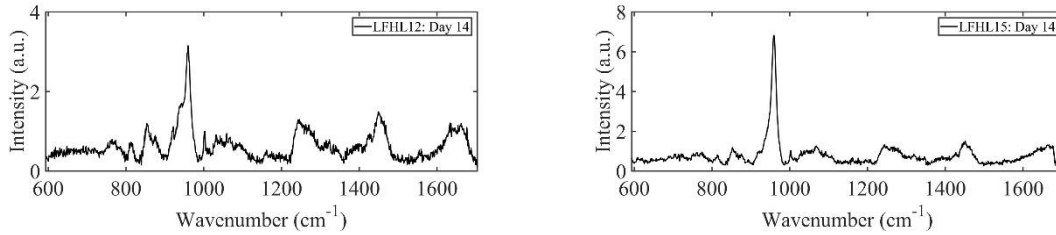


Figure 32h: Average spectra for remineralised tendons – day 14 (young; LFHL-12 and old; LFHL-15)

Commencing day 3 changes to the mineral content of the tendons were evident (**Figure 32c**). These changes were more definitive in the young tendon compared to old tendon. Comparing them chemically along the length of a tendon revealed greater detail to changes which took place in the collagen aside from the mineral content (**Figure 33**). Day 3 initiates the trend where mineral regions were present in areas of low amide III:I ratio intensity. This is observed particularly at distal and proximal ends of the tendon and progressing proximally along the tendon (**Figure 33**).

A threshold is reached where the highest peaks of amide: phosphate intensity ratio overlays with a region of high amide III: amide I; **region C & D**. This is a region that is indicative of a non-mineral region, which is most likely to never become mineralised (**Figure 33**).

By day 6, mineral content continues to increase with the young tendon starting to overtake the old one particularly in the right tendon (**Figure 32d**). In the old tendon at this day specifically, the shape of amide III: I ratio (collagen) almost mirrors that of the mineral; amide III: phosphate ratio (**Figure 33**). This confirms a natural progression of mineral deposition in the old tendon whereby the collagen seems to change by responsively adapting to the increased deposition of mineral. This is very different to the young tendon.

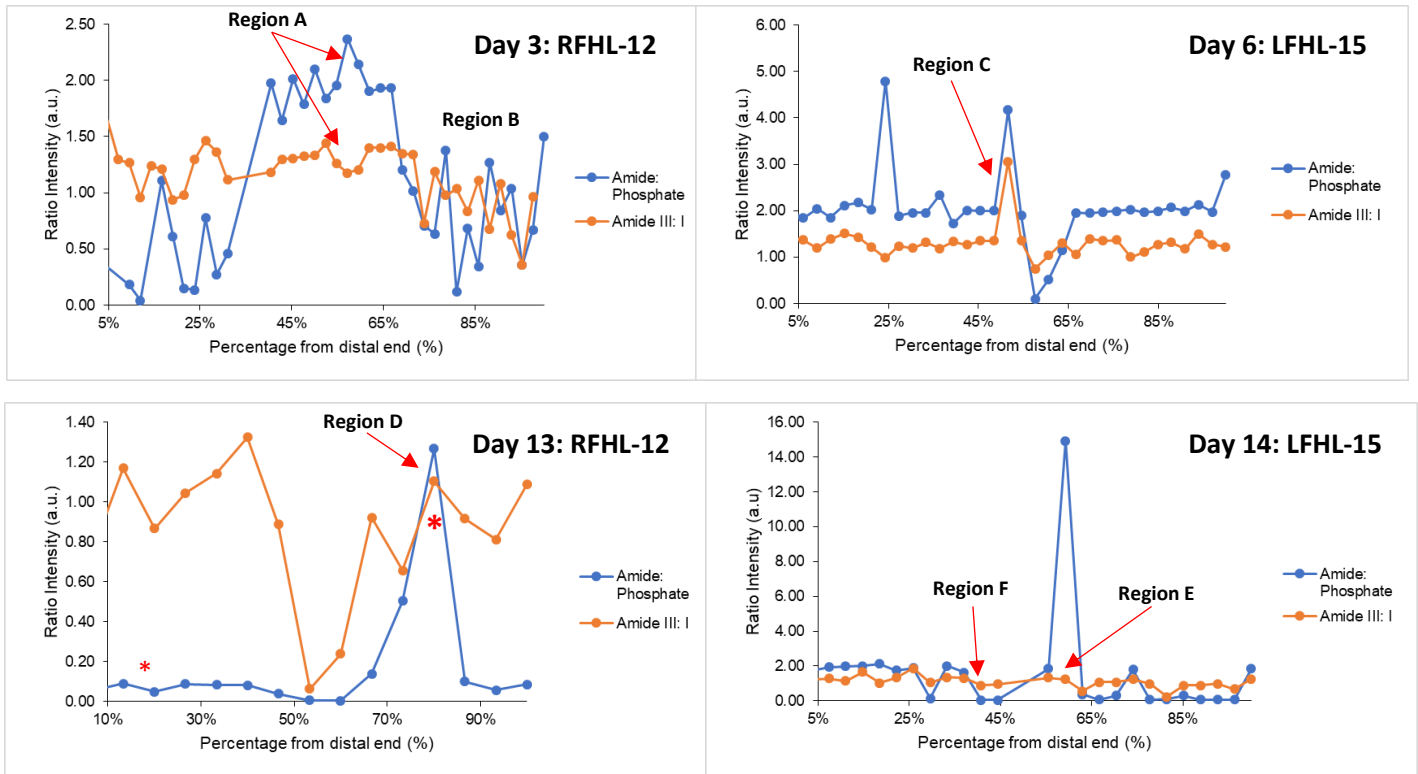


Figure 33: Chemical analysis of mineral and collagen changes along length of young and old tendon at various timepoints during the incubation with SBF. * indicates a transition zone from mineral to non-mineral.

Looking closely along the length of the tendon at day 13 there is a percentage shift of **region D**. **Region D** is distributed further proximal in young (RFHL-12) tendon compared old (LFHL-15) tendon; **Region E**. This could be the potential cause of the young tendon (RFHL-12) snapping in solution at day 6 (**Figure 33**). This suggests this trend is a feature of the earlier stages of remineralisation; day 3 & 6 as opposed to the endpoint; day 14 whereby the high amide III: phosphate coincides with a reduced amide III: amide I, **region E**. By day 7; the halfway mark of the experiment, the young right tendon became fully mineralised, losing almost half its weight (in overall mass) (**Table 8**). Day 10 saw both young and old left tendons producing almost identical spectra. It was interesting to see how these tendons would progress from here.

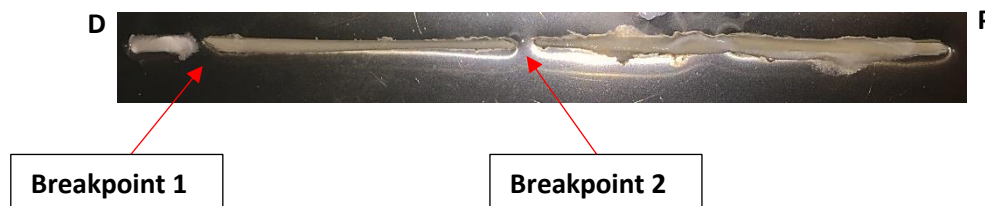


Figure 34: Breakpoints in RFHL-12 tendon found at day 6 of SBF incubation

The mineral content of both old and young tendon increased but the young tendon (right) seemed to increase at rate faster than expected per day. This was clarified in day 13 and became apparent when the tendon snapped at specific regions adjunct with mineralisation zones (*) earlier on in the duration of the

experiment (**Figure 33**). Both breakpoints were in non-mineral regions with the first breakpoint being a predicted “Never mineralised” region if this tendon were to age. This is indicative of the chemical changes in the collagen at these specific regions. By day 12 along much of the length of the tendon, the ratio intensity of amide III: phosphate is very low (under 0.1) indicating a very high amount of phosphate (mineral content). It was very likely that the RFHL-12; young tendon would become the most mineralised by the end of the experiment which was confirmed by day 14. Despite day 13 being quite close to day 14 in duration with both young and old tendons now having a high profile of mineralisation, the collagen properties; amide III and amide I varied.

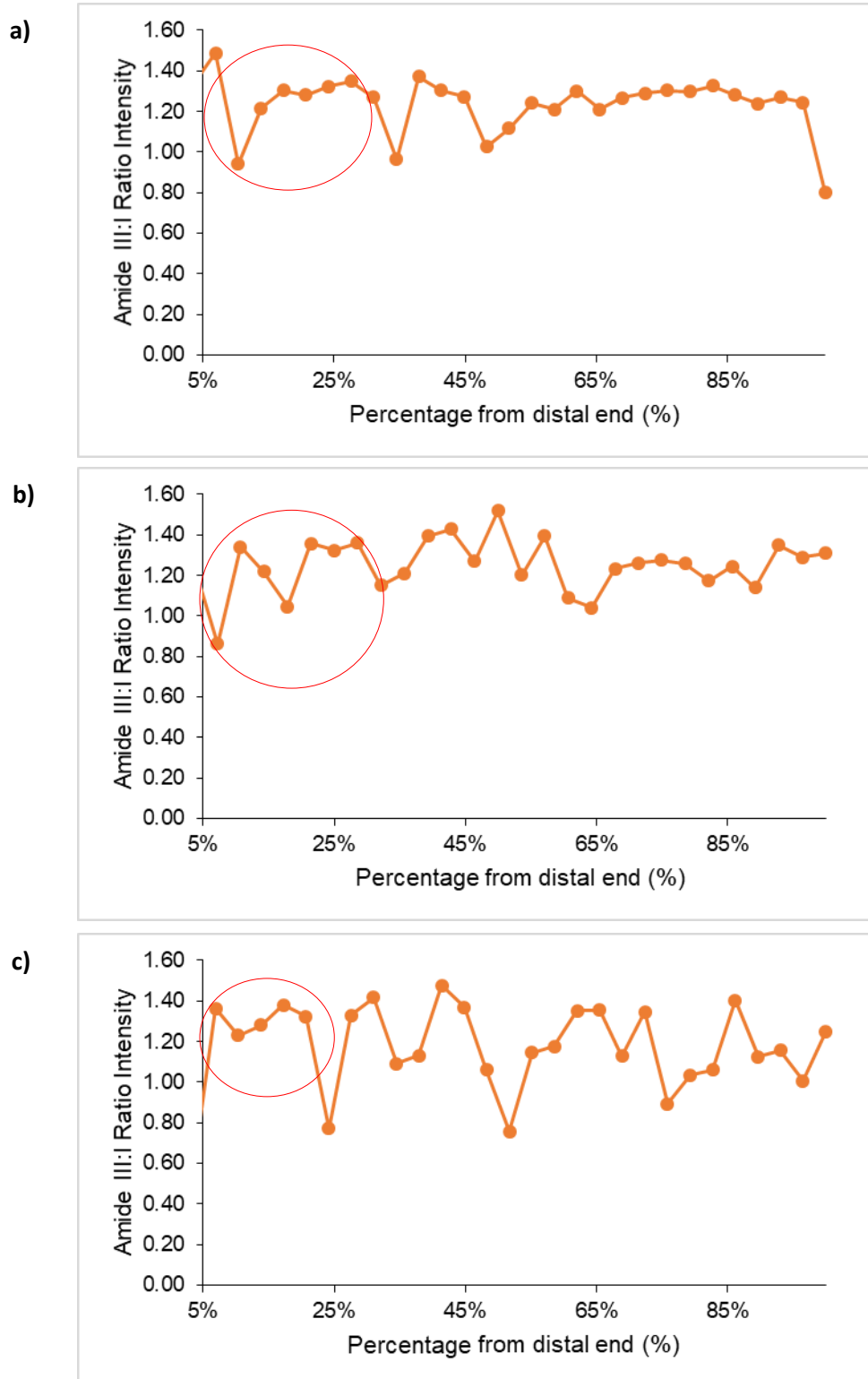


Figure 35: Changes in the collagen of the right old tendon along length during incubation with SBF at a) day 3 b) day 7 c) day 13. Circles indicate regions of similar amide III:I ratios thus collagen chemistry retained through SBF incubation

Comparing the amide III: I ratio intensity was indicative of changes that occurred in the structural integrity of the collagen throughout incubation with SBF. Changes are very subtle in fact the range of values of the ratio intensity stays relatively the similar throughout progression of the right old tendon fluctuating between 0.8-1.5. Looking across the length, the chemistry at particular regions has been retained. The red circle shows this trend in the 1st mineral region (**Figure 35**).

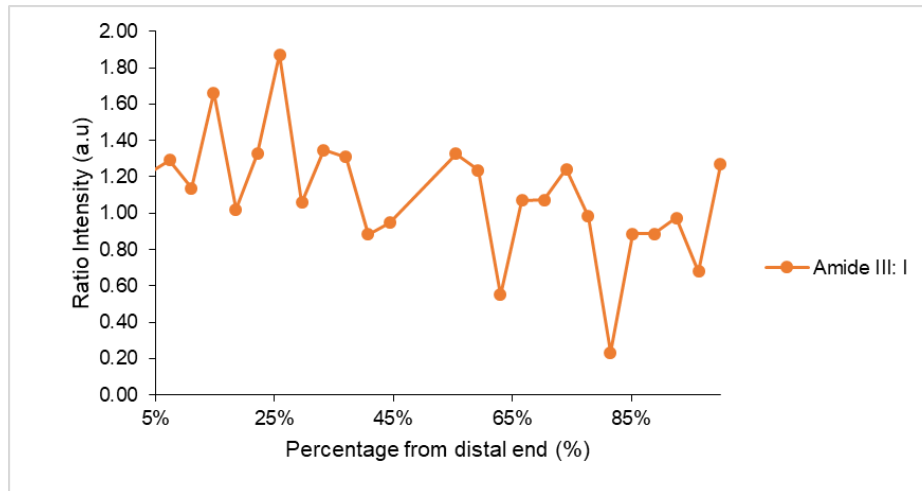


Figure 36: Collagen analysis (Amide III: I) in Left old tendon; Day 14

The experiment ended on day 14 marked and all tendons were removed from SBF. The left young (LFHL-12) tendon did not follow in the footsteps of the right young tendon (RFHL-12) in overtaking its old counterpart (LFHL-15) in mineralisation level (**Figure 32h**). Looking at the left old tendon there is a more natural mineral profile adjunct to changes in the collagen by the end of the experiment (**Figure 36**). The amide: phosphate intensity along the length of the tendon remains quite low; an indication in regions of high mineral content; **region F**. In non-mineralised regions, ~26% from the distal end, the amide III intensity is 2-fold higher than the amide I ratio. Overall there is a continual decrease in amide III:I ratio intensity moving proximally to increased mineral with the lowest point of amide III:I region coinciding with the lowest amide III: phosphate ratio intensity; **region F** (0.04 – 41% from distal end).

Initially the downward trend in the amide III: I ratio intensity which coincided with high amide III: phosphate regions seen in day 3 of RFHL12 tendon is characteristic of no mineral presence (**region A**). As the sample is left in SBF for an increased period of days, by day 12 it is in fact a region further proximal; **region B** which remains un-mineralised and not **region A**. **Region B** persisted as non-mineralised until Day 12 (labelled as **region D**). Compared to the old tendon LFHL15, it is possible that chemical changes in the collagen occurring within this region happened at a faster rate than it should have (**Figure 36**). The normal rate of mineralisation is seen the old tendon; day 14 (**Figure 33**).

Table 8: Variation in the weight of the tendons before, during and after incubation in SBF

Tendon	Weight before SBF incubation (g)	Weight after 1 wk of incubation (g)	Weight after 2 wks of incubation; end (g)
LFHL-12	0.75	0.48	0.47
RFHL-12	0.68	0.31	0.31
LFHL-15	1.10	1.17	0.89
RFHL-15	0.63	0.67	0.67

Monitoring the weights of the tendons showed a decrease in weight of the young tendons and a very small increase in weight of the old tendons, which was evident from the halfway point of the experiment (**Table 8**). This also showed that as well as the youngest tendon becoming oversaturated with mineral, the most mineralised lost a substantial amount of mass compared to its less mineralised counterparts (**Table 8**). By the end of the 2-week period all tendons had lost weight except the right old tendon (RFHL-15). It is expected that the tendon should weigh more with greater mineral as the tissue become more densely packed due to the addition of mineral, however the rate of mineralisation that took place points in the direction of a very fast and unnatural process causing the mineral to also replace the water content within the tendons, hence dehydrating them which would explain the brittle appearance of the highly mineralised tendons and their final lower weights (g). Previous literature has shown that increased mineralisation leads to tougher tendons and increased hardness but also at a compromise to the structure, which is brittle (92).

4.6.2 Analysis of SBF results

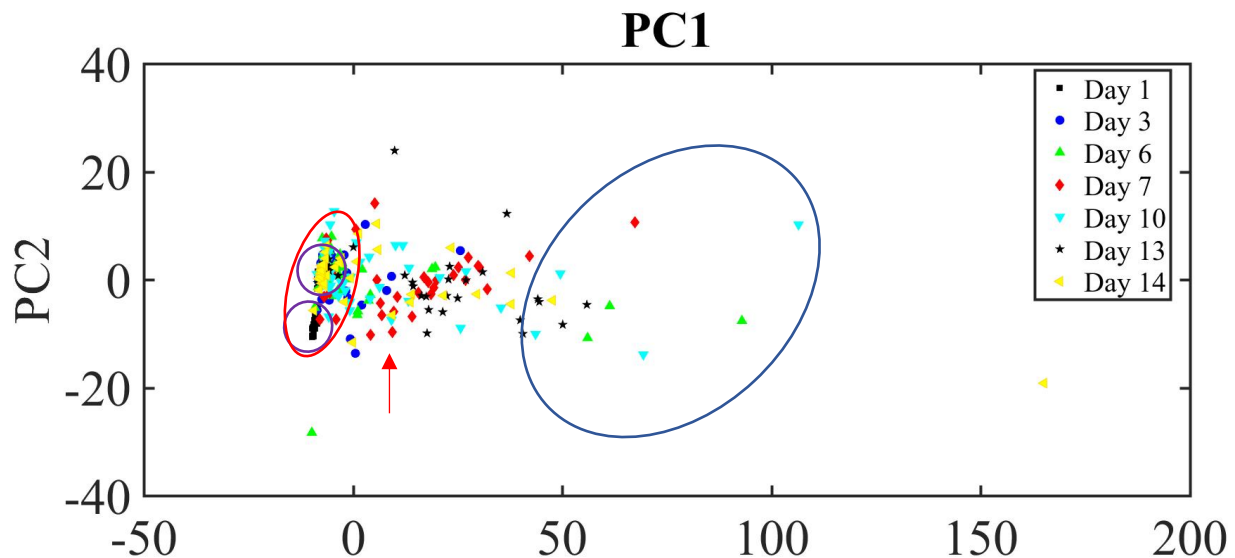


Figure 37: PCA plot showing distribution of tendons during incubation with SBF relative to PC1 and 2. Blue circle indicates spread of the data in this area of the plot while red circle indicates the clustering of spectra within this region particularly the purple circles within this circle are groups of spectra from day 1

(bottom) and day 14 (top) respectively. The red arrow highlights the days in which spectra begins to become more spread. Data is colour coded according to day of chemical analysis; day 1-14.

The same colour code was used in the PCA plot legends for easy comparison between PCA plots (**Figure 37-40**). Initially looking at the right young tendons, they were more similar in chemical composition (mineral content) in days 3-7 and start to differentiate as the days progress suggesting a change in the level of mineral which is shown in the PCA plot. Most of the spread in young right tendon was occurring due to spread further along the progression of the experiment e.g. day 10 and become more spread as the days progressed. The right tendons were more spread in PC2 than PC1. This correlated to a similar level of mineralisation in the earlier days 3-7 thus the trend seen in PC1. PC2 showed a greater level of changing collagen organisation contributed to the mineralisation profile in the young tendons as the days progressed (**Figure 43**). The spread became more apparent after the halfway mark of the experiment period (red arrow) (**Figure 41**); day 6,7 until 14 respectively showing a difference in the way the tendon regions was mineralised accompanied by the rate of mineralisation described earlier (**Figure 32**).

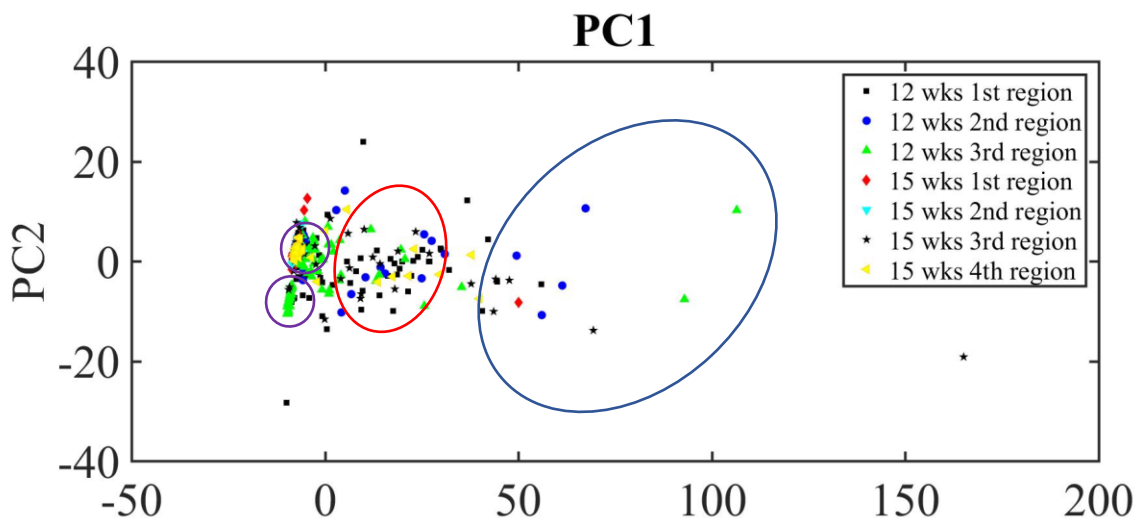


Figure 38: PCA plot showing distribution of tendons during incubation with SBF according to region with respect to age relative to PC1 and 2. Blue circle indicates spread of the data in this area of the plot. Red circle identifies the regions of the young tendon which contribute to the variation in day 3. Purple circles identifying the regions of tendons spectra within day 1 (bottom purple circle) and 14 (top purple circle).

After day 14 and with knowledge of the type of regions in young and old tendons prior to SBF it was possible to categorise the data according to the number of regions present in each age group. They could not be classified as the distinct mineral and non-mineral regions because there was a changing level of mineralisation throughout the progression of this experiment and so it was possible that the position of these regions could change. The young tendons had 3 possible regions while the old tendons had 4 possible regions (**Figure 38**). This made results comparable to the distribution of data with known mineralisation profile thus distinct regions of mineral and non-mineral (**Figure 39**). The right young tendons showed a different chemical profile from other tendons. By day 3, all 3 regions of the right young tendon (red circle) (**Figure 38**) varied chemically from the big initial cluster of spectra from the other tendons (red circle) (**Figure 37**).

There were minimal differences in the position spectra other than the right young tendon spectra relative to PC1 and 2 because of the chemical similarity in the old tendons up until day 10 (**Figure 37**). By day 14, 7/13 left old tendon spectra caused the spread of the data (blue circle) (**Figure 38**). This was followed by the left young tendon in the 3rd region specifically a spectrum in day 6 and another in day 10 (green triangles in blue circle) (**Figure 38**). These regions compared to the non-min regions before SBF incubation. Overall the left tendons had the most variance. There were also some spectra in the left tendon which remained chemically similar in day 1 as day 14 (**Figure 37**). In the old tendons these were mineral regions and in the young tendons were non-mineral regions. Through the progression of SBF incubation it became apparent that the tendon regions that did not mineralise by day 14 were most likely to never mineralise. These spectra clustered in a similar way to those in the “Never min” region before SBF (**Figure 40**) therefore this underlying chemical element was conserved despite remineralisation. This region was characterised between 37.9 – 62.1% from distal end in most old tendons therefore points of the tendons anyway between this region could potentially never mineralise.

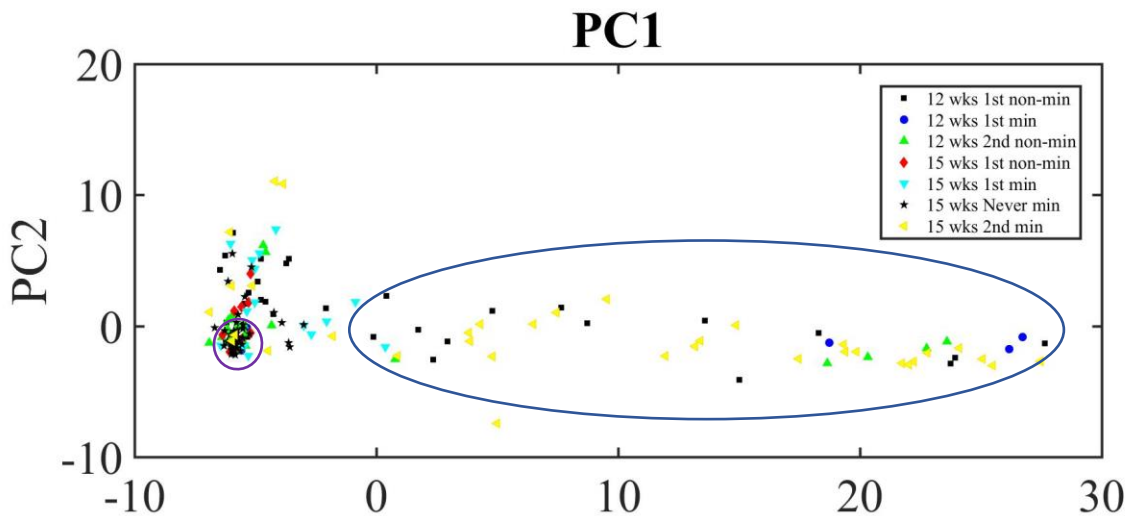


Figure 39: PCA plot showing distribution of tendons before SBF incubation with respect to chemical regions and age relative to PC1 and 2.

Comparing PCA after SBF (**Figure 38**) with PCA before (**Figure 39**), there are 2 main groups of data. These were more easily identifiable before SBF compared to after. It was possible to determine the nature of the level of mineralisation in the 2 areas (red circles) in the PCA plot post SBF (**Figure 40**). Within the blue circle (**Figure 38**), the heavily mineralised tendons regions by day 13 after SBF incubation were the only group to be in a similar position relative to PC1 and 2 before SBF (**Figure 39**). They would be spectrally similar the 2nd mineral region of the (15 wks) old tendons (**Figure 39**) due to the spectra present being the the 4th region along the old tendon which was previously defined as the 2nd mineral region along the length of the old tendon (**Figure 38**). This outcome was expected because PC1 is separated by the level of mineralisation with high mineral at the opposite end to low mineral (**Figure 41**).

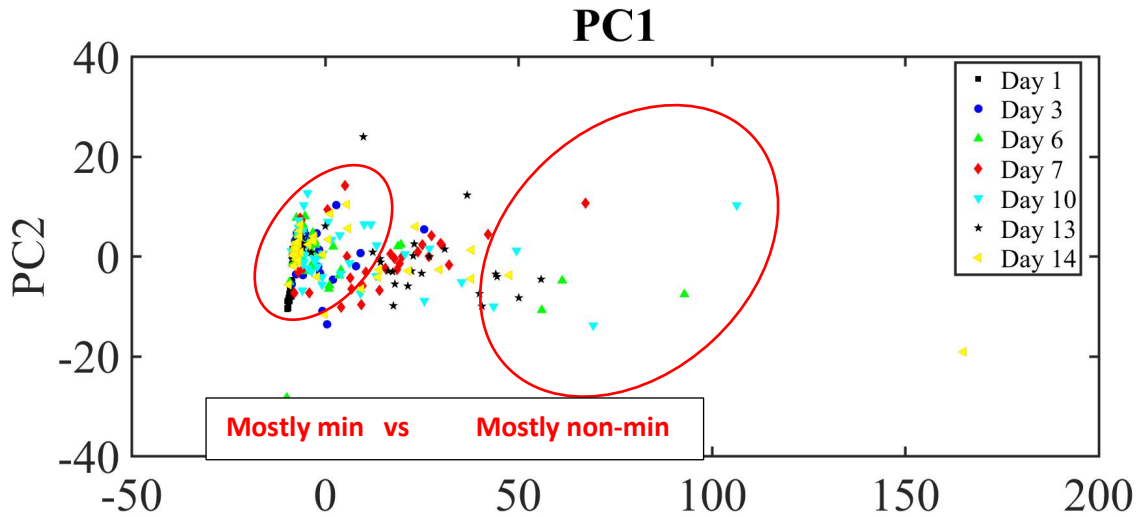


Figure 40: PCA scores plot of the difference in the level of mineralisation across the plot. Spectra were colour coded according to day of chemical analysis during SBF incubation.

The most noticeable difference between both experiments is the way the data is distributed relative to PC1 and PC2. Comparing loading plots from both sets of data the mineral peak is the same chemical feature which contributes to the most variance along PC1 which is expected (**Figure 41**). The smaller red circle consisted mostly of tendon regions which were spectrally similar hence the cluster. These spectra were identified from mostly mineralised regions compared to the spectra allocated by the bigger red circle. These were spectrally dissimilar displaying high variance amongst the data and were identified from non-mineralised regions. This was very different compared to the cause of the high variance and interclass variation before incubation with SBF (**Figure 39**). There was a shift from mineralised regions to non-mineralised regions attributing to the spread of the data. Before SBF incubation although some tendon regions with non-min components - 12 wks 1st non-min region (**Figure 39**), they remained contributors to the high interclass and intraclass variance there was an increase in this number and a decrease in the number of mineral regions contributing to the spread. This was interesting as it revealed there was a difference in way the tendons mineralised after remineralisation with SBF.

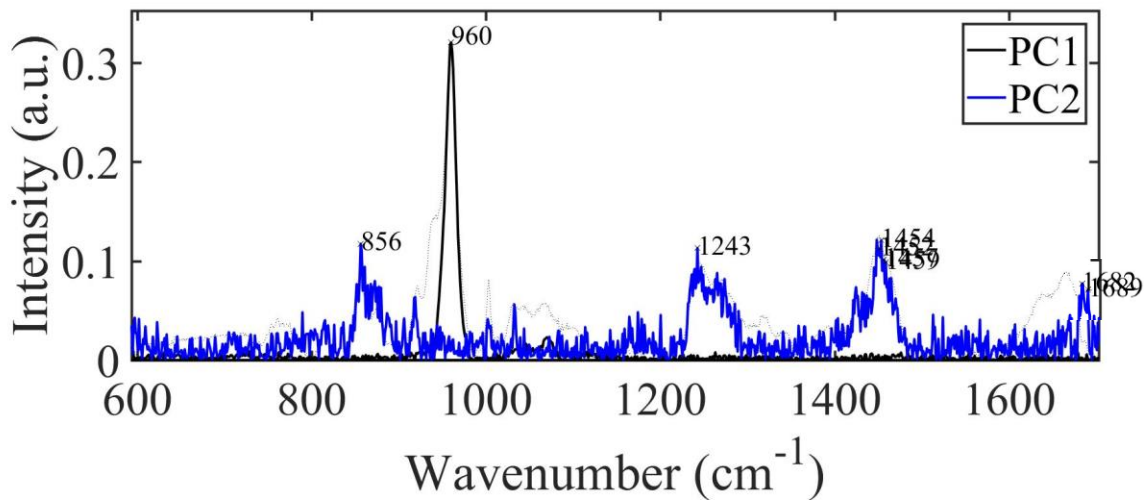


Figure 41: PCA loadings plot identified the mineral phosphate at 960 cm^{-1} as the main factor contributing to the spread of the data along PC1. PC2 identified a range of structural chemical components as the contributing factors to the collagen organisation as the mineralisation varies through the day to day progression of SBF incubation.

4.6.3 Visualising the effect of SBF

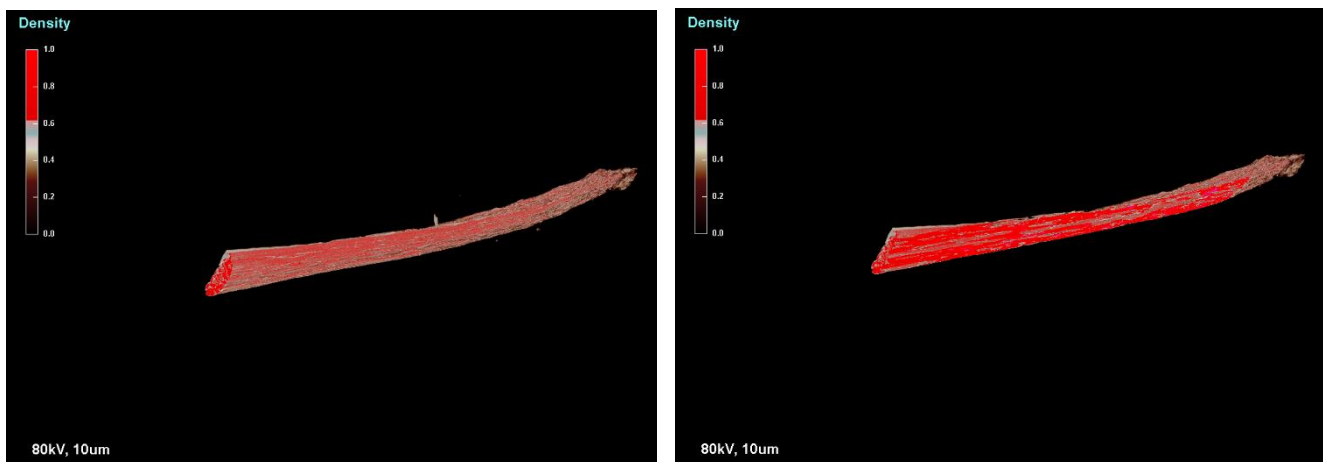


Figure 42: Micro-computed tomographic (micro-CT) imaging of young tendon

Left: Surface rendered 3D model showing mineralised region in the proximal end of treated RFHL12 tendon
Right: Reconstructed cross section of RFHL12 tendon with discrimination between densely packed mineralised collagen fibrils (red) embedded under surface of tendon (white) rendered with CTvox.

Tendons were scanned under microCT to visualize the difference structurally from changes to the chemistry. Micro-CT imaging showed density ratios within tendon after incubation in SBF. Regions of greater mineralisation were associated with greater density as the tissue within the tendon is more densely packed (93). **Figure 42** shows, linearity and regular arrangement of the collagen fibrils. The collagen fibrils become more aligned during mineralisation (35). Thus, the regions on the colour chart associated with higher density are an indication of the mineralisation profile within the tendon. As we cut

into the tendon using CTvox software (Skyscan 1275, Bruker, Belgium) the mineralisation profile increases thus revealing that mineralisation is embedded in the tendon. This young tendon (**Figure 42**) looks to be oversaturated with mineral having the highest mineral peak at the end of the 2-week period (**Figure 32g**). However, understanding that the micro-CT used X-rays to produce this image it can be appreciated that density is relative to the surface of the tendon and showed clearly that mineral deposits just under the surface of the tendon.



Figure 43: Micro-CT imaging of old tendon

Left: Reconstructed cross section of untreated LFHL15 tendon (distal region) with discrimination between non-mineralised collagen fibrils; brown, embedded under surface of tendon; white, rendered with CTvox (SkySan 1275, Bruker, Belgium). Right: Surface rendered 3D model of proximal end in LFHL15 tendon with detail of density distribution along surface of tendon.

It is easy to see the difference between a mineralised region and a non-mineralised region. Cutting into the old tendon (**Figure 43**) depicts a non-mineralised zone displayed at a brown region in the density colour chart and lower down on the scale indicating tissue which is less dense (**region E**). This confirms the chemical analysis of this region with a no/little mineral present in this area and/or the low level of mineralisation present around the surface of this area as seen in the surface rendered 3D model at the proximal end of this tendon (**Figure 43**). The chemical and structural difference is also clear between the young (RFHL-12) and old tendon (LFHL-15) evident in the way the two mineralised (**Figure 42 & 43**). By the end of the 2-week period the young tendon having a substantial amount of mineral compared to the old tendon which has previously demineralised prior to mineralisation by SBF.

5 Discussion

The turkey-leg tendon system is a strong model for the mineralisation process in collagen (49). This study has specifically defined 3 main factors which have the greatest contribution to the way this process takes places in collagenous tissue. This includes the structural integrity which defines the underlying chemistry and its importance for assessing the predetermined assembly of the collagen triple helix in tendons and how this tissue compares to bone. Collagen is the major protein component of the organic matrix in bone, thus using bone as reference point to see if the mineralisation in tendons was expected. The mechanical integrity, which puts this type of connective tissue in the context of its function for locomotion in the domestic turkeys, *Meleagris gallopavo* (42). The tissue bioactivity conducted *in vitro*, which mimics changes in an *in vivo* system; using the TLT model to analyse how this tissue will adapt/develop to a changing environment. Therefore, evaluating all these factors using novel testing techniques allowed an in-depth investigation of the link between mineralisation and problems that can arise during ageing.

5.1 Collagen's structural integrity

Literature has proposed that regions of turkey tendons as young as 12-weeks in the TLT system start to mineralise and become fully mineralised by 18 weeks. Changes in the collagen properties are evident in as young as 11-weeks (35) (48) (51). These regions are distinct and using several multidisciplinary techniques, the properties which contribute to these differences could be analysed. In this study 12 and 15-weeks-old turkeys were examined to analyse these two age groups during the occurrence of mineralisation and how changes progress from old to young.

Multidisciplinary techniques revealed great variability in the mineral profile in both age groups. This was indicative of differences that occurred in the level of mineralisation between the young and old tendons. This included differences in the maturity (**Table 4a**) and the number of mineral regions. It was expected that old tendons had at least two distinct zones of mineralisation while young tendons had one zone or points of immature mineral (**Figure 21**). The collagen organisation predetermined the maturity of each region thus regions furthest proximal from the distal end always have more mature mineral. The 1st mineral region (distal) in the old tendon was less mature than the 1st mineral region (proximal) in the young tendon. The 1st mineral region had less mature mineral than the 2nd mineral region in the old tendon (**Table 4a**). The mineral region in the young tendon at the proximal end of the tendon encompassed a combination of low and high mineral maturity therefore included mineral that was more mature than the 1st mineral region (distal) of the old tendon.

Comparing bone to tendon, bone's 2nd mineral region had the most mature mineral which was the 2nd furthest proximal from the distal end (middle region). While bone's 1st mineral region in the young bone which was at the distal end (Figure 3b). Unlike tendon the mineral maturity of the old bone did not vary much because much all regions along the bone are mineralised. The difference in maturity of bone takes place during the remodelling of bone cells causing changes to level of mineralised tissue during bone growth (2). These changes were more evident in the young bone than the old bone indicative of the level of growth from the young to the old bone (**Table 4b**).

There was an overlap in the level of mineralisation across specific zones along the length of the tendon which was expected because of the proximity of regions from one another with the start of a mineral region being adjacent to the end of a non-mineral region. The overlap was due to the same chemical

properties across both age groups which are conserved due to the nature of the tendon for its function on a day to day basis of maintain elastic energy during load bearing activities in the life of a turkey (50).

Raman spectral signatures in combination with PCA confirmed these differences between old and young tendon very effectively. It is evident that LDA resulted in the overfitting of the data and a lack of extrapolation that could be gathered from spectral differences between old and young tendon (**Figure 20**). PCA-LDA was considered but it was clear that the trend displayed by the data was adequate to identify variance in the chemistry of the tendons. PCA-LDA conveyed the difference between regions and particularly mineralised regions which were already visualised in PCA. PCA-LDA was unable to provide any additional information (**Figure 19**). This was expected because there was not enough spectral data to show differences within groups. No further information could be extracted using PCA-LDA (**Figure 20**) compared to PCA (**Figure 16**). This was because there was no change in the chemical features which caused the variance in both forms of analysis. Overall, as PCA is an unsupervised technique, and identifiable specific differences, compared to the supervised PCA-LDA, it was used as the primary analysis technique with the added benefit of reducing the chance of bias. Other analysis techniques are available and could be explored in future such as partial least square (PLS) (94).

Collagen parameters revealed from PCA were great indicators of the chemistry of the underlying structure in relation to the mineral (**Figure 15**). Much of the non-mineralised collagen in young tendon was more easily influenced by changes induced in mechanical testing (**D & E; RFHL-12 - Figure 15i**). Young tendons are more likely to exist in the non-linear state (**Figure 26**) because they possessed crimp morphology hence less energy is required to work against mechanical load (95). This differs in old tendons; the collagen becomes less easily influenced with age particularly when transitioning into mineralisation zones causing a loss of crimp morphology. Crimps straighten, altering the structural integrity thus harden the tissue resulting in high modulus. Old tendons had higher moduli because they possessed more of these mineral regions (**Figure 26**). The collagen here adopts a regular arrangement. There was increased organisation whereby mineral influenced change in the density of the tissue depositing around and within collagen fibrils (**Figure 32**).

A range of collagen parameters had a specific influence on the change seen in mineralisation profile in young vs old tendons. Changes in amide bands, specifically conformational changes are attributed to the changing of the structure of the collagen network and are adapted for onset of mineralisation. The collagen becomes more rigid by the alignment of collagen matrix becoming more uniform in a regular self-assembled structure preparing the tendon for mineral deposition (51). The changes in amide III:I ratio intensity seen in old tendons were very similar before and after tensile loading as the extra fortification of the triple helix of the collagen prior to mineralisation made it harder for structure to change (**A & B; Figure 15i**). Therefore, when there was a change in structure this was followed by increasing work done mechanically in old age for the same functional process in young tendons (80-100% from distal end of old tendon).

The changes in the apatite transition during mineralisation were indicative of the crystal maturity because this occurred spontaneously with higher mineral phosphate peaks (**Table 4**). Immature mineral contains greater amounts of carbonate in the apatite; the inorganic crystal component of the mineral (**G & H; Figure 15ii**). As mineral matures OH^- replaces CO_3^{2-} ions increasing amounts of hydroxyapatite as oppose to carbonated apatite. Hydroxyapatite (HA) is one of the most stable forms of the mineral salt; calcium phosphate. Its strong anisotropic properties determine the orientation pattern of the crystal which is

known to increase the macroscopic mechanical properties therefore stability of the mineral and its collagen bonding ability (96). For this reason, it was also harder to change the structure of more maturely mineralised tissue during tensile load.

Stability was another consistent feature influencing mineralisation within the tendon. Changes in hydroxyproline: proline ratio is associated with stability of collagen. Higher ratio of hydroxyproline is indicative of higher stability; collagen stability. Hydroxyproline is an important amino acid which denotes structural integrity. Hydroxylation of lysypyridinoline is associated with increased mineralisation. The collagen triple helix here hence the collagen backbone was fortified in more regions after mechanical load (**K; Figure 15ii**). Hydroxyproline is unique to collagen and should be consistent (~14% of collagen weight) (97). Therefore, changes in the hydroxyproline: proline intensity ratio were indicative of changes caused by proline. Hydroxyproline permits sharp twisting of the collagen triple helix and is necessary for repair in damaged areas (98). This provides the appropriate environment for the required mineralisation levels with increasing mineral around the collagen backbone thus strengthening the tendon structure.

5.2 Collagen's mechanical integrity

The structural integrity of the tendons was affected by the mechanical properties displayed by the tendon. Tendons existed in a viscoelastic state encompassing a variation of strains corresponding to toe, linear and yield regions during uniaxial loading. Young tendons were more flexible because of the position of hydroxyproline relative to proline (99). This makes the collagen strong elastically. The mechanical properties of collagen were not hindered by the mineral and able to withstand higher strain (**Table 5**). These tendons do not reach yield region too early at lower strains because the collagen fibrils can orientate themselves efficiently in the direction of tensile load. In old tendons this action is compromised (due to mineralisation) in particular in mineral regions as the collagen is surrounded by mineral. The collagen fibrils here are orientated into organisation with respect to mineral and so if the tensile load is trying to orient the collagen fibrils more than the mineralised tissue can withstand, this affects the ability for the collagen to change thus strain which could be applied was reduced (5-2.5%). The decreased strain at the point close to failure of old tendon was due to the increased number of cross-links within the collagen fibril (51). This could also be due to several other factors such as the cycling of elastic strain energy in the older tendons (42). Therefore, the elastic potential of the collagen tissue is affected, as well as affected by the tendons being tested mechanically ex-vivo.

The cross-links of the collagen fibrils were important. At very high strains the cross-links between the collagen fibrils would break due to mechanical deformation. Chemical cross-links stabilise collagen fibrils resulting in high tensile strength (100). These include enzymatic (hydroxylation) and non-enzymatic cross-links (glycation). PGs such as decorin regulate the formation of enzymatic cross-links (101). AGEs correspond to the amount of non-enzymatic cross-links and are regulated by glucose-mediated reactions (10) (102). As the collagen matures there is an increase in trivalent cross-links (103). This produces pyrrole and pyridinolines. The ratio of pyrrole: pyridinoline varies between bone and tendon with mineralised tissue having low levels of pyridinoline (104). Young tendons mainly consisted of non-mineral regions therefore have more hydroxylysyl-pyridinoline cross links (35). Old tendons have an increased number of mineral regions thus more lysyl-pyridinoline mature cross-links (35) contributing to underlying collagen's tensile capacity in this region.

Old tendons reach physiological upper limits of yield earlier due to mineralisation. It was expected that calculating the Young's modulus would provide a consistent value for the tensile strength of the tendon (42). FHL tendons from turkeys weighing between 3.1-4.0 kg (~7-8 weeks old) (105) would possess an EM around 1479 ± 106 MPa while FD tendons are a bit lower at $948 \pm 85 - 1390 \pm 82$ MPa (42). Therefore, it is expected that old tendons should have greater EM according to the literature (42). There were differences in values according to the literature and the results from mechanical testing due to increased mineralisation as the TLT matures.

There was also variation between actual EM results in young and old tendons. It was difficult to determine whether this was caused due to the unique nature of the testing used (**Table 5**). Common methodological challenges that can arise with this approach include clamping of the tendons. This can result in an underestimate of the tendon's strength due to slipping or damage at interface between tendon and clamp (42). This may provide a reason for the very low EM for young tendon (RFHL-12) (**Table 5**). The linear region of the stress-strain activity in old tendons had a higher gradient thus increased modulus. Much of this effect results from a combination of all regions present in the tendon with the mineral region greatly influencing the modulus on the tendon overall. The older tendon was able stretch further beyond resting limit compared to young tendon thus a larger elastic modulus (**Table 5**). This is advantageous in non-mineralised regions of the old tendon with high ratio of hydroxyproline: proline increasing the mechanical integrity at these regions. There are several regions within tendons which contribute to the overall strength and stiffness, therefore the modulus at each region needs to be measured to determine the overall mechanical integrity. This factor probes finding the moduli with respect to different regions.

It was expected the novel iMetrum VG system would visualise the stress/strain activity with respect to regions of different collagen chemistry relative to the level of mineralisation (82). It is likely that tendon displays different moduli per unit region of the viscoelastic behaviour displayed in the tendon, thus varying stress-strain values as the tendon was subject to tensile loading. The Young's modulus would be ill-defined if coining an effective single modulus for the stress-strain activity of the tendon during tensile loading. This is evident in the experimental data for each tendon revealing different length of each stage of the viscoelastic curve i.e. toe region, linear region and yield and field were different per tendon (**Figure 26**). However, the Young's modulus was valid for the linear region it was taken from per tendon and calculations retained a consistent method (91). The VG system was useful in testing the non-linear and viscoelastic component of the tendon, a rarity because of the difficulty of testing these components. Marking the tendon in a regular pattern made it possible to visualise changes in the collagen over a variation of strain. Through this there was confirmed inhomogeneity within the same tendon thus changing moduli throughout the tendon because of physical stretching when subjected to mechanical stress. This adds to the difficulty in coining a single effective modulus per tendon.

Because of the non-trivial nature of the tendon with no standards in determining the modulus, fitting a range of models (82) (81) (91) to calculating the modulus has revealed the potential limitation to the current techniques thus the implementation that can be made to the new system. Finite element analysis (76) was used to model the tendon as a structure with either distributed or variable elastic properties as shown in **chapter 3**. This model shows looking at the displacement there is no obvious difference between varying modulus distributed along the length of the tendon (**Figure 31b**). But if you can compare strain relative to position therefore its distribution along the length of the tendon you could calculate the difference in modulus depending on whether modulus changes in a constant, linear or exponential manner. This novel technique can have remarkable implications in the future. This kind of pattern is

important because instead of producing results as a function of time in the current iMetrum system could calculate a value for a position along the length of the tendon relative to the actual strain at that position.

By using this FEA theoretical model (**Figure 31**), it would be possible to calculate a more accurate and unifying modulus which can class local modulus per distribution of strain. This would make it possible to map a breakpoint in the tendon which occurred during mineralisation (**Figure 36**) and determine whether this was a region of high modulus or low modulus. Subsequently putting this into context it would be possible to predict which regions were more likely to break during tensile loading hence locomotive function. It could be inferred that structural integrity of the tendon here are weakened due to the way the mineral is deposited on the tendon (**Figure 36**) and indicative of problems which may occur during ageing.

Further works would also include calculating the rate of change from one modulus to the next in mineralised regions thus a measure of the rate of mineralisation that occurs between age groups. Based on this model implementations to this system would help provide a more accurate range of moduli characterising regions in an ageing tendon. An effective way of marking the tendon for this system would be needed such as using a surface marker that would eradicate the issue of inconsistency in the pattern marked onto the tendon. Previous techniques explored the use of surface markers or pins glued at regular intervals along the length of the tendon with pins specifically inserted transversely to minimise damage to the tendons (42). The VG system requires meticulous detail to capture the minute stress/strain activity which makes a big difference to the modulus (82).

5.3 Collagen chemistry as related to function

SBF influenced chemical changes of collagen in the tendon through its ability to drive apatite formation during remineralisation (87). Isolating the tendons in an environment with an abundance of ions needed to promote apatite formation revealed information about the bioactivity of the mineralisation process. Mineralisation rate differed between tendons after incubation in SBF (**Figure 33**). The right tendon mineralised faster than left and this was seen particularly in the young tendons. In addition to the results from the previous experiment it is clear the dominance in the right side is inherent and not occurred due to the mineralisation of the tendon. The structure of the collagen in the tendon became adapted during incubation in addition to demineralisation of the old tendons which removed the element of mineral completely, clarifying dominance occurs before mineralisation.

Hindlimbs mineralise in a specific way suggestive of their anatomical location & biomechanical function playing a role in their adaptation (40). The right young tendon became over-mineralised when given an optimum ionic environment compared to the left inferring the right side adapted to greater mechanical load during locomotion. This was an interesting result because the right young tendon became over-mineralised causing the tendon to break spontaneously in solution. This tendon snapped at the transition zone between the “never mineralised” region to mineral region. This region was a small area but the difference in the collagen were unstable causing the tendon to break. The viscoelastic behaviour of the tendon surpassed the upper limits of stress/strain activity in the yield of tendon thus became a weak-point in the overall structural integrity of the tendon leading to its failure. PCA revealed despite the majority of tendon becoming flooded with mineral this region remained un-mineralised. The never mineralised region retains this property because of the absence of specific non-collagenous phosphopeptides; O-phosphoserine and O-phosphothreonine, and γ -carboxyglutamic acid containing peptides which allow the binding of Ca^{2+} amino acids for mineral deposition in the collagen (106). This is

predetermined prior to the onset of mineralisation. This new finding revealed the importance of collagen at structural level for determination of function. Further work would explore when in the ageing process this feature is determined, and the cells embedded in the collagen responsible for this kind of signalling.

It was also evident that the tendons which were demineralised prior to remineralisation mineralised more naturally compared to tendons which were just incubated under SBF. This was expected because the rate of mineral uptake was too fast for natural deposition of mineral within the collagen fibrils. *In vivo*, ECM expression shows differentiation of tenocytes is likely to be responsible for the progression of ossification (40). The precursor for the signalling element governing changes in the collagen was absent from the type of mineralisation that occurred in the tendons in this experiment. Incubation with SBF showed that the tissue favoured calcification over ossification in the event of copious amounts of mineral, thus clarifying the morphological differences that determine which mineralisation process takes place. Ossification is favoured when there is a signalling component usually derived from remodelling. This involves tenocytes which are no longer viable in the SBF experiment because of the timeframe *ex vivo* and the tendon had been frozen. Ossification is more likely *in vivo* at the tendon-bone intersect (107).

The collagen fibrils within the tendon were forced to adapt to the fast occurrence of mineralisation particularly in tendons which did not undergo demineralisation prior to mineralisation. Since tendons were unviable, there are no signalling components to direct the deposition of mineral and slow or counter the influx of excess ions in apatite formation. In a viable tendon, the signalling between within the collagen would be controlled by tenoblasts also known as fibroblasts which differentiate to elongated fibroblasts (tenocytes) with age (108). These regulate the dynamic network between collagen cross links and cell driven ECM interactions (108). Without the influence of these cells the structural component of the tendon; the collagen and the organisation of its fibrils is left to guide the deposition of mineral. To take on copious amounts of mineral, the collagen undergoes changes in its morphology. The collagen fibrils within the collagen becomes straightened within their elastic potential limit (108). This enables a more regular and tight assembly of the fibrils identified by the density of the tissue (**Figure 42**).

Incubation in SBF has shown there is a limit before changes in the collagen at this rate compromises its structural integrity whereby mineralisation becomes a disadvantage to function of the tendon as previously seen in the tensile loading of the tendon (**Table 5**). This is because fibrillar crimps within the collagen fibrils have a limit to their elastic capacity indicative of its stress/strain behaviour at yield point (108). The level of mineralisation means the tendon reaches yield point quicker thus excess mineral beyond this would cause the tendon to fail. With no signalling component it is inevitable that if this experiment was continued for several more weeks eventually most of the tendons would break following in the same footsteps as the right young tendon. If the cells were viable tenocytes would prevent over-mineralisation. Fibroblasts would increase the elastic potential of the tendon by upregulating fibrillogenesis (108). Thus, increase the collagen content to accommodate the increased mineral.

In old tendons at specific mineral regions after mineral was removed, the collagen would retain some of the organisation of the fibrils throughout remineralisation (**Figure 35**). This organisation is characteristic of a loss in crimp morphology thus collagen fibrils are straighter and ordered (108). This process is irreversible so in theory the level of organisation in the collagen thus the amide III:I ratio intensity should be the same as if the tendon remained demineralised (**Figure 15i**). This is not the case because there is loss of collagen (109). This is shown by the weight loss in the tendons while remineralisation continued to accommodate the collagen with mineral. Therefore, to simultaneously allow the uptake of excess mineral,

the collagen had to compromise its structural integrity. This is seen in the varying ratios of amide III: I indicative of the level of organisation as well as the loss of amide III vs loss of amide I (**Figure 33**). Further works is needed to fully elucidate the chemistry of the irreversible nature of the collagen organisation immediately after demineralisation.

Overall collagen is very important factor to the way both young and old tendons mineralised shown by Raman spectroscopy combined with multivariate analysis. Changes in mineral which are not backed up by substantial collagen structural change led to weak-points in the tendon. Breaking points would arise in areas of high modulus associated with regions of high strength along the tendon because the collagen must surpass its strain capacity to accommodate mineral content in and within its fibrils. Subsequent weight lost signified uptake of mineral. Literature has shown this corresponds to replacement of collagen reducing collagen's stability (89). Uptake of mineral also leads to dehydration of tendon making it more prone to failure of function (unable to withstand mechanical load during locomotion). It becomes brittle because of the replacement of water which reduces the tendon strength displaying effects of age in an accelerated system (**Figure 36**). This is indicative of problems that can occur in over-mineralised collagenous tissues.

6 Strengths and Limitations

The strength of this study was using a multidisciplinary approach to identify the links between mineralisation and potential problems which can arise leading to unhealthy ageing of collagenous tissue. A combined approach of chemistry with biomechanics of components of collagen mineralisation other than the mineral content of the tendon allowed the collagen to be investigated in-depth. This revealed the importance of collagen at structural level for determination of function. Methods were also kept consistent thus making results reliable and comparable. The number of freeze-thaw cycles were kept to a maximum of five which reduced any effects this would have on the spectral data during Raman analysis. The limitations to this study was the range of age groups and number of tendons. Only two age groups were used to classify young and old TLT. Although the number of age groups were low, across both old and young TLTs there were large amounts of data produced (**List of Figures & Appendix**). This is associated with the timeframe which was another limitation. Other limitations associated with the mechanical testing such as a lack of sample numbers caused a decrease in the reliability and potentially using 2 different strains for uniaxial loading of young vs old tendon (strain reduced from 5 to 2.5% for old tendon as test failed at higher strain). Thus, it was difficult to determine whether the trend in stress-strain activity seen in some tendons were specific to those tendons or caused by a problem which may have occurred during mechanical testing. Particularly, the unexpected initial shape of the force-displacement curve of some tendons compared to the literature (110). There was also a lack of statistical analysis of the mechanical properties of the tendon. The decreased reliability and statistical analysis still leaves some results unexplained such as the large increase in length of tendons compared to young tendons. Given more time, more age groups could be collected to increase the consistency and reliability of the results as well as statistics to show the significance of the results. Thus, possible explanations for unexpected trends in this new technique for mechanical testing tendons can be provided.

7 Future works

In this study PCA was a very adequate multivariate technique to show spectral differences within the TLT model. Future work would explore other analysis techniques such as partial least square (PLS). PLS is a supervised technique which creates a linear combination of variables from the wavenumbers in the same way as PCA however it produces a linear regression of new variables between predicted variables which are maximumly correlated to observable variables (94).

Characterising a single effective modulus of the TLT model was difficult due to the viscoelastic nature of tendon thus the tendon displaying a variety of moduli depending on which region of the stress/strain activity was calculated. Future work would build on the FEA model and include calculations of the rate of change from one modulus to the next in mineralised regions thus a measure of the rate of mineralisation that occurs between age groups. In addition, Raman analysis could be conducted simultaneous during tendon loading. This would help to provide a more accurate range of moduli characterising regions in an ageing tendon alongside the varying moduli present in the TLT. This would include a surface marker that would eradicate the issue of inconsistency and would not compromise the structural or mechanical integrity of the tendon. In addition, features such as measuring diameter of each tendon more accurately may influence results e.g. using a calipers. Though a small change, this could make a big difference to the accuracy of the overall results.

Much of the literature explores tendons from 11 weeks of age to show mineralisation does not occur in turkeys, *Meleagris gallopavo* up until around 11-12 weeks (35) (48) (51). This study warrants further investigation in tendons younger than 11 weeks due to the predetermined changes in the collagen which occur before the onset of mineralisation. Particularly in the region which never mineralises, there will be differences in the fibroblasts embedded in the collagen involved in signalling which determines the chemistry of these region that manifest in old tendons. Proteoglycans such as decorin play an important role in the inhibition of mineralisation of fibrillar collagen (108). Extracting tendons at the age these cells are most active and viable would contribute to results indicative of the transition from undefined functionalised collagenous tissue to never mineralised tissue.

During the remineralisation experiment, tendons lost weight due to a combination of dehydration (water loss) and loss of collagen content from mineral deposition. Future work could be done to quantify the exact percentage of water and collagen lost by weight. By repeating the remineralisation experiment the addition of a control group would be useful for comparison. This would include media functioning only to preserve the integrity of the tendon vs SBF solution with the necessary ionic environment to promote apatite formation. Through this it would be possible to fully elucidate the chemistry of the irreversible nature in the collagen organisation immediately after demineralisation in TLTs. In addition, mechanical testing could be conducted after mineralisation with SBF to see the final changes that occurred in the mechanical properties of the tendon thus determining the effect of age on the mechanical integrity of the tendon.

8 Conclusions

To conclude mineral regions, mineral maturity and regions that will never become mineralised are all predetermined by the tendon's collagen chemistry. These factors are responsible for the tendon's complex mechanical behaviour supported by a range of mechanical tests. There was an overarching theme of leg dominance revealed by differences such as the tendon's adaptation for greater mechanical load, the over-mineralisation and the loss of collagen content in remineralisation. These factors were consistent in the right tendon across both age groups evidenced in the inherent nature of collagen's structure before the onset of mineralisation. Due to the changing combinations of these factors with age the transition of mineralisation is not as simple as one linear progression but rather a group of processes working together to counteract compromises to the mechanical integrity to the best of their ability and balance the rate of these adaptations for effective function.

The results support the hypothesis that distinct regions where mineralisation occur are accompanied by a change in the biomechanical properties of collagen. The collagen becomes more aligned and adapted to the mechanical demand of the tendon however when over-mineralisation occurs these regions are a disadvantage to the tendon's overall structural integrity. Additionally, this research has shown the absence of higher signalling components (such as tenocytes in the collagen matrix and proteoglycans present in the ECM) results in a perturbed mineralisation system. Mineralisation is a conserved process which is limiting. Due to the specific locomotive activity of the turkeys and the anatomical position of these tendons, they have evolved as a mechanism of function, supposedly to conserve the mechanical integrity of tendons however the laws of physics govern this process as a hinderance to the tendon's innate function to absorb elastic energy during movement. This energy is absorbed by the tendon to reduce the impact on bone significantly thus the viscoelastic nature of tendon. By the tendon becoming more 'bone-like' in mineralised regions, the turkey can balance its mass and the elastic potential of the tendon for efficient locomotion. However, the level of 'bone-like' similarity can counteract the overall tendon function.

This research justifies the advantage of the structural integrity of non-mineralised collagen. Being able to characterise tissue that never mineralises in a perturbed mineralisation system provides the possibility of controlling mineralisation. The regeneration of this type of tissue can exponentially improve the longevity of collagenous tissue and open opportunities for new therapeutic agents to target tissues with disrupted mineralisation in a range of metabolic diseases.

Word Count: 25,230

9 References

1. Currey JD. *Bones: Structure and Mechanics*: Princeton University Press; 2013.
2. Bellido T, Plotkin LI, Bruzzanitti A. Bone Cells. In: Burr DB, editor. *Basic and Applied Bone Biology*: Academic Press; 2013. p. 27.
3. Charles JF, Aliprantis AO. Osteoclasts: more than 'bone eaters'. *Trends in molecular medicine*. 2014;20(8):449-59.
4. Lau AN, Adachi JD. Bone Aging. In: Nakasato Y, Yung RL, editors. *Geriatric Rheumatology: A Comprehensive Approach*. New York, NY: Springer New York; 2011. p. 11-6.
5. Rochefort G, Pallu S, Benhamou C-L. Osteocyte: the unrecognized side of bone tissue. *Osteoporosis Int*. 2010;21(9):1457-69.
6. Premkumar S. *Biology of Bone and Cartilage Textbook of craniofacial growth 1ed*: JP Medical Ltd; 2011. p. 14.
7. Berger C, Goltzman D, Langsetmo L, Joseph L, Jackson S, Kreiger N, et al. Peak bone mass from longitudinal data: implications for the prevalence, pathophysiology, and diagnosis of osteoporosis. *Journal of Bone and Mineral Research*. 2010;25(9):1948-57.
8. Lu J, Shin Y, Yen M-S, Sun SS. Peak bone mass and patterns of change in total bone mineral density and bone mineral contents from childhood into young adulthood. *Journal of Clinical Densitometry*. 2016;19(2):180-91.
9. Boskey AL, Coleman R. Aging and Bone. *J Dent Res*. 2010;89(12):1333-48.
10. Armitage OE, Oyen ML. Indentation across interfaces between stiff and compliant tissues. *Acta Biomater*. 2017;56:36-43.
11. Viguet-Carrin S, Follet H, Gineyts E, Roux J-P, Munoz F, Chapurlat R, et al. Association between collagen cross-links and trabecular microarchitecture properties of human vertebral bone. *Bone*. 2010;46(2):342-7.
12. Nyman JS, Roy A, Acuna RL, Gayle HJ, Reyes MJ, Tyler JH, et al. Age-related effect on the concentration of collagen crosslinks in human osteonal and interstitial bone tissue. *Bone*. 2006;39(6):1210-7.
13. Saito M, Marumo K. Effects of collagen crosslinking on bone material properties in health and disease. *Calcif Tissue Int*. 2015;97(3):242-61.
14. Allen MR, Burr DB. Bone Modelling and Remodelling In: Burr DB, editor. *Basic and applied bone biology*: Academic Press; 2013. p. 87.
15. Jilka RL, O'Brien CA, Roberson PK, Bonewald LF, Weinstein RS, Manolagas SC. Dysapoptosis of osteoblasts and osteocytes increases cancellous bone formation but exaggerates cortical porosity with age. *Journal of Bone and Mineral Research*. 2014;29(1):103-17.
16. Health UDo, Services H. *Bone health and osteoporosis: a report of the Surgeon General*. Rockville, MD: US Department of Health and Human Services, Office of the Surgeon General. 2004;87.
17. Rey C, Combes C, Drouet C, Glimcher MJ. Bone mineral: update on chemical composition and structure. *Osteoporosis Int*. 2009;20(6):1013-21.
18. Liu XQ, Qu XH, Nie T, Zhai ZJ, Li HW, Ouyang ZX, et al. The Beneficial Effects of Bisphosphonate-enoxacin on Cortical Bone Mass and Strength in Ovariectomized Rats. *Front Pharmacol*. 2017;8:8.
19. Heaney R, Abrams S, Dawson-Hughes B, Looker A, Marcus R, Matkovic V, et al. Peak bone mass. *Osteoporosis Int*. 2000;11(12):985-1009.
20. United States Public Health Service States GSGU. *The Basics of Bone in Health and Disease. Bone Health and Osteoporosis: A Report of the Surgeon General* University Press of the Pacific; 2004.
21. Pietschmann P, Skalicky M, Kneissel M, Rauner M, Hofbauer G, Stupphann D, et al. Bone structure and metabolism in a rodent model of male senile osteoporosis. *Experimental gerontology*. 2007;42(11):1099-108.

22. Nagaraja S, Lin AS, Guldborg RE. Age-related changes in trabecular bone microdamage initiation. *Bone*. 2007;40(4):973-80.
23. Seref-Ferlenguez Z, Kennedy OD, Schaffler MB. Bone microdamage, remodeling and bone fragility: how much damage is too much damage [quest]. *BoneKEy reports*. 2015;4.
24. O'Brien FJ, Brennan O, Kennedy OD, Lee TC. Microcracks in cortical bone: how do they affect bone biology? *Current osteoporosis reports*. 2005;3(2):39-45.
25. Karim L, Vashishth D. Bone Microdamage and Its Contribution to Fracture. In: Silva MJ, editor. *Skeletal aging and osteoporosis: Biomechanics and Mechanobiology* Springer; 2013. p. 94.
26. Chen A, Gupte C, Akhtar K, Smith P, Cobb J. The global economic cost of osteoarthritis: how the UK compares. *Arthritis*. 2012;2012.
27. Pye SR, Reid DM, Smith R, Adams JE, Nelson K, Silman AJ, et al. Radiographic features of lumbar disc degeneration and self-reported back pain. *The journal of Rheumatology*. 2004;31(4):753-8.
28. Winter J. Admitted patient care, England 2013–2014. Health and Social Care Information Centre. 2015.
29. Kanis J, Johnell O, Oden A, Sernbo I, Redlund-Johnell I, Dawson A, et al. Long-term risk of osteoporotic fracture in Malmö. *Osteoporosis Int*. 2000;11(8):669-74.
30. Siris E, Adler R, Bilezikian J, Bolognese M, Dawson-Hughes B, Favus M, et al. The clinical diagnosis of osteoporosis: a position statement from the National Bone Health Alliance Working Group. *Osteoporosis Int*. 2014;25(5):1439-43.
31. O'Connor EM, Durack E. Osteocalcin: The extra-skeletal role of a vitamin K-dependent protein in glucose metabolism. *Journal of Nutrition & Intermediary Metabolism*. 2017;7:8-13.
32. Brion A, Zhang G, Dossot M, Moby V, Dumas D, Hupont S, et al. Nacre extract restores the mineralization capacity of subchondral osteoarthritis osteoblasts. *J Struct Biol*. 2015;192(3):500-9.
33. Tomoaia G, Pasca R. On the Collagen Mineralization. A Review. *Clujul Medical*. 2015;88(1):15-22.
34. Burr DB, Akkus O. Bone Morphology and Organization In: Burr DB, editor. *Basic and Applied Bone Biology* Academic Press; 2013. p. 23.
35. Kerns JG, Buckley K, Churchwell J, Parker AW, Matousek P, Goodship AE. Is the Collagen Primed for Mineralization in Specific Regions of the Turkey Tendon? An Investigation of the Protein-Mineral Interface Using Raman Spectroscopy. *Analytical Chemistry*. 2016;88(3):1559-63.
36. Franchi M, Ottani V, Stagni R, Ruggeri A. Tendon and ligament fibrillar crimps give rise to left-handed helices of collagen fibrils in both planar and helical crimps. *Journal of anatomy*. 2010;216(3):301-9.
37. Docheva D, Müller SA, Majewski M, Evans CH. Biologics for tendon repair. *Advanced drug delivery reviews*. 2015;84:222-39.
38. Freeman J, Silver F. Analysis of mineral deposition in turkey tendons and self-assembled collagen fibers using mechanical techniques. *Connective Tissue Research*. 2004;45(3):131-41.
39. Thorpe CT, Riley GP, Birch HL, Clegg PD, Screen HRC. Effect of fatigue loading on structure and functional behaviour of fascicles from energy-storing tendons. *Acta Biomater*. 2014;10(7):3217-24.
40. Agabalyan NA, Evans DJ, Stanley RL. Investigating tendon mineralisation in the avian hindlimb: a model for tendon ageing, injury and disease. *Journal of anatomy*. 2013;223(3):262-77.
41. Jones W, Roberts R. *Pathological calcification and ossification in relation to Leriche and Policard's Theory*. SAGE Publications; 1933.
42. Matson A, Konow N, Miller S, Konow PP, Roberts TJ. Tendon material properties vary and are interdependent among turkey hindlimb muscles. *Journal of Experimental Biology*. 2012;215(20):3552-8.
43. Thorpe C, Clegg P, Birch H. A review of tendon injury: why is the equine superficial digital flexor tendon most at risk? *Equine veterinary journal*. 2010;42(2):174-80.
44. Reddy GK, Stehno-Bittel L, Enwemeka CS. Glycation-induced matrix stability in the rabbit achilles tendon. *Archives of Biochemistry and Biophysics*. 2002;399(2):174-80.

45. Thorpe CT, Godinho MSC, Riley GP, Birch HL, Clegg PD, Screen HRC. The interfascicular matrix enables fascicle sliding and recovery in tendon, and behaves more elastically in energy storing tendons. *J Mech Behav Biomed Mater*. 2015;52:85-94.
46. Thorpe CT, Streeter I, Pinchbeck GL, Goodship AE, Clegg PD, Birch HL. Aspartic Acid Racemization and Collagen Degradation Markers Reveal an Accumulation of Damage in Tendon Collagen That Is Enhanced with Aging. *Journal of Biological Chemistry*. 2010;285(21):15674-81.
47. Burger C, Zhou H-w, Wang H, Sics I, Hsiao BS, Chu B, et al. Lateral packing of mineral crystals in bone collagen fibrils. *Biophysical journal*. 2008;95(4):1985-92.
48. Kłosowski MM, Carzaniga R, Shefelbine SJ, Porter AE, McComb DW. Nanoanalytical electron microscopy of events predisposing to mineralisation of turkey tendon. *Scientific reports*. 2018;8(1):3024.
49. Raspanti M, Reguzzoni M, Protasoni M, Congiu T. Mineralization-related modifications in the calcifying tendons of turkey (*Meleagris gallopavo*). *Micron*. 2015;71:46-50.
50. Silver FH, Freeman JW, Seehra GP. Collagen self-assembly and the development of tendon mechanical properties. *J Biomech*. 2003;36(10):1529-53.
51. Silver FH, Christiansen D, Snowhill PB, Chen Y, Landis WJ. The role of mineral in the storage of elastic energy in turkey tendons. *Biomacromolecules*. 2000;1(2):180-5.
52. Silver FH. *Mechanosensing and mechanochemical transduction in extracellular matrix: Biological, chemical, engineering, and physiological aspects*: Springer Science & Business Media; 2006.
53. Kerns JG, Gikas PD, Buckley K, Shepperd A, Birch HL, McCarthy I, et al. Evidence from Raman Spectroscopy of a Putative Link Between Inherent Bone Matrix Chemistry and Degenerative Joint Disease. *Arthritis Rheumatol*. 2014;66(5):1237-46.
54. Coello B, López-Álvarez M, Rodríguez-Domínguez M, Serra J, González P. Quantitative evaluation of the mineralization level of dental tissues by Raman spectroscopy. *Biomedical Physics & Engineering Express*. 2015;1(4):045204.
55. Morris MD, Mandair GS. Raman assessment of bone quality. *Clinical Orthopaedics and Related Research*®. 2011;469(8):2160-9.
56. Bumbrah GS, Sharma RM. Raman spectroscopy—Basic principle, instrumentation and selected applications for the characterization of drugs of abuse. *Egyptian Journal of Forensic Sciences*. 2016;6(3):209-15.
57. Butler HJ, Ashton L, Bird B, Cinque G, Curtis K, Dorney J, et al. Using Raman spectroscopy to characterize biological materials. *Nature protocols*. 2016;11(4):664-87.
58. Buckley K, Kerns JG, Birch HL, Gikas PD, Parker AW, Matousek P, et al. Functional adaptation of long bone extremities involves the localized “tuning” of the cortical bone composition; evidence from Raman spectroscopy. *J Biomed Opt*. 2014;19(11):111602-.
59. Kerns JG, Buckley K, Parker AW, Birch HL, Matousek P, Hildred A, et al. The use of laser spectroscopy to investigate bone disease in King Henry VIII's sailors. *Journal of Archaeological Science*. 2015;53:516-20.
60. Reichenbacher M, Popp J. *Vibrational spectroscopy. Challenges in Molecular Structure Determination*: Springer; 2012. p. 63-143.
61. Le Pevelen DD. NIR FT-Raman. In: Lindon JC, Tranter GE, Koppenaal D, editors. *Encyclopedia of spectroscopy and spectrometry*: Academic Press; 2016. p. 98-109.
62. Rojalín T, Kurki L, Laaksonen T, Viitala T, Kostamovaara J, Gordon KC, et al. Fluorescence-suppressed time-resolved Raman spectroscopy of pharmaceuticals using complementary metal-oxide semiconductor (CMOS) single-photon avalanche diode (SPAD) detector. *Analytical and bioanalytical chemistry*. 2016;408(3):761-74.
63. Wieboldt D. *Understanding Raman Spectrometer Parameters*. 2010.
64. Baena JR, Lendl B. Raman spectroscopy in chemical bioanalysis. *Current opinion in chemical biology*. 2004;8(5):534-9.

65. Depciuch J, Kaznowska E, Zawlik I, Wojnarowska R, Cholewa M, Heraud P, et al. Application of Raman spectroscopy and infrared spectroscopy in the identification of breast cancer. *Applied spectroscopy*. 2016;70(2):251-63.
66. Movasaghi Z, Rehman S, Rehman IU. Raman spectroscopy of biological tissues. *Applied Spectroscopy Reviews*. 2007;42(5):493-541.
67. Mandair GS, Morris MD. Contributions of Raman spectroscopy to the understanding of bone strength. *BoneKEy reports*. 2015;4.
68. Timchenko E, Zherdeva L, Timchenko P, Volova L, Ponomareva U. Detailed Analysis of the Structural Changes of Bone Matrix During the Demineralization Process Using Raman Spectroscopy. *Physics Procedia*. 2015;73:221-7.
69. Baeten V, Hourant P, Morales MT, Aparicio R. Oil and fat classification by FT-Raman spectroscopy. *Journal of Agricultural and Food Chemistry*. 1998;46(7):2638-46.
70. Ferraro JR, Nakamoto, K. & Brown, C. W. *Introductory Raman Spectroscopy*: Elsevier; 2003.
71. Waller L, Tian L, Barbastathis G. Transport of intensity phase-amplitude imaging with higher order intensity derivatives. *Optics express*. 2010;18(12):12552-61.
72. Tarcea N, Popp J. Raman data analysis. *Raman spectroscopy applied to earth sciences and cultural heritage*, PPT. 2012.
73. Khmaladze A, Ganguly A, Kuo S, Raghavan M, Kainkaryam R, Cole JH, et al. Tissue-engineered constructs of human oral mucosa examined by Raman spectroscopy. *Tissue Engineering Part C: Methods*. 2012;19(4):299-306.
74. Rieppo L, Saarakkala S, Närhi T, Helminen H, Jurvelin J, Rieppo J. Application of second derivative spectroscopy for increasing molecular specificity of Fourier transform infrared spectroscopic imaging of articular cartilage. *Osteoarthritis and cartilage*. 2012;20(5):451-9.
75. Jolliffe IT, Cadima J. Principal component analysis: a review and recent developments. *Phil Trans R Soc A*. 2016;374(2065):20150202.
76. Fearn T. *Discriminant analysis*. 1 ed. New York: John Wiley & Sons 2002.
77. Reddy GK. Glucose-mediated in vitro glycation modulates biomechanical integrity of the soft tissues but not hard tissues. *Journal of orthopaedic research*. 2003;21(4):738-43.
78. Chen L, Wu Y, Yu J, Jiao Z, Ao Y, Yu C, et al. Effect of repeated freezing–thawing on the Achilles tendon of rabbits. *Knee Surgery, Sports Traumatology, Arthroscopy*. 2011;19(6):1028-34.
79. Pascart T, Cortet B, Olejnik C, Paccou J, Migaud H, Cotten A, et al. Bone samples extracted from embalmed subjects are not appropriate for the assessment of bone quality at the molecular level using Raman spectroscopy. *Analytical chemistry*. 2016;88(5):2777-83.
80. Cadusch P, Hlaing M, Wade S, McArthur S, Stoddart P. Improved methods for fluorescence background subtraction from Raman spectra. *Journal of Raman Spectroscopy*. 2013;44(11):1587-95.
81. ISO S. 527-1 (2012), *Plastics-determination of tensile properties-Part 1: General principles*. 2018.
82. Milad M, Green S, Ye J. Mechanical properties of reinforced composite materials under uniaxial and planar tension loading regimes measured using a non-contact optical method. *Composite Structures*. 2018.
83. Boyce MC, Arruda EM. Constitutive models of rubber elasticity: a review. *Rubber chemistry and technology*. 2000;73(3):504-23.
84. Seibert D, Schoche N. Direct comparison of some recent rubber elasticity models. *Rubber chemistry and technology*. 2000;73(2):366-84.
85. Dell'Isola F, Sciarra G, Vidoli S, editors. *Generalized Hooke's law for isotropic second gradient materials*. *Proceedings of the Royal Society of London A: Mathematical, Physical and Engineering Sciences*; 2009: The Royal Society.
86. Nikookar M, Nikookar H, Arabani M, editors. *Unconfined compressive strength of lime-stabilized peat*. *Proceeding of the International Conference 7th SASTech, In*; 2013.

87. Kokubo T, Takadama H. How useful is SBF in predicting in vivo bone bioactivity? *Biomaterials*. 2006;27(15):2907-15.
88. Chirchir H. Limited trabecular bone density heterogeneity in the human skeleton. *Anatomy research international*. 2016;2016.
89. Shoulders MD, Raines RT. Collagen structure and stability. *Annual review of biochemistry*. 2009;78:929-58.
90. Gasser TC. An irreversible constitutive model for fibrous soft biological tissue: a 3-D microfiber approach with demonstrative application to abdominal aortic aneurysms. *Acta Biomater*. 2011;7(6):2457-66.
91. Testing ASf, Testing MCE-oM. Standard test method for Young's modulus, tangent modulus, and chord modulus: ASTM International; 2004.
92. Benjamin M, Toumi H, Ralphs J, Bydder G, Best T, Milz S. Where tendons and ligaments meet bone: attachment sites ('entheses') in relation to exercise and/or mechanical load. *Journal of anatomy*. 2006;208(4):471-90.
93. Li Y, Aparicio C. Discerning the subfibrillar structure of mineralized collagen fibrils: a model for the ultrastructure of bone. *PloS one*. 2013;8(9):e76782.
94. Kelly JG, Trevisan J, Scott AD, Carmichael PL, Pollock HM, Martin-Hirsch PL, et al. Biospectroscopy to metabolically profile biomolecular structure: a multistage approach linking computational analysis with biomarkers. *Journal of proteome research*. 2011;10(4):1437-48.
95. Spiesz EM, Thorpe CT, Thurner PJ, Screen HR. Structure and collagen crimp patterns of functionally distinct equine tendons, revealed by quantitative polarised light microscopy (qPLM). *Acta Biomater*. 2018;70:281-92.
96. Wenk H-R, Heidelbach F. Crystal alignment of carbonated apatite in bone and calcified tendon: results from quantitative texture analysis. *Bone*. 1999;24(4):361-9.
97. Rumian AP, Wallace AL, Birch HL. Tendons and ligaments are anatomically distinct but overlap in molecular and morphological features—a comparative study in an ovine model. *Journal of orthopaedic research*. 2007;25(4):458-64.
98. Cheraghali Z, Mohammadi R, Jalilzadeh-Amin G. Planimetric and biomechanical study of local effect of pulegone on full thickness wound healing in rat. *The Malaysian journal of medical sciences: MJMS*. 2017;24(5):52.
99. Schumacher MA, Mizuno K, Bächinger HP. The crystal structure of a collagen-like polypeptide with 3 (S)-hydroxyproline residues in the Xaa position forms a standard 7/2 collagen triple helix. *Journal of Biological Chemistry*. 2006.
100. Avery N, Bailey A. Enzymic and non-enzymic cross-linking mechanisms in relation to turnover of collagen: relevance to aging and exercise. *Scandinavian journal of medicine & science in sports*. 2005;15(4):231-40.
101. Thorpe CT, Birch HL, Clegg PD, Screen HR. The role of the non-collagenous matrix in tendon function. *International journal of experimental pathology*. 2013;94(4):248-59.
102. Schmidt F, Zimmermann E, Campbell G, Sroga G, Püschel K, Amling M, et al. Assessment of collagen quality associated with non-enzymatic cross-links in human bone using Fourier-transform infrared imaging. *Bone*. 2017;97:243-51.
103. Fujimoto D, Moriguchi T, Ishida T, Hayashi H. The structure of pyridinoline, a collagen crosslink. *Biochemical and biophysical research communications*. 1978;84(1):52-7.
104. McNerny EM, Gardinier JD, Kohn DH. Exercise increases pyridinoline cross-linking and counters the mechanical effects of concurrent lathyrogenic treatment. *Bone*. 2015;81:327-37.
105. Nutrition SP. *Nutrient Requirements of Poultry: Ninth Revised Edition, 1994. Illustrated, reprint, revised ed: National Academies Press; 1994. 157 p.*

106. Glimcher MJ, Brickley-Parsons D, Kossiva D. Phosphopeptides and γ -carboxyglutamic acid-containing peptides in calcified turkey tendon: Their absence in uncalcified tendon. *Calcif Tissue Int.* 1979;27(1):281-4.
107. Apostolakos J, Durant TJ, Dwyer CR, Russell RP, Weinreb JH, Alae F, et al. The enthesis: a review of the tendon-to-bone insertion. *Muscles, ligaments and tendons journal.* 2014;4(3):333.
108. Franchi M, Trirè A, Quaranta M, Orsini E, Ottani V. Collagen structure of tendon relates to function. *The Scientific World Journal.* 2007;7:404-20.
109. Galloway MT, Lalley AL, Shearn JT. The role of mechanical loading in tendon development, maintenance, injury, and repair. *The Journal of bone and joint surgery American volume.* 2013;95(17):1620.
110. Maganaris CN, Narici MV, Maffulli N. Biomechanics of the Achilles tendon. *Disability and rehabilitation.* 2008;30(20-22):1542-7.

10 Appendix

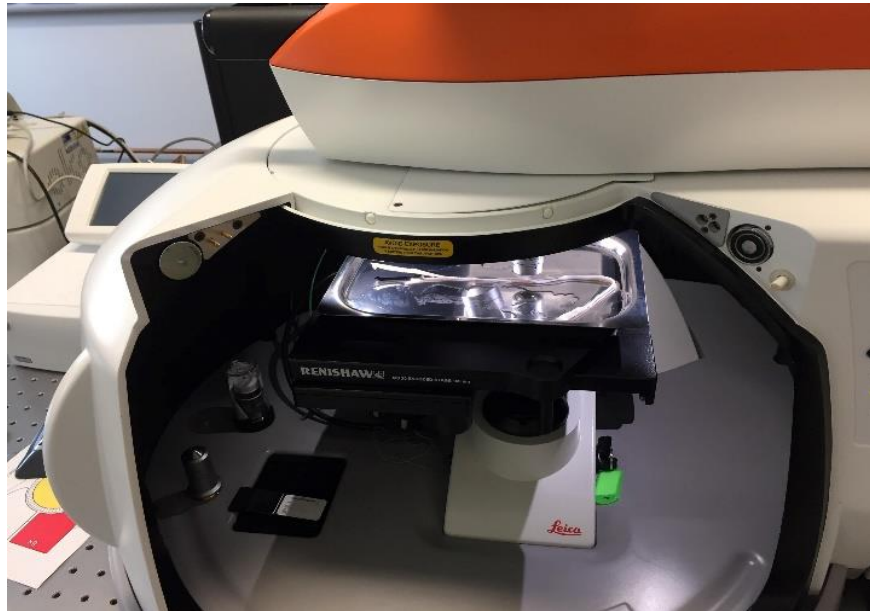


Figure 44: TLT setup for spectral data collection using Raman spectrometer (Renishaw plc, Gloucestershire, UK).

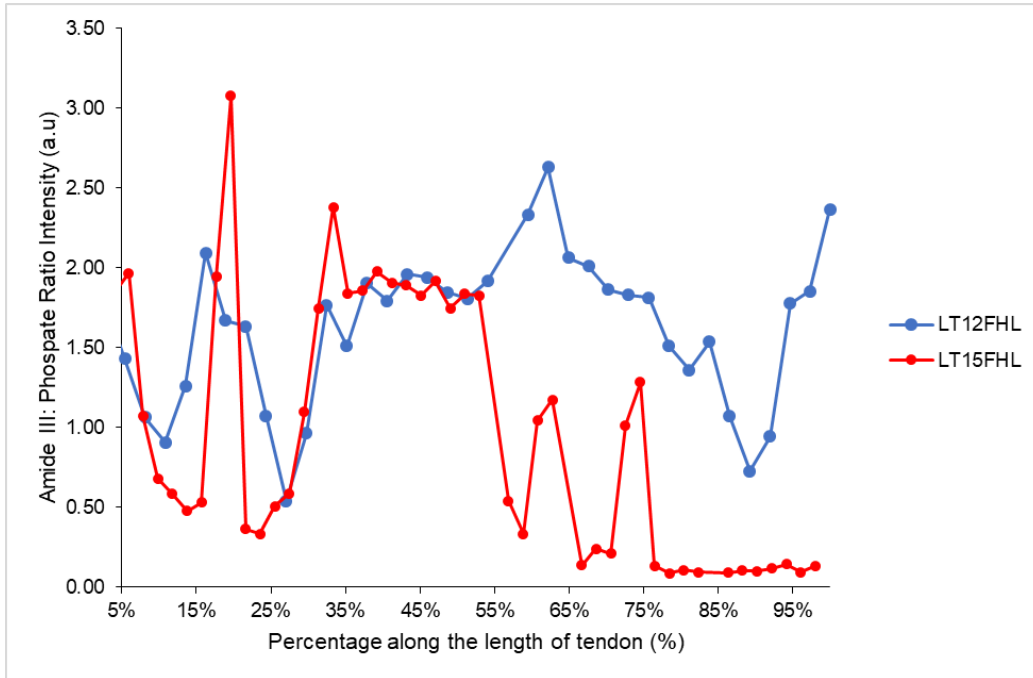


Figure 45: Amide III: Phosphate ratio intensity from the distal end of the left tendon before mechanical testing.

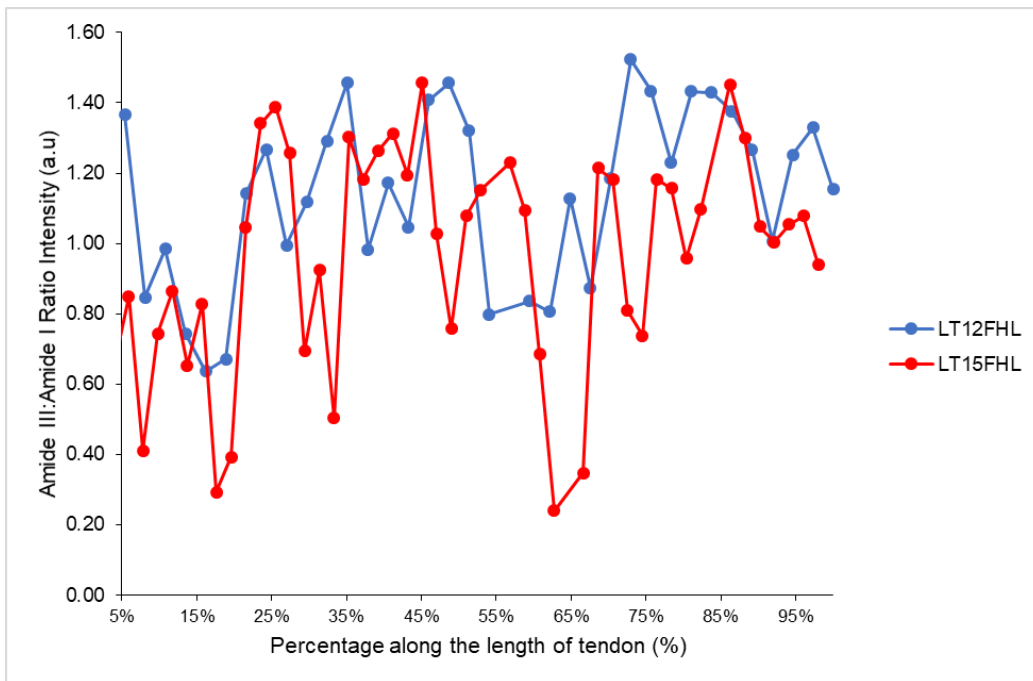


Figure 46: Amide III: Amide I ratio intensity from the distal end of the left tendon before mechanical testing.

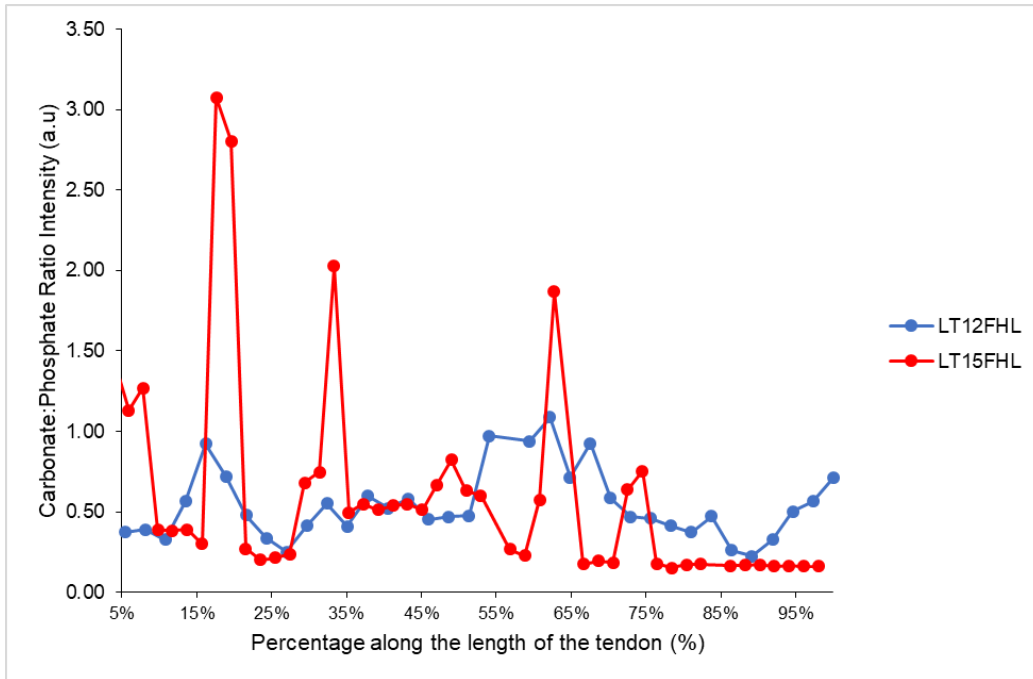


Figure 47: Carbonate: Phosphate ratio intensity from the distal end of the left tendon before mechanical testing.

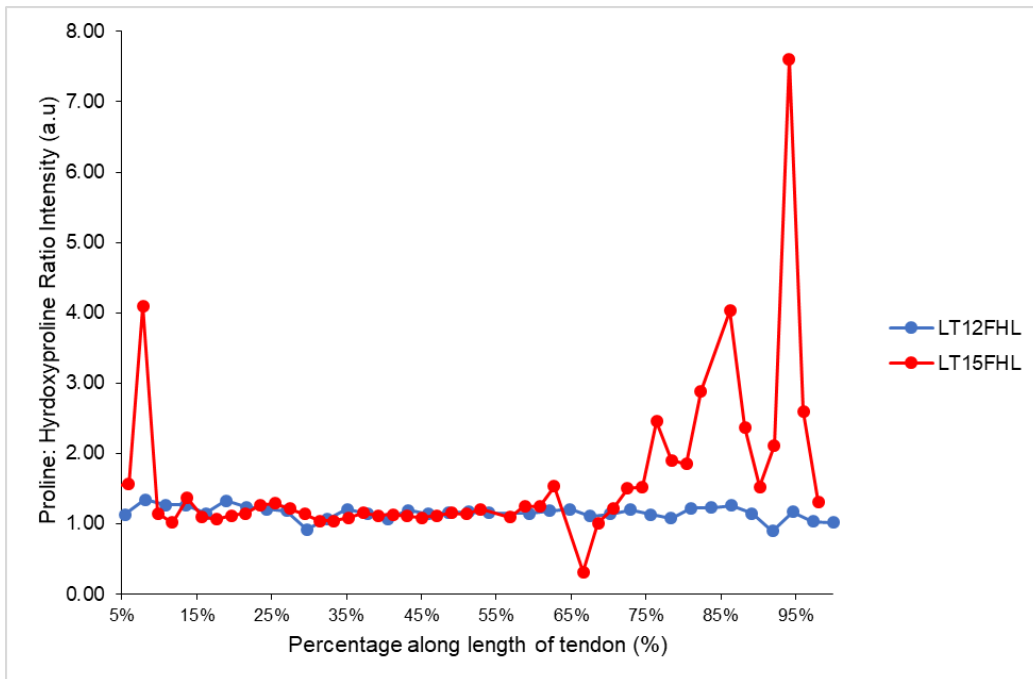


Figure 48: Proline: Hydroxyproline ratio intensity from the distal end of the left tendon before mechanical testing.

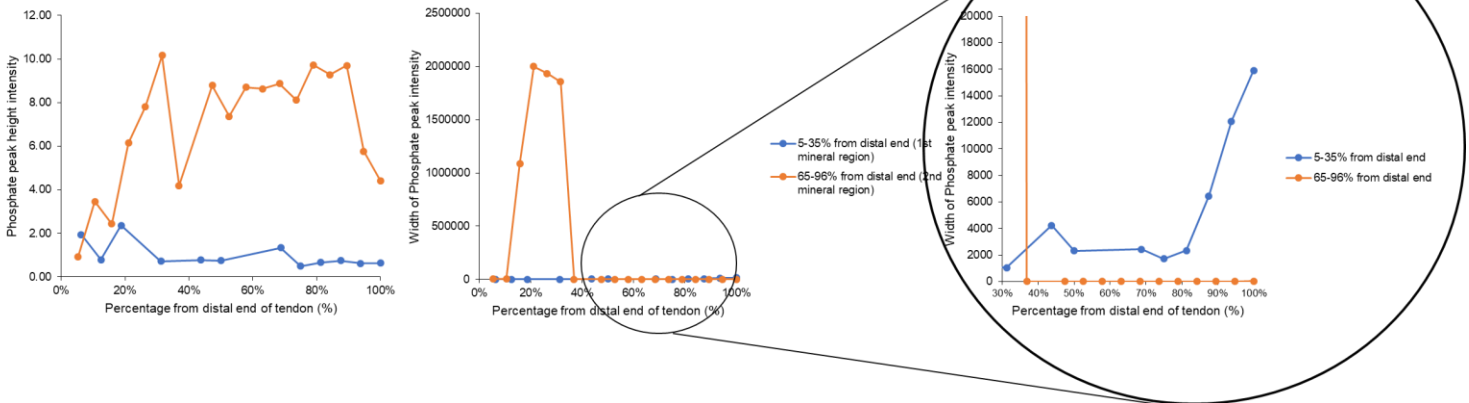


Figure 49: Differences in level of mineralisation in 1st and 2nd mineral regions of right old tendons (15 wks), both height (left) and width (right) giving an indication of maturity of mineral component.